TAMPEREEN TEKNILLINEN YLIOPISTO
TAMPERE UNIVERSITY OF TECHNOLOGY

TELMO SUBIRÁ RODRÍGUEZ

ANALYSIS, OPTIMIZATION AND MINIATURIZATION OF AN 18-MHZ BASIC AM TRANSMITTER

Master of Science Thesis

Examiners: Dr. (Tech.) Jari Kangas &
Dr. (Tech.) Olli-Pekka Lunden
Examiner and topic approved by the
Faculty Council of the Faculty of
Computing and Electrical Engineering
on 9th March 2016

ABSTRACT

TAMPERE UNIVERSITY OF TECHNOLOGY
TELMO SUBIRÁ RODRÍGUEZ: Analysis, optimization and miniaturization of an 18-MHz basic AM transmitter
Master of Science Thesis, 77 pages, 8 Appendix pages
March 2016
Exchange Student from the Universidad Politécnica de Madrid
Major: Telecommunication Engineering
Examiners: Dr. (Tech.) Jari Kangas & Dr. (Tech.) Olli-Pekka Lunden

Keywords: AM transmitter, Optimization, Amplitude Modulation, Crystal Oscillator, LC Oscillator, Power Efficiency, ADS, RF layout, PCB fabrication, 3D model

Amplitude Modulation is one of the oldest and most known modulation techniques. It is still widely used because of its simplicity. *Practical RF Electronics: First Principles Applied* course at Tampere University of Technology used a basic AM transmitter to make the students put into practice many concepts of RF electronics. This thesis project focuses on the optimization of the original design of the AM transmitter. The thesis provides the future students of the course with a functioning demonstration device similar to the original one.

Because of the didactic purpose of the transmitter, the schematic should remain as simple as the original one. Simplicity has been the most important restriction of this optimization project, so that every block and component in the circuit has a clear purpose, helping students understanding.

To highlight the weakest points of the transmitter design, an analytical work was made for a deeper characterization of the transmitter performance. Analytic methods, circuit simulations, and laboratory measurements were carried out for the optimization process.

Improvements, modifications and replacements were implemented on the original schematic design. These changes involved the use of low-current transistor types, adjustment of several passive component values, and the design of a custom crystal oscillator to generate an 18.432-MHz carrier.

As a result, the optimized transmitter provides 26% lower power consumption, 5 times higher power efficiency, and double transmission distance using the same dipole antenna. On the other hand, the first harmonic distortion degraded by some 9 dB from the original design.

Once the schematic was optimized, the device was miniaturized by designing and fabricating the transmitter on a printed circuit board (PCB). The project included an additional task of 3D modelling and printing for the package of the final device. As a result, the final fabricated transmitter has a small, reliable, and user-friendly form factor to be used as a demonstration.

PREFACE

This project rises after the experience of the author as a student in the *Practical RF Electronics* course, during his exchange year at TUT. The work has been carried out entirely by the author, with the guidance and advice of his supervisors. It is the intention of this thesis to prove the acquired knowledges of the author about analog and radio-frequency electronics, while offering the course a final product with a didactical purpose.

Because of that, it is the author's desire that the contents shown in this thesis may be of use for any MSc student, while working with analog transmitters, as a reference material. Optimization methods, measurement setups and debug information are provided so that anyone with similar background could replicate the fabrication of the final device.

Thesis document makes use of pictures, summary tables and graphs very commonly, and it highlights also important concepts using bold letters. This is intended to help the reader during fast reading and information searching. References and bibliography follow the IEEE referencing guidelines.

The author would like to thank all the guidance, support and attention provided from his both examiners Jari and Olli-Pekka. Additionally, the author is grateful with all the Tampere University of Technology institution for giving him the opportunity to finish his formation period and enjoy its installations, resources and education system during the last year. He thanks also all the staff from the *Universidad Politécnica de Madrid* who made this exchange experience possible during his Master's degree studies.

In Tampere, Finland, on 23 May 2016

Telmo Subirá Rodríguez
Universidad Politécnica de Madrid
Tampere University of Technology
telmosubirar@gmail.com

CONTENTS

LIST OF FIGURES

LIST OF TABLES

LIST OF SYMBOLS AND ABBREVIATIONS

Acronyms and abbreviations

.stl – stereo lythography

3D – three dimensional

AC – alternating current

ADS – Advanced Design System

AM – amplitude modulation

BJT – bipolar junction transistor

CAD – computer-aided design

C/N – carrier-to-noise ratio

DC – direct current

FSR – frequency of self-resonance

H_2O – water (hydrogen monoxide)

H_2O_2 – hydrogen peroxide

HCl – hydrogen cloride

HP – Hewlett-Packard

LED – light-emitting diode

PCB – printed circuit board

P_{HD} – harmonic distortion power

RF – radio frequency

SMD – surface mount device

TH – through-hole

TUT – Tampere University of Technology

UV – ultraviolet

Symbols and Units

cm – centimeter

dB – decibel

dBc – decibels relative to the carrier

dBm – decibel-miliwatt

h – hour

Hz – hertz

j – imaginary unit

kHz – kilohertz

kΩ - kiloohm

m – meters

mA – miliamper

mAh – miliamper-hour

MHz – megahertz

mm – millimeter

mVpp – millivolt peak-to-peak

mW – miliwatt

PPM – parts per million

V – volt

Vpp – Volt peak-to-peak

Z – impedance

ω – angular frequency

Ω - ohm

1. INTRODUCTION

The transmitter is one of the most important parts in any wireless communication system. Transmitters transform some kind of information (e.g. sound or data) into radio signals, and deliver these signals to antennas [1]. Most of wireless transmissions nowadays are digital, but traditionally transmitters send analog information. Many analog transmitters are still in use despite the increased use of digital techniques.

In a transmitter, the information signal is used to modify one or more properties of another signal that will carry the message. This process is called modulation. Many modulation techniques have been developed since the first days of radio transmission, working on a three-sided compromise between bandwidth, throughput and power consumption. Nevertheless, old and simple modulation techniques such as amplitude and frequency modulation are still widely used around the world [2].

Amplitude Modulation (AM) was the first modulation technique used in voice transmissions by radio, used in 1900 by a Canadian engineer [3]. Because of its simplicity it is still found in many applications, such as broadcast transmissions, remote sensing [4], or civil aviation [5]. In addition to that, it is typically one of the first modulation techniques learned and practiced by students of electronics and RF.

1.1 Thesis objectives

During the *Practical RF Electronics: First Principles Applied* course [6] at TUT, students carried out the analysis, building and testing of a basic AM transmitter. The RF course and the didactical purpose of the AM transmitter are the context in which this project is based.

This thesis focuses on the optimization of the transmitter used as the case of study in the course. The objective of this optimization is to provide a functional demonstration device for the future RF students. Additionally, performance parameters are analyzed and several improvements are implemented, so that students can easily understand and assimilate the concepts of the course.

The design should be kept simple. The purpose of each block and component in the schematic should be clear. In addition, the demonstration device requires a reliable, small, and user-friendly physical interface. Power efficiency will be also a valuable parameter in the optimization process, so that the battery lifetime is not unnecessarily reduced.

This text provides documentation about the optimization of the transmitter, so that the final device could be easily replicated and debugged if necessary. Besides that, optimization process and important choices are detailed for better understanding of the results. Every part of this thesis, form the fabricated device to the contents in this text, could be used as didactic material for master students.

1.2 Document organization

Chapter 2 starts with a brief theoretical explanation of some key concepts related to the topic. In the references one can find further information about these matters.

Chapter 3 defines the working procedures carried out for the optimization. They include several analyses, characterization, design and fabrication methods explained for the replication of the process.

Chapter 4 discusses qualitative and quantitative analysis of the original basic AM transmitter. This chapter explains the transmitter behavior based on the schematic, providing simulation and prototype results.

In Chapter 5, the implementation of several improvements on the schematic are explained. It includes also information and decisions taken about the PCB design, the fabrication, and the 3D modelling for the package.

Chapter 6 provides the optimization results and comparisons with the original device and an intermediate version. It includes the complete bill of materials of the transmitter, with price data and comparisons. This information is completed with debug information for future replications of the device.

Finally, Chapter 7 summarizes the key points of the project and gives conclusions.

2. THEORETICAL BACKGROUND

An optimization process involves many tasks, in which different concepts and techniques are essential for the correct development of the solution, depending on the specific case. This project focuses on the optimization of a basic AM transmitter with didactical purposes, and this chapter explains the most important concepts that will help to understand the optimization of the transmitter.

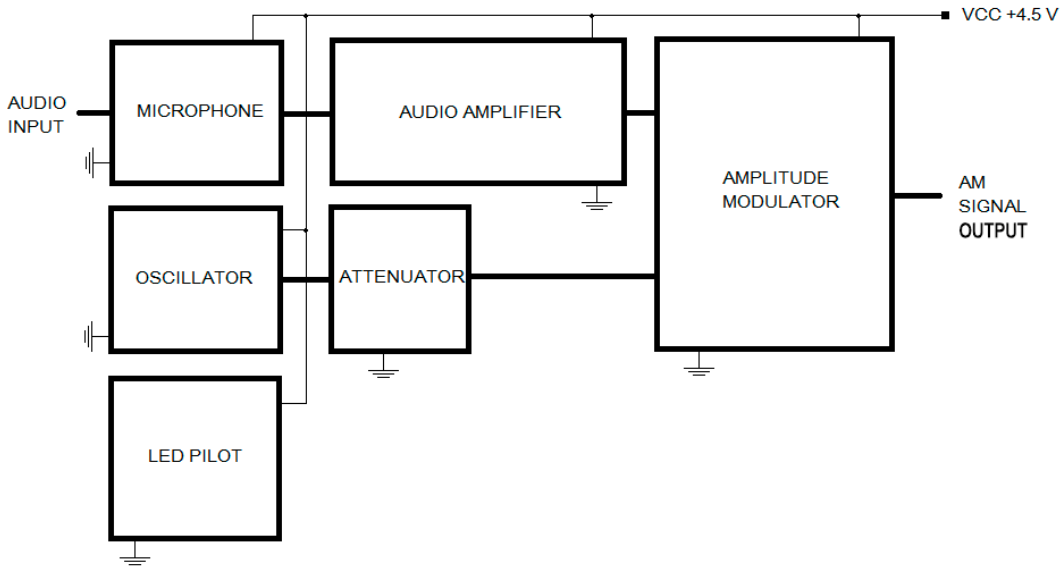

Figure 1 Block-diagram for the AM transmitter from the "Practical RF Electronics: First Principles Applied" course.

Having a look at the diagram of the transmitter in Figure 1, we can identify circuit blocks performing different analog functions. They are explained in more detail in Chapter 4, but from here we can assume the signal path starting from the microphone block. It goes through the audio amplifier block, and reaches the output through the amplitude modulator block as an AM signal.

Because of that, **amplitude modulation theory** presents an important role as the optimization basis. Additionally, the basic **oscillator theory** is also considered a key part in the optimization. An oscillator will generate the carrier signal, and the carrier generation will be one of the main design tasks implemented in this project. Power optimization of the schematic design will make use of several **power efficiency** concepts as well.

All these background concepts will help us understand the transmitter, the decisions made and the optimization results. Following subchapters give a very brief explanation of all these concepts.

2.1 AM modulation

AM is probably the simplest and oldest modulation technique in RF transmission. A **modulating signal** contains the information to be sent. This signal changes the amplitude of a high-frequency **carrier** according to its waveform. The time-domain result can be observed as a high-frequency signal with variable amplitude, so that the envelope corresponds to the modulating signal waveform [7]. Figure 2 shows an example using a sine wave as the modulating signal.

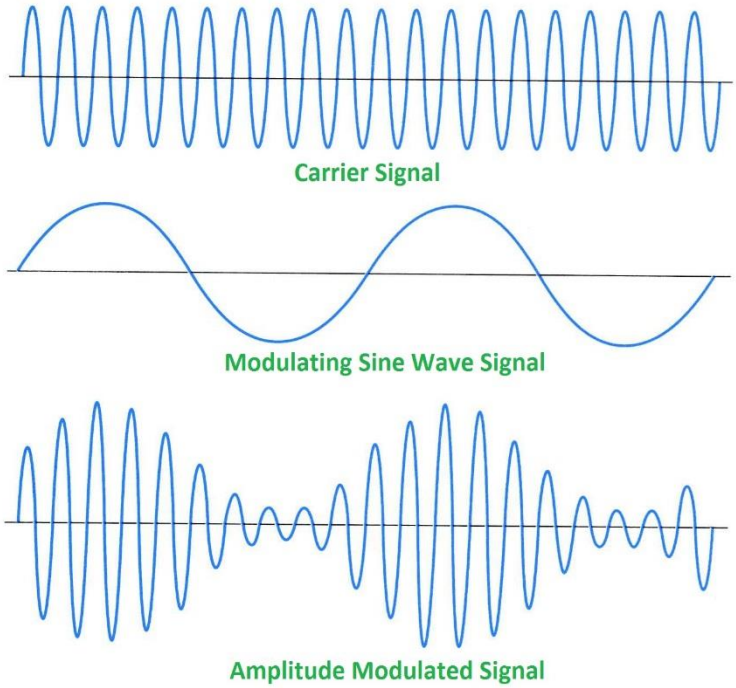

Figure 2 Amplitude Modulation signals example. [8]

We can consider the sinusoidal modulating signal v_m as

$$v_m = V_m sin 2\pi f_m t \tag{1}$$

where V_m is the peak amplitude, f_m is the modulating frequency and t is the time. The carrier signal v_C can be

$$v_C = V_C sin 2\pi f_C t \tag{2}$$

where V_C is the peak amplitude and f_C is the carrier frequency. Then, the AM signal v_{AM} produced by the combination of them is

$$v_{AM} = v_C(1 + v_m) = V_C sin2\pi f_C t + (V_m sin2\pi f_m t)(sin2\pi f_C t) \quad (3)$$

Considering the trigonometric identity

$$sinA\ sinB = \frac{\cos(A-B)}{2} - \frac{\cos(A+B)}{2} \quad (4)$$

and replacing *(sinA)(sinB)* = $(sin2\pi f_m t)(sin2\pi f_C t)$ in equation (3) we obtain a new representation for the AM signal v'_{AM} as

$$v'_{AM} = V_C sin2\pi f_C t + \frac{V_m}{2} cos2\pi t(f_C - f_m) - \frac{V_m}{2} cos2\pi t(f_C + f_m). \quad (5)$$

From equation (5) we can see that the frequency **spectrum** for an AM signal will present three components. The **carrier** component at f_C and **two sidebands**, "upper" and "lower" separated from the carrier at the modulating frequency f_m as it can be seen in Figure 3.

An important concept about the amplitude modulation is the **modulation index** [9]**,** also called modulation depth when expressed in percentage form. This index gives us an idea of how much the carrier amplitude is being changed from its original one. It will play a key role for the AM power measurement as seen in equation (8).

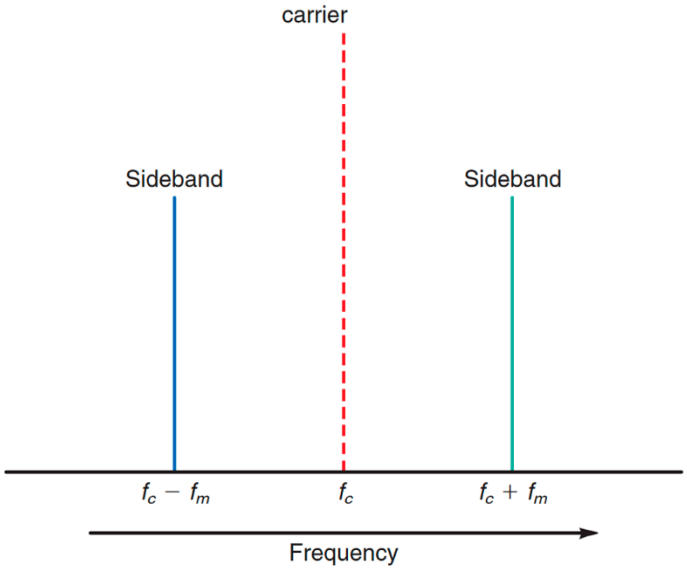

Figure 3 AM spectrum for a carrier with frequency f_c and a modulating signal with frequency f_m. Adapted from [9].

Taking Figure 4 as a reference, modulation index can be calculated from the time-domain waveform as

$$m = \frac{V_{max} - V_{min}}{V_{max} + V_{min}} \tag{6}$$

where m is the modulation index.

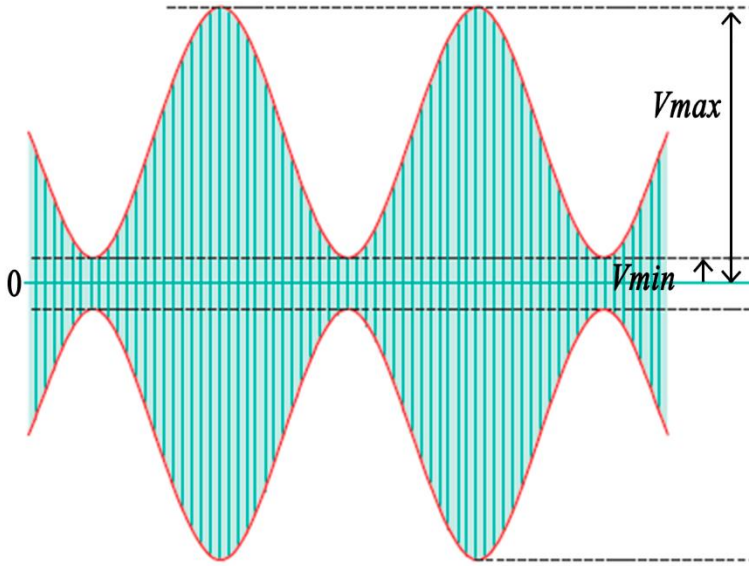

Figure 4 AM signal example with modulation index parameters. Adapted from [9].

2.2 Power efficiency

Power efficiency in electronic devices can be considered as the relation between the output power delivered by the device (i.e. output power for the AM signal) and the DC power consumption [10]–[13]

$$P_{eff} = \frac{P_{out}}{P_{DC}} = \frac{P_{out}}{VI} \tag{7}$$

where P_{eff} is the power efficiency, P_{out} is the output signal power, P_{DC} is the DC power consumption of the device, V is the DC voltage supply, and I is the DC current consumption of the device.

For the AM transmitter case, it can be shown that **AM power** is calculated using the carrier power and the modulation index information [9] as

$$P_{AM} = P_C\left(1 + \frac{m^2}{2}\right) \tag{8}$$

where P_{AM} is the AM power, P_C is the carrier power and m is the modulation index. According to this, power efficiency for the AM transmitter may be calculated as

$$P_{effAM} = \frac{P_{AM}}{P_{DC}} = \frac{P_C\left(1 + \frac{m^2}{2}\right)}{VI} \tag{9}$$

where P_{effAM} is the power efficiency of the AM transmitter. It is important to notice at this point that even when the efficiency is high, the power consumption may also be high. In order to design a low-power transmitter, efficiency will not be the most important parameter, but the DC current sourced from the battery. In the same way, efficiency itself does not provide information about the output power requirements.

2.3 Feedback Oscillators

As we saw in the transmitter diagram in Figure 1, the carrier signal for the AM transmitter is generated in an oscillator block. Feedback oscillator theory [14], [15] shows us that they are composed by an amplifier block and a feedback block forming a signal loop as shown in Figure 5. ***A* is the voltage gain of the amplifier** and ***β* is the attenuation of the feedback network**, usually called feedback factor in some oscillator schemes. V_o is the oscillation signal at the output of the oscillator, and V_f is the feedback signal closing the loop.

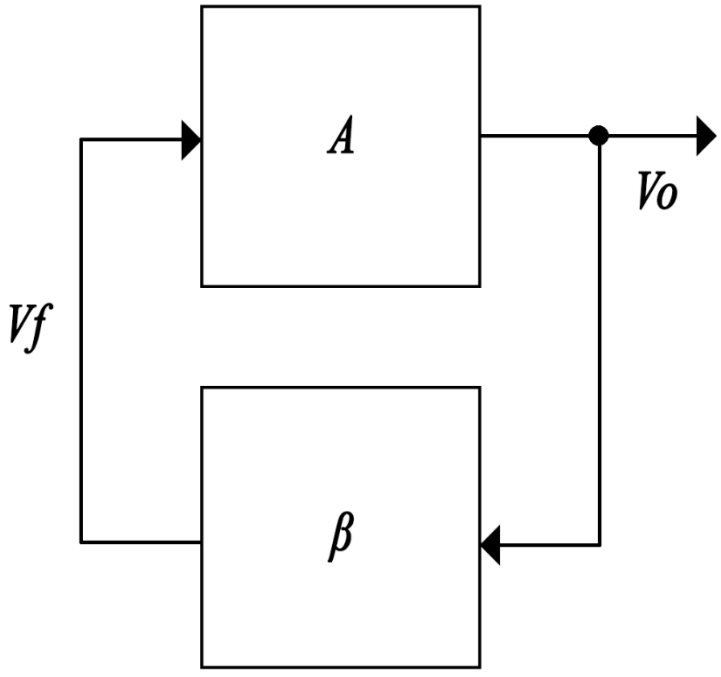

Figure 5 Feedback oscillator block diagram. Amplifier block (top) and feedback network (bottom).

Barkhausen Criteria [16], [17] states two **necessary conditions** for stability in oscillators:

1. **Amplitude condition**. Loop gain |G| = |A|·|β| = 1. Lower gain would result on attenuation of the oscillations, and higher gain may produce an unstable behavior. In simple oscillators without trigger input signals, gain must be initially over 1 so that the circuit could start oscillating by amplifying the background noise [18].
2. **Phase condition**. Loop phase shift has to be integer multiple of 360º (or 0º). In most cases, this phase shift is achieved by combining an inverting amplifier (that has 180º phase shift) and a phase-shift network such a resonator circuit. This phase-shift circuit includes the additional 180º shift required for the phase condition.

   LC resonators are used for this task in Colpitts and Clapp designs. Their tank circuits resonate at the oscillation frequency, filtering other undesired frequencies. Another common and stable option is the use of a piezoelectric crystal as a mechanical resonator.

An important parameter of oscillators is the **frequency stability**. It is defined as the random variations of the oscillation frequency over time, and they are usually separated in long-term and short-term instabilities [19]–[21].

- **Long-term instabilities** affect the oscillation frequency over time by progressive changing it because of temperature or aging effects.
- **Short-term instabilities** affect the instantaneous oscillation frequency, which will always slightly vary around the desired frequency.

This thesis project will pay special attention to short-term instabilities, because they should remain small enough so that the AM signal can be successfully transmitted and received. The variations in frequency are usually measured in Part Per Million (PPM), as the ratio between the variation in Hz and the operating frequency in MHz.

2.3.1 Colpitts oscillator

This oscillator scheme [19], [22] is based on an **LC resonator** [23], [24] tank circuit in the feedback loop. Figure 6 shows the schematic of basic Colpitts oscillator. Two capacitors C_1 and C_2 create the capacitive voltage divider that provides feedback to the amplifying step. An inductor is placed with them to create a resonator. The resonator induces 180º phase shift, while filtering frequencies other than the resonance frequency. The oscillation frequency is determined by the resonance as

$$f_r = \frac{1}{2\pi\sqrt{L_1 C_T}} \tag{10}$$

where L_1 is the inductance of the inductor and C_T is the series capacitance of C_1 and C_2

$$C_T = \frac{C_1 C_2}{C_1 + C_2}. \tag{11}$$

Feedback ratio β or feedback factor [19] is calculated in Colpitts oscillators as the ratio between C_2 and C_1, corresponding to the attenuation of the in the feedback network. This factor has to be took into account to make the oscillator meet the amplitude condition as defined in Chapter 2.3.

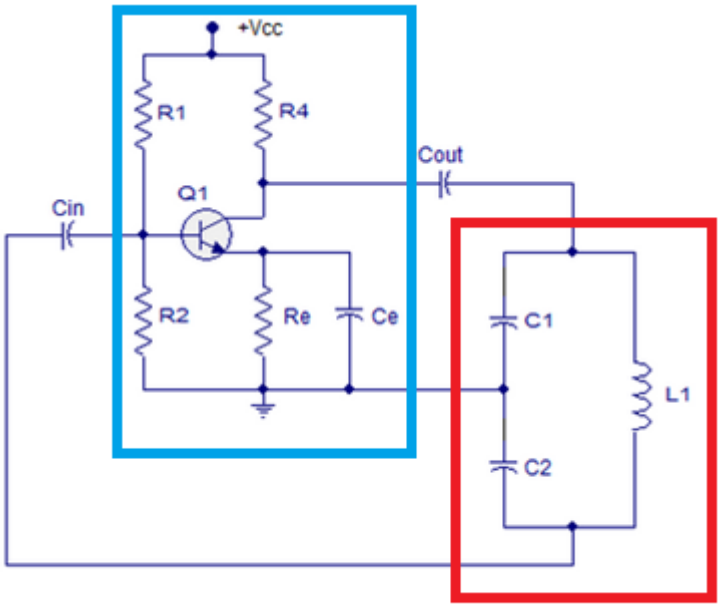

Figure 6 Example of a schematic for a Colpitts Oscillator. Feedback tank circuit in the right side (red) and inverting amplifier in the left side (blue). Adapted from [22].

2.3.2 Clapp oscillator

Colpitts' oscillation frequency is often affected by the stray capacitances of the amplifier. Clapp [19], [25] design is an enhanced version in which an **additional capacitor** C_S is placed in series with the inductor.

Oscillation frequency can be calculated using the same equation (10) as in the Colpitts case, but now considering also the effect of the C_S in the calculation of C_T. The capacitance for the series capacitor C_S is usually much lower than the others, so that the oscillation frequency will be mostly determined by its value. Frequency stability is higher because the value of the series capacitor is not affected by the stray capacitances of the amplifying step. [25]

Using a variable capacitor for C_S is a common technique for designing tunable frequency oscillators, since the oscillation frequency will mainly depend on this capacitance. Nevertheless, in this thesis project the oscillator has been designed with a single-fixed oscillation frequency.

2.3.3 Crystal oscillator

Piezoelectric materials such as **quartz crystals** can be used for oscillator design [26], [27] as the core of the feedback circuits. A piece of crystal is placed between electrodes, so that when an electric field is applied, the piezoelectric material reacts by generating a mechanical vibration.

The frequency of this vibration can be controlled by tailoring the physical dimensions of the crystal during the manufacturing process. A quartz crystal can replace an LCR resonator with the electrical equivalent circuit shown in Figure 7. The values of the components in the equivalent circuit may be found in the datasheet of the crystal, but the information varies depending on the manufacturer.

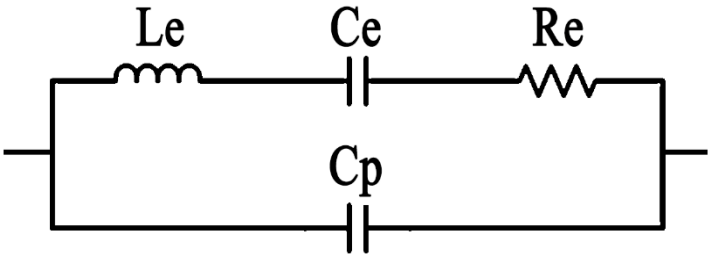

Figure 7 Quartz Crystal electrical equivalent circuit.

Crystal oscillators present a very stable oscillation frequency and they are widely used in the industry [26]. The fundamental resonant frequency f_o increases when decreasing the thickness of the crystal, and this implies a limitation in the highest f_o. Manufacturers offer crystals with different f_o, from several kHz up to 30 MHz. Crystals can be operated also with their overtones up to 250 MHz [19], [26].

One of the simplest schematics for a crystal oscillator is the Pierce oscillator. The schematic for the Pierce oscillator [19] looks exactly as the LC Colpitts oscillator as it can be seen in Figure 8, just replacing the series inductor with the quartz crystal (*XTAL*). The feedback ratio is defined approximately as $\beta = C2/C1$ as in the LC cases commented, and the frequency of oscillation will depend on the crystal.

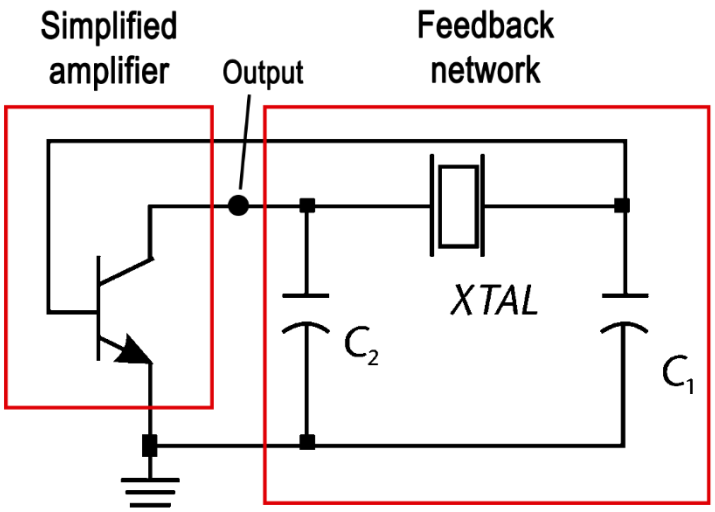

Figure 8 Pierce Crystal oscillator schematic. Adapted from [19].

According to [19], the Pierce oscillator meets the amplitude condition when

$$\frac{g_m}{\omega_o^2 R_e C_1 C_2} > 1, \tag{12}$$

where g_m is the transconductance of the transistor, ω_o is the working angular frequency, and R_e is the equivalent series resistance of the quartz crystal.

3. METHODS AND PROCEDURES FOR THE OPTIMIZATION PROCESS

This chapter describes the different working procedures, methods and setups used in the transmitter optimization process.

3.1 Optimization methodology

Optimization of electronics devices may be approached from many different points of view. For this basic AM transmitter, the optimization process has followed several steps:

1. **Identification of the optimization goals**. Before to start working on the optimization itself, the project objectives, restrictions and requirements must be set. Taking into account the didactical purpose for the optimized AM transmitter, every modification or improvement implemented on the transmitter schematic has to be oriented to clarify the transmitter behavior.
   Reduced power consumption, small size and enhanced usability are also considered optimization goals. They should improve the quality of the final device to be used as a demonstration for future RF students.
2. **Analysis of the original AM transmitter**. Qualitative studies, theoretical and mathematical calculations provide the first point of view in the study of the original transmitter. Simulations and prototyping give additional information about the performance of the schematic of the transmitter.
   The objective of this step is to find the weakest points in the schematic design so that they could be optimized. Low performance and unclear or complex blocks are detected, so that they can be modified afterwards.
3. **Implementation of modifications on the schematic.** Iterative cycles of simulation and prototyping are used to modify the transmitter schematic. Several trade-offs typically rise when doing modifications. The original objectives have to be present in order to decide what results can be accepted as an optimized result.
   The antenna has not been considered as a part of the transmitter during this thesis project. Since the antenna characteristics may be important when doing some design choices, we have assumed in all cases a 50-ohm impedance antenna for the carrier frequency.
4. **Miniaturization and usability design.** This last step focuses on the printed circuit board (PCB) design and fabrication. The result is a small form-factor and user-friendly interface for the demonstration device. Package design has been included to improve the usability and reliability of the final device.

3.1.1 Simulations

Circuit simulation software allow us to have a first idea of the circuit behavior. Because of its good RF simulation and design characteristics [28], [29], **Advanced Design System** (ADS) software from Keysight has been used for all the simulation and PCB design tasks in this project.

Simulations have been done generally **using ideal components**. The results obtained from them could be used then as a rough approximation to the real circuit behavior.

In all cases, the microphone input signal has been simulated as a single frequency sinusoidal wave. On the other hand, the carrier signal coming from the quart-crystal oscillator module has been created as a single frequency signal.

In most cases the simulations executed have been **Transient**, **DC point** and **Harmonic Balance** to obtain results providing information about power, waveforms and frequency. The original transmitter, as well as the optimized prototypes, have been simulated in this way.

3.1.2 Measurements setup

Breadboard [30] **prototypes** of the original transmitter and the improved version have been built and tested, using discrete through-hole (TH) components.

Time-domain measurements have been done following a **path-analysis**. Different points in the paths of the signals have been measured for checking their characteristics (amplitude, noise, waveform…). Figure 9 highlights the key points tested on a block diagram.

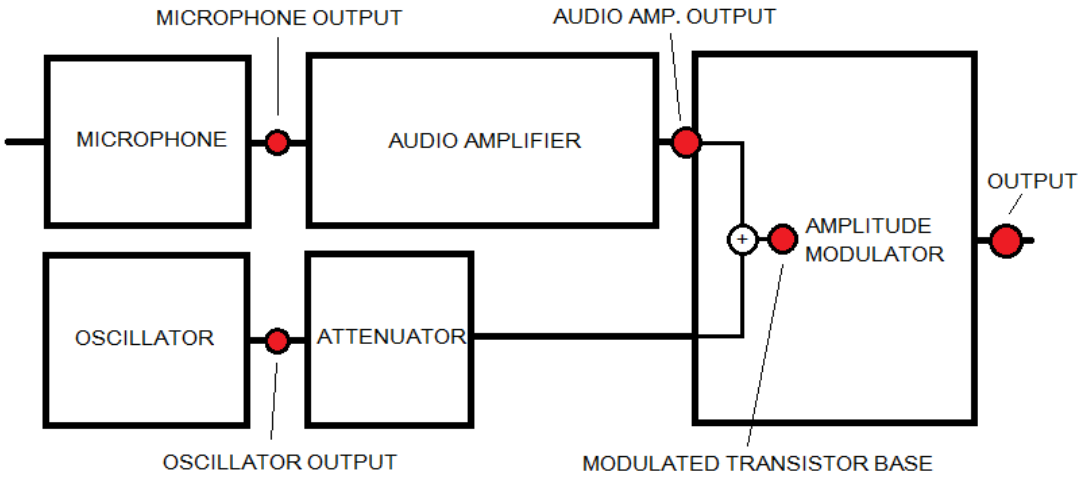

Figure 9 Blocks diagram of the transmitter with path-analysis points highlighted.

Figure 10 shows a block diagram of the measurements setup used for time-domain testing. The speaker has been placed at approximately 3 cm from the microphone. The speaker transduces to an acoustic wave the sinusoidal signal coming from the waveform generator.

An oscilloscope has been used to measure the different voltages and waveforms in the circuit. Batteries are replaced during the tests by a DC Power Supply, supplying 4.5 V and a 50 mA current limit to protect the circuit from short-circuits or placement mistakes.

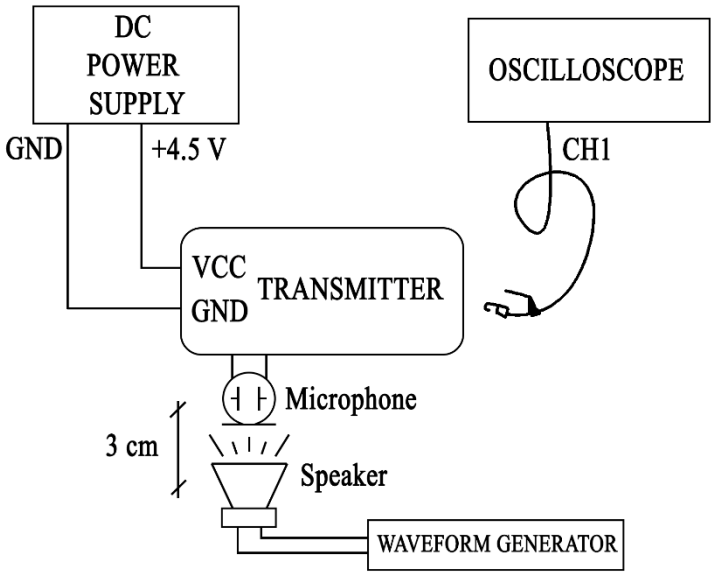

Figure 10 Time-domain measurements setup.

The **speaker** used for the measurements is a round-shaped 35 mm diameter speaker with 21.4 Ω output impedance at DC. See Figure 11.

Figure 11 Speaker top (left) and bottom (right) views.

For the **frequency-domain** measurements, the same setup has been used except for the measurement device. A spectrum analyzer has replaced the oscilloscope. Oscillation and modulated **frequencies**, signal-to-noise ratio (**C/N)**, AM **modulation depth** and AM **power** measurements have been done using this setup.

Additionally, several **multimeters** connected in parallel or series have been used for DC voltage and current measurements.

A **standard 4 kHz** sinusoidal signal generated with the waveform generator with **3 Vpp** amplitude and 0 V offset has been used as a **reference for comparisons**. See Figure 12. This frequency has been selected because it is included in the human voice spectrum, and both the speaker and the microphone can work with it. Even when most of the normal speech spectrum is below 4 kHz, spectrum of singing voices has also a high 3-4 kHz component [31], and the human hearing is more sensitive to the range of 4-5 kHz [32].

The transmitter response will depend highly of the input signal, so the results may be very different depending on the audio waveform, the volume, or the distance of the speaker from the microphone. This standard sine wave helps us to compare quantitatively the different versions of the AM transmitter by using the same sample signal.

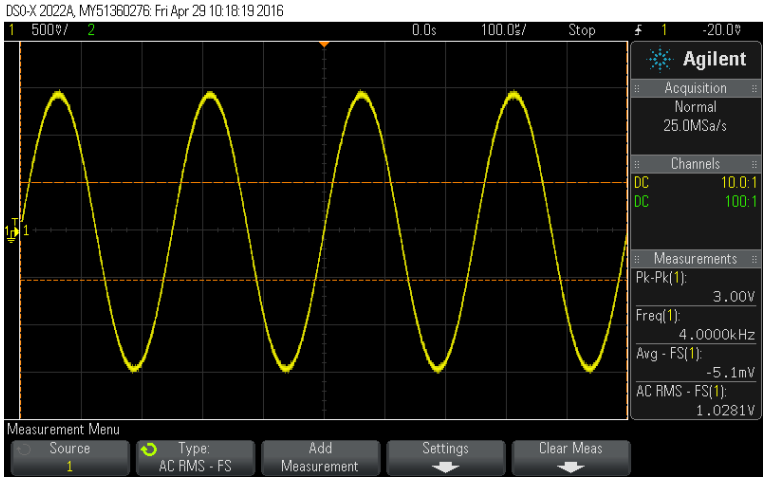

Figure 12 Preview of 4 kHz 3 Vpp sinusoidal reference signal.

All the laboratory **equipment** used in the measurements setup is included in Appendix 1.

3.1.3 Field testing

An important task in the characterization of this transmitter is the field test. In this case, field testing has been done using a **dipole antenna** and a real radio receiver. It has been done outdoors.

The objective is getting an approximate measurement of the **distance reached** by the AM transmission. We can also check if the **frequency stability** is enough to ensure the

reception. In addition to that, we check that the audio transmitted (i.e. voice) can be recognized.

3.2 PCB design methodology

ADS is used also for the **PCB design** of the final optimized schematic. The design process followed several steps:

1. Define the Surface Mount Device (SMD) and TH components to be used and draw the **final circuit schematic** based on the previous analysis and prototypes.
2. Select or create the **footprints** for every component used.
3. Import the circuit **connections** from the ADS schematic. Place every footprint and label them according to the schematic, keeping the board size as small as possible. SMD components should remain in the traces layer, while TH components may be placed in the opposite one.
4. **Trace** every connection trying to keep them in the same layer. A **common ground plane** is placed in the opposite layer. Trace width has been defined as 0.5 mm for ensuring a good manual fabrication. Taking into account that the maximum current in the circuit will be under 40 mA, this width is high enough for the power requirements of the circuit [33].
   Traces shall remain as short as possible to avoid radiation losses or interferences. Since the wavelength for the HF carrier will be around 16 m, keeping them under 16 cm long should be enough for discounting the radiation effects.
5. Place **vias** [34] to connect the required traces and components from the top layer to the ground plane. For matching to the drill sizes available in the workshop, vias have been defined with 1 mm diameter.
6. Check the **connectivity** of every node.

3.3 Fabrication methodology

The fabrication of the final PCB transmitter has been carried out manually using the different resources available at TUT. A double-sided photoresist circuit board has been used as substrate. An ultraviolet-light exposure unit has been used for the **exposure** step. Appendix 2 includes more information about the fabrication process.

4. BASIC AM TRANSMITTER ANALYSIS

This chapter will analyze and explain the **basic AM transmitter** functioning, as a starting point for the next optimization steps. Qualitative analysis together with **simulation** results and **prototype** measurements will show the transmitter behavior.

4.1 Schematic and block diagram description

Figure 13 includes the **original schematic** for the AM transmitter used during the RF course. We can define some different blocks with their respective purposes.

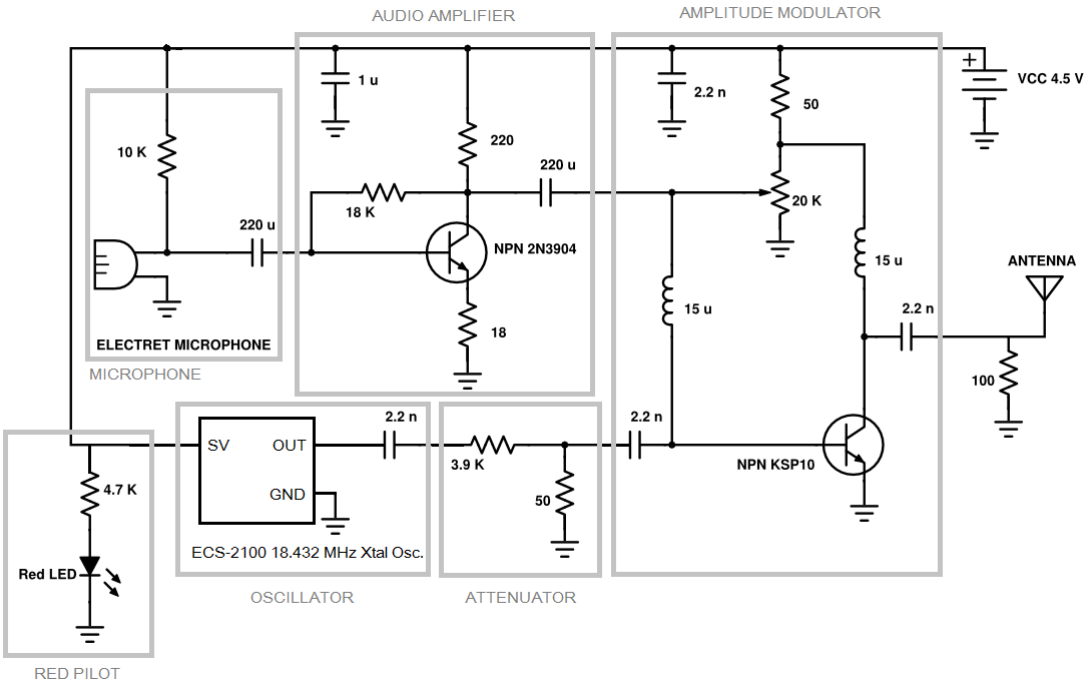

Figure 13 Original basic AM transmitter schematic.

Audio signal is received and converted into an electrical signal by an electret **microphone**, in the top left of the figure.

That electrical signal, which contains the information of the audio we want to transmit, is amplified by the **audio amplifier** block.

After being amplified, the signal is used to modify the instantaneous bias point in the **amplitude modulator.** This modification of the bias point changes the output amplitude of the carrier signal at the collector node. This carrier is generated in the **crystal oscillator** module and **attenuated** to fit into the modulator levels.

By doing that, the transistor is generating an **amplitude modulated** (AM) signal containing the audio information, which is connected to the antenna for being sent as electromagnetic radiation. The next subchapters will explain in more detail all of these blocks.

4.1.1 Microphone block

The **electret microphone** [35], which has two pins, is connected to the ground and to the output node that will be used as an input for the audio amplifier. This node also receives the power supply from the 4.5 V battery through a 10 kΩ resistor. It generates an electric audio signal according to acoustic signals received between approximately 50 Hz and 16 kHz according to the datasheet.

Electret microphones do not really require power supply to work [36], [37], since they have been prepolarized and they can work during many years on their own. Nevertheless, the electret microphone module contains usually a FET amplifier that requires some power supply, and it is the reason for the 10 kΩ bias resistor providing a supply path from the battery. As a result, the DC point at the microphone output is around **2.4 V**.

4.1.2 Audio Amplifier block

The acquired audio signal is amplified using a **Class A common-emitter Bipolar Junction Transistor (BJT) amplifier** [38], [39] based on a 2N3904 BJT [40]. A collector resistor R_C and a collector-base resistor R_{CB} are used for setting the bias point of the transistor, and this DC component is separated from the RF signal in the input and output points of the amplifier block using coupling capacitors (also known as "DC blocks") [41].

The amplifier gain can be calculated approximately, without any load [42], by

$$G \approx \frac{-R_C}{R_E} = \frac{-240}{18} = -13.3 \tag{13}$$

where G is the gain, R_C is the collector resistor and R_E is the emitter resistor. See Figure 12. This equation is valid only if R_E exists, otherwise the gain must be calculated then by using the small signal model of the BJT, and it will depend on the transistor parameters. Gain may be increased by removing this resistor of by adding a bypass capacitor for the AC component.

Since the gain is negative, we can appreciate that it is working as an **inverting amplifier** with around 22.5 dB gain and 180º phase shift.

Figure 14 represents the ADS schematic used for the Audio Amplifier simulation. In this case, the audio amplitude is 20 mVpp, and the frequency is 15 kHz, which allow us to do fast simulations and it is within the microphone frequency limits.

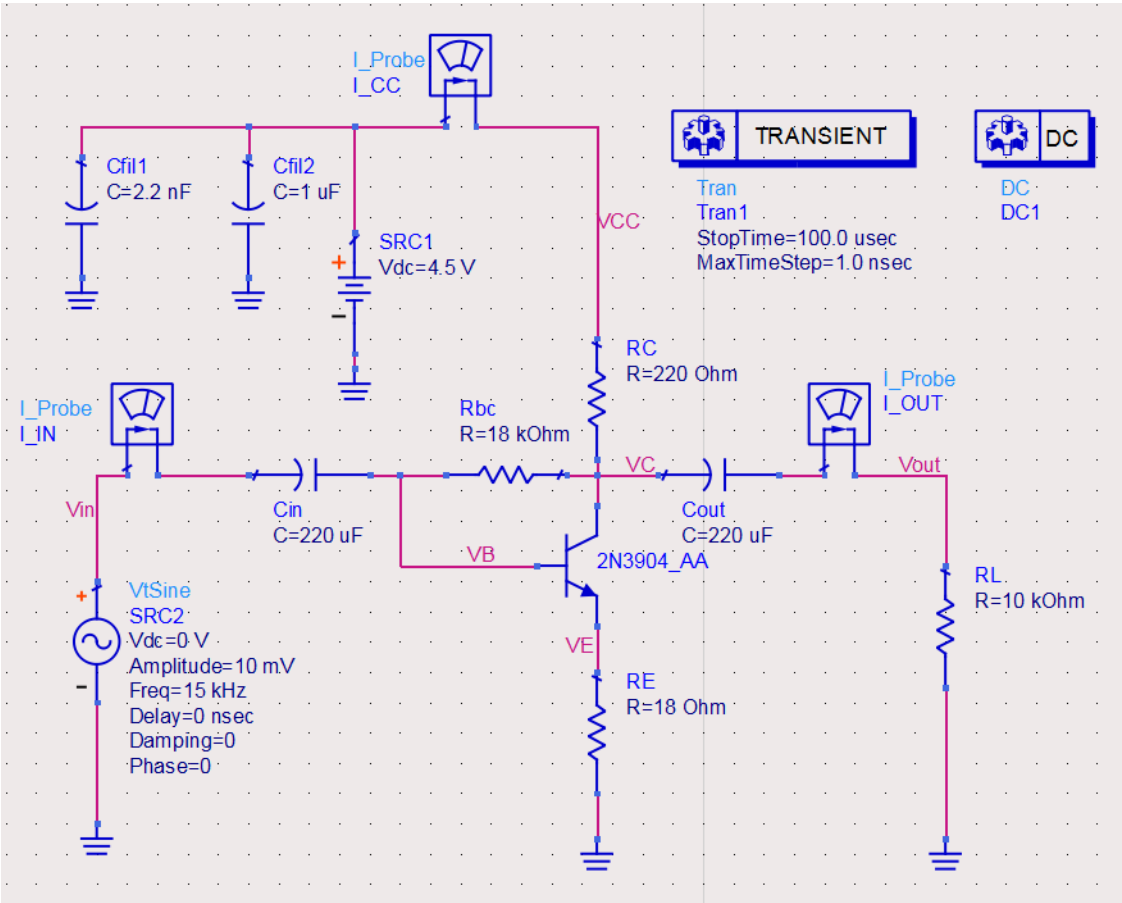

Figure 14 Schematic in ADS for the audio amplifier simulations.

The DC analysis provides the different biasing levels for the BJT. As it can be seen in Figure 14, DC voltages for the base (VB), collector (VC) and emitter (VE) of the BJT have been calculated. Table 1 shows their values during the simulation.

The transient analysis allows us to see the time-domain waveforms shown in Figure 15 and to calculate the gain of the amplifier.

Table 1 Audio amplifier simulation DC points.

	VB	VC	VE	VBE
Voltage (DC)	919.6 mV	2.089 V	197.2 mV	722.4 mV

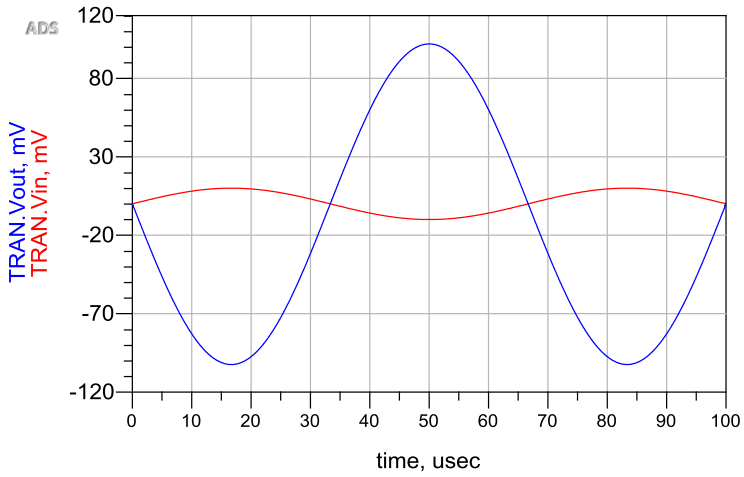

Figure 15 Audio input (red) and audio output (blue) signals from the audio amplifier simulation results.

As it is shown, the output amplitude (blue) is higher than the input signal amplitude (red). The waveform remains very similar, so the amplifier is working linearly. Note that it is inverted, and the gain has been calculated as -10.219, which is a bit lower than the theoretical approximation. This is because the audio amplifier is working now with a 10 kΩ resistive load at the output that produces a little gain decrease. The lower the load resistance, the lower will be the gain. This it because the gain is affected by the load [42] approximately according to

$$G \approx \frac{-R_C \,//\, R_L}{R_E} \tag{14}$$

where R_L is the load resistance. However, this is a rough approximation since the resulting gain from equation (14) would be around -12 by using the components from Figure 14. Equation (14) is valid only when the resistance of the load is much higher than the output resistance of the circuit [42]. The real gain has certain limitations that are not considered in (14), depending on the output resistance and the g_m of the BJT.

4.1.3 Crystal Oscillator block

An ECS-2100 **crystal oscillator** module [43] generates the constant 18.432 MHz carrier signal required for the AM modulation. This module just needs the 4.5 V supply as an input and a ground connection for generating the 18 MHz output, which will be switching from 0 V to approximately 4.5 V. This block includes also a coupling capacitor at the output for filtering any DC component, so that the signal will be used as a symmetric square wave with 2.25 V amplitude.

Nevertheless, the oscillation is not a perfect square wave by far. We can see from the oscilloscope capture that the waveform presents several underdamping peaks on every switch, giving as a result a much higher peak-to-peak measurement. See Figure 16.

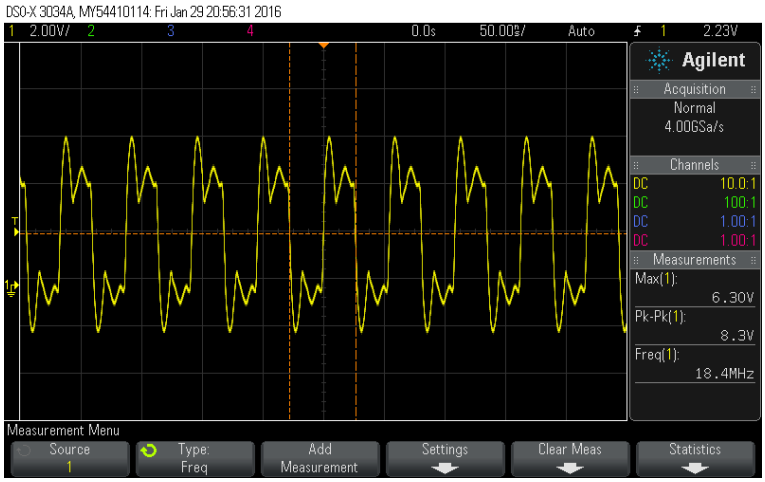

Figure 16 ECS-2100 crystal oscillator module output with 4.5 V supply. Scale: 2.00 V/division vert. 50.00 ms/division horiz.

Without any load, the **current consumption** for this oscillator with 4.5 V is **5 mA.**

4.1.4 Attenuator block

This block is a simple **voltage divider** [44] used to lower the amplitude of the carrier. Two resistors divide the input signal in a factor of 79, so that for a 4.5 Vpp input signal we will have around 57 mVpp output signal. This base amplitude, in addition to the bias voltage, will be low enough for not saturating the BJT.

4.1.5 Amplitude Modulator block

The Amplitude Modulation is performed using another **common-emitter BJT amplifier** working as a **modulated-gain amplifier**. It is based on a KSP10 [45] BJT, different from the transistor used in the audio amplifier.

In this case, both audio and carrier signals are applied to the base. The biasing circuit is selected so that the initial collector current is around 4 mA, adjusting the potentiometer. The variations in the audio amplitude make the instantaneous bias point in the base to change, so the collector current changes and the transistor gain is varying according to the audio waveform. The 18 MHz carrier is getting amplified this way, producing the **AM output signal** at the collector node.

Coupling capacitors are used again for separating the DC component from the AC components. Two RF chokes [46], [47] of 15 µH are preventing the carrier signal from affecting the biasing circuit. RF chokes provide a high impedance for the 18 MHz signal as

$$Z_{18M} = j\omega L = j2\pi \cdot 18 \cdot 10^6 \cdot 15 \cdot 10^{-6} = j1696.46\ \Omega \qquad (15)$$

while the impedance for the audio signal (~16 kHz maximum) is much lower as

$$Z_{16k} = j\omega L = j2\pi \cdot 20 \cdot 10^3 \cdot 15 \cdot 10^{-6} = j1.885\ \Omega\,. \qquad (16)$$

The 100 Ω resistor (*Rstab*) at the output has the purpose of stabilize the modulator. On the other hand, this resistor is working as a shunt connection at the output and it is dissipating a certain amount of power that will not reach the antenna.

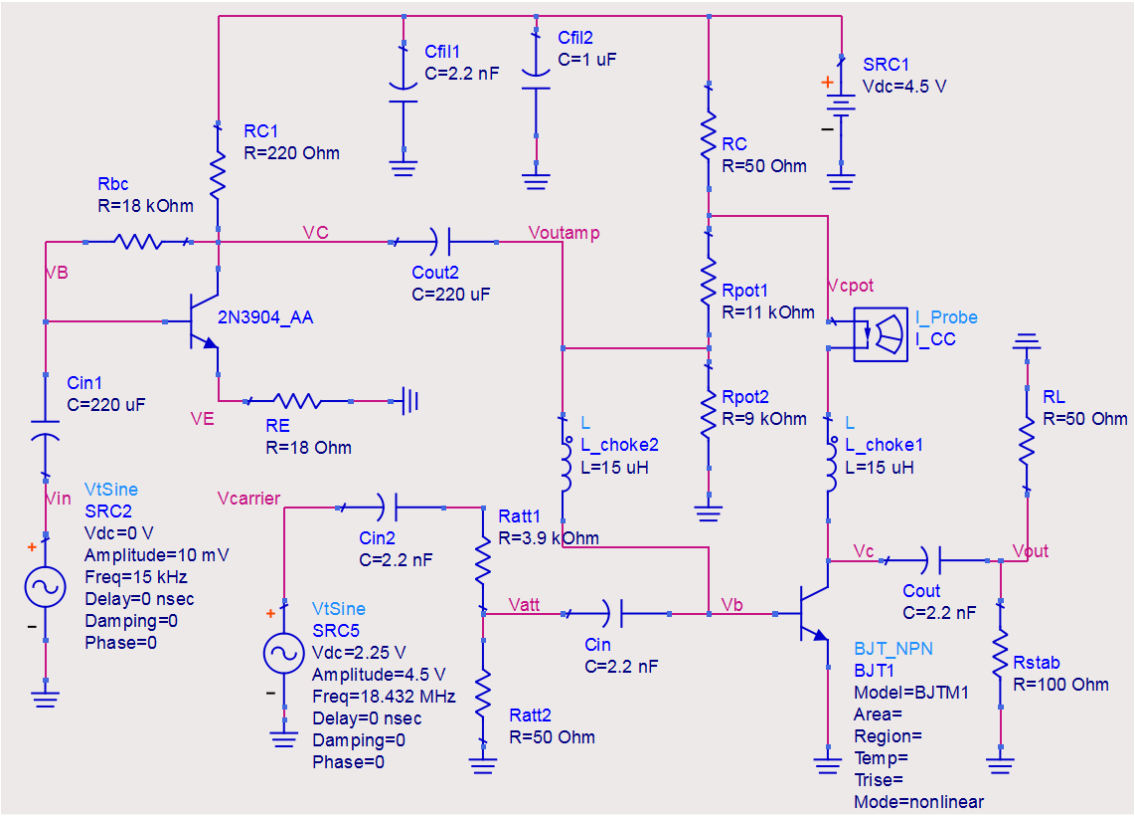

Figure 17 ADS schematic for the original basic AM transmitter.

For the simulations of this transmitter, the audio amplifier output is connected to the audio input for the amplitude modulator as seen in Figure 17. The audio input is a 20 mVpp sinusoidal wave, while the crystal oscillator has been replaced by an 18.432 MHz signal generator with 4.5 Vpp.

Figure 18 shows the output voltage obtained in the transient simulation. The envelope of the output waveform is sinusoidal, according to the AM theory.

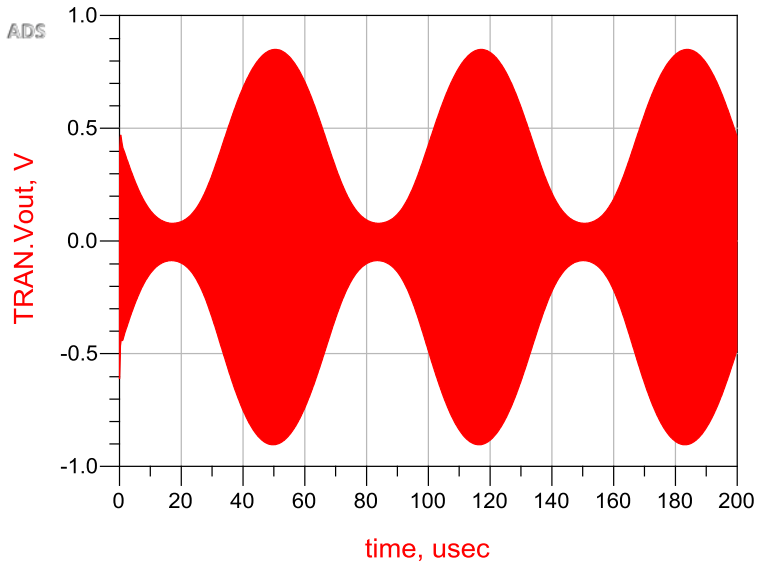

Figure 18 AM signal (red) from the original basic AM transmitter simulations. 15 kHz audio input and 18.432 MHz carrier.

On the other hand, the amplitude modulator circuit is loading the output of the audio amplifier, affecting its behavior. Now, the output of the amplifier in Figure 17 (blue) appears distorted and very different as in the simulations in Chapter 4.1.2. The higher cycles of the output signal are much smaller than the lower cycles, and some high-frequency noise coming from the carrier signal. In this case, the gain of the amplifier is much lower than in the previous simulations: about 7 for the upper cycles and 3.5 for the lower. Farther discussion about the source and analysis of this non-linearity in the audio amplifier can be seen in Appendix 3.

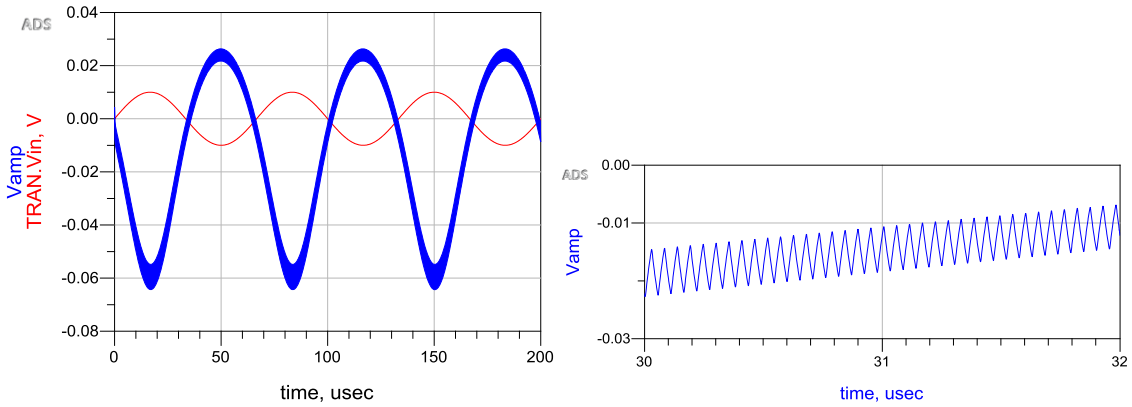

Figure 19 Audio input (red) and audio output (blue, left) signals from the original basic AM transmitter simulations. Zoomed/in view of high-frequency noise (blue, right) at the output of the audio amplifier.

When the amplitude of the input signal is higher (i.e. 40 mVpp from the microphone), the AM signal at the output gets distorted. The amplitude modulator works in the saturation region and the output signal shows little “valleys” in the peak positions, so the waveform envelope does not follow the sinusoidal input anymore.

On the other hand, when the input levels are lower (e.g. 10 mVpp) the BJT works correctly in the linear region. In a real scenario, the audio levels from microphone will not usually go over 20 mVpp according to voice tests with the microphone. The microphone was tested by measuring the output, talking from different distances at normal speech volume. Only in extreme cases, when speaking loudly and very close to the microphone (less than 2 cm), the output increased further up to 30 - 35 mVpp.

In normal cases, the amplifier will remain then in the linear region and the output will be less distorted. Of course ultimately, input amplitude will always depend on the source of the sound, and its distance from the microphone.

Power efficiencies of the audio amplifier and the amplitude modulator are **very low**. Because of this, the overall efficiency of the device is very low as it can be seen in Table 2. These power efficiencies will depend also on the input signal, but this case shows an approximation of the normal use case efficiencies using the 20 mVpp input.

Table 2 Power efficiency simulations for the basic AM transmitter.

Amplitude Modulator efficiency	Total efficiency
14.693%	9.929%

Nevertheless, these simulation results are **very optimistic** compared with the measurements of the real device shown in the following subchapter. Additionally, the oscillator current consumption has not been taken into account in these simulations, so that the real efficiency will be consequently lower.

4.2 Basic transmitter prototype

Figure 20 presents the breadboard prototype layout, highlighting the distribution of the blocks seen in Figure 13.

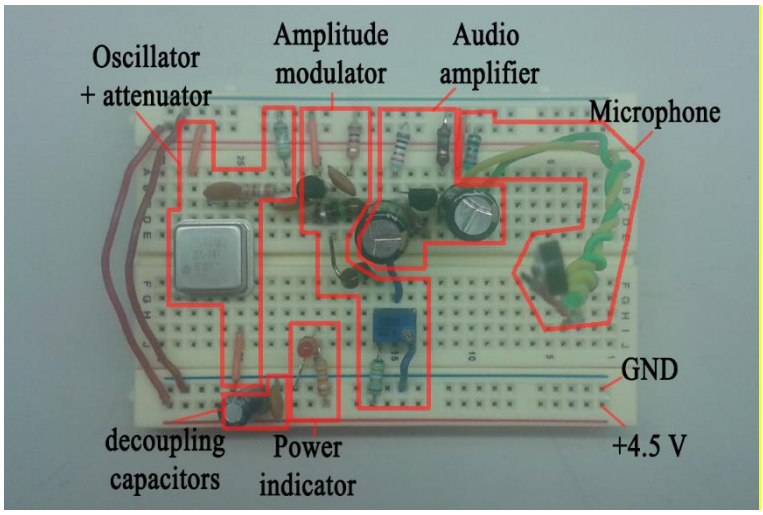

Figure 20 Breadboard prototype for the original basic AM transmitter.

4.2.1 Silence scenario

As an initial scenario, we test the behavior of the transmitter without any input signal from the microphone (**silence scenario**). The amplitude modulator must work in this case as a **constant gain amplifier** for the carrier signal, as it can be seen in the Figure 21 from the oscilloscope. This is because there is not any modulating signal to modify the amplitude of the carrier,

The 18.432 MHz signal is amplified from some 60 mVpp to around 1.1 Vpp, and there is not any amplitude modulation, as one can expect. Looking at the audio amplifier output, we see that there is certain **high-frequency noise** at 18.4 MHz, coming from the carrier signal. This high-frequency noise goes through the common ground and supply paths to the other blocks of the circuit. It can be measured even in the microphone output, so that it is being amplified together with the audio from the microphone. This fact makes the first blocks to work with a very noisy audio signal.

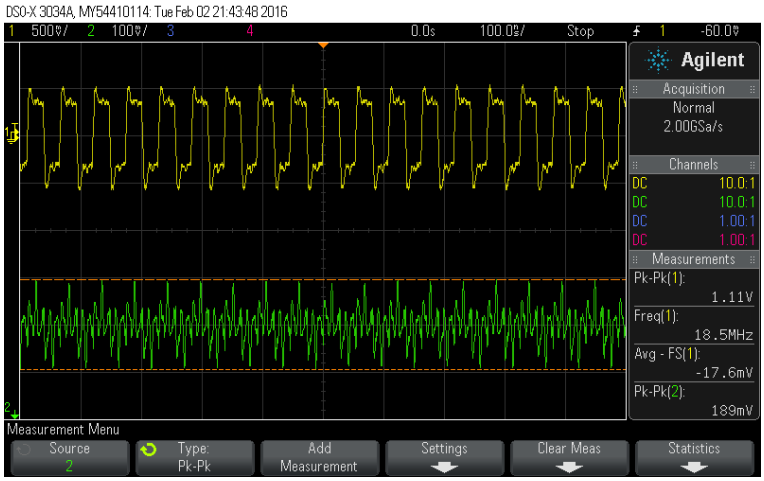

Figure 21 Original basic AM transmitter output (yellow) and audio amplifier output (green) from silence scenario measurements.
Scale: 5.00 V/division vert. 100.00 ms/division horiz.

4.2.2 Audio inputs scenario

After measuring the output without any input signal from the microphone, we test the performance of the transmitter with **different audio inputs**, so that the expected AM output may be observed.

Figure 22 shows the response of the system to a whistle in the microphone. The waveform envelope seems to be very similar to a sinusoidal wave.

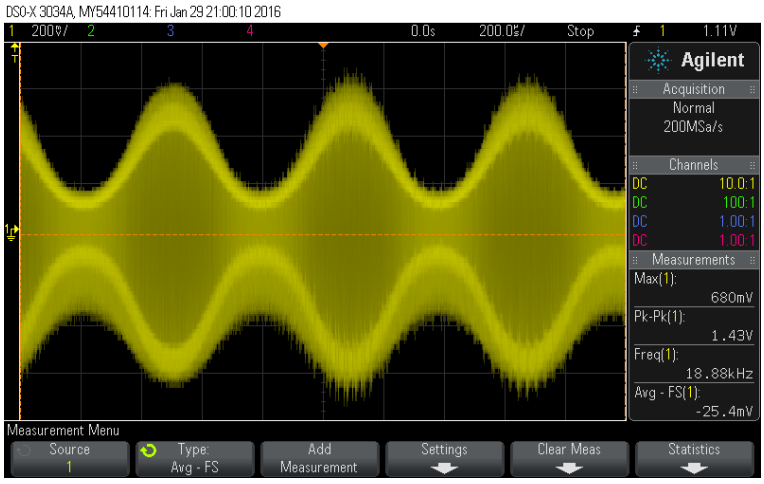

Figure 22 Original basic AM transmitter output AM signal from a whistle-input measurement. Scale: 200.00 mV/division vert. 200.00 ms/division horiz.

The next step is using the speaker shown in the setup diagram seen in Figure 10. Using the waveform generator, we produce different audio tones of constant frequency. Figure 23 shows the output response for a 3 kHz tone and a 7 kHz tone, where the sinusoidal waveform can be easily seen as the **envelope of the carrier signal**.

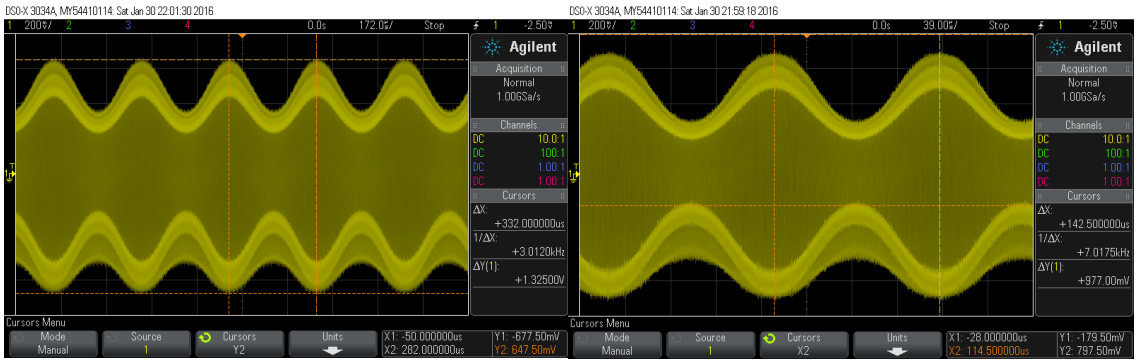

Figure 23 Original basic AM transmitter output AM signals from 3 kHz (left) and 7 kHz (right) input measurements. Scale: 200.00 mV/division vert. (both) 172.00 ms/division horiz. (left) 39.00 ms/division horiz. (right).

It can be seen that the maximum amplitude of the AM signal is around 1.3 V, and this amplitude is approximately the same for different frequencies. The modulation is not completely perfect: we can see little differences between half cycles. The signal presents also different amplitude levels (the different bright-yellow sinusoidal lines inside the waveform in Figure 23) corresponding to the peaks present on the waveform of the carrier from Figure 21.

The input levels for the audio signal and the carrier are critical to make the modulator work properly. The biasing of the BJT has to be taken into account to adjust the gain. This is done by modifying the ratio in the potentiometer. Recommended values are summarized in Table 3.

Table 3 Recommended settings for the amplitude modulator.

***Voutamp* – audio input**	100 - 150 mVpp
***Vatt* – carrier input**	50 – 70 mVpp
I_{RC} – DC current through R_C	4 – 5 mA

4.2.3 Frequency response and field testing

The last point to analyze from the basic AM transmitter is the frequency response. Following the measurements setup described in Chapter 3.1.2, we proceed using a spectrum analyzer. The **C/N** measured with the carrier is about **65 dB**. This measurement depends of the spectrum analyzer, and the C/N will be used to compare this transmitter with improved versions, measured in the same way. The **first harmonic distortion** power P_{HD} [48] is **22.5 dBc** as it can be seen in Figure 24.

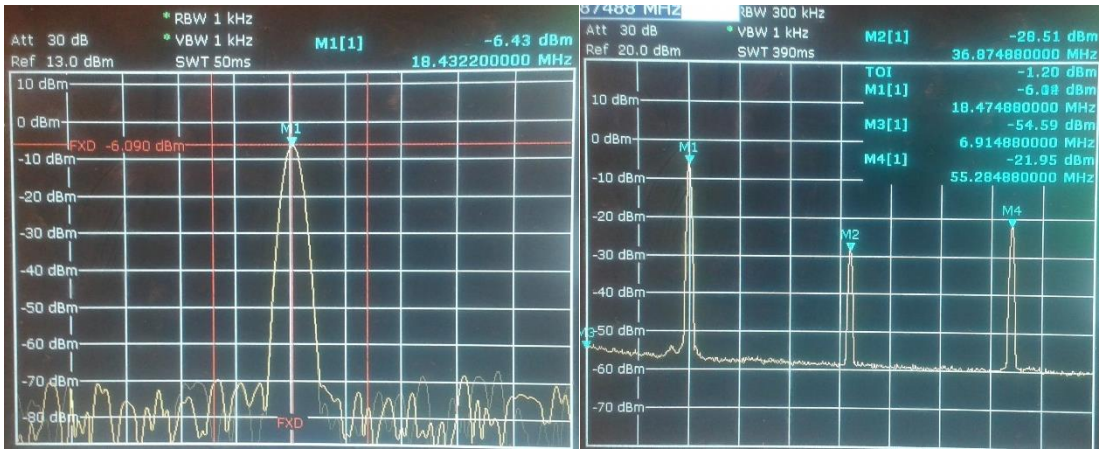

Figure 24 Original basic AM transmitter C/N (left) and P_{HD} (right) measurements.

By using the 4 kHz tone (described in Chapter 3.1.2) to measure the modulation depth, we can calculate the output AM power. Taking into account the DC power consumption, we can calculate the power **efficiency** of the transmitter as it was explained in Chapter 2.2. It results to be very low (not even 0.2%), as it can be seen in Table 4 together with the most important parameters commented in this chapter.

Field testing gives us an approximate distance reach of **65 meters**. Voice can be easily recognized, and the frequency remains stable enough so that the reception does not get interrupted. The 18.432 MHz carrier has good short-term stability thanks to the crystal oscillator module.

Table 4 Original basic AM transmitter performance summary table.

DC Voltage Supply	4.5 V
DC Current consumption	38 mA
DC Power consumption	171 mW
Output carrier power	0.254 mW
Modulation depth (4 kHz tone)	51 %
AM power (4 kHz tone)	0.287 mW
Power Efficiency (4 kHz tone)	0.168 %
Carrier C/N	~65 dBm
P_{HD}	22.5 dBc
Transmission distance	~65 m

Chapter 6 includes further discussion and comparisons between these results and the results of the optimized version of the transmitter.

5. OPTIMIZATION AND DESIGN

The optimization process requires the implementation of different modifications in the original design analyzed in Chapter 4. This chapter details the scope and limitations for the modifications, and how these changes have been carried out.

5.1 Restrictions and Trade-offs

Once the original transmitter has been analyzed, it is time to consider how to optimize the circuit. Several restrictions and goals affect the scope of the optimization process.

- Do **not change or add additional blocks** to the schematic. The original simple block-diagram shall remain.
- Keep all the functioning **blocks as basic as possible**, so that they may be explained and used as didactical material for electronics students. Clarify every block function by using simple schemes and component values.
- Use the **same components** in different blocks when they are performing **similar functions**, so that the list of materials remains simple and easy to understand.
- Reduce, if possible, the **power consumption** of the transmitter so that the battery lifetime increases. Increase the **power efficiency** of the transmitter.
- Keep the **overall price** low, taking the original one as a reference.
- **Reduce the size** of the final device that will be used as a demonstration for the students.
- Design a **user-friendly interface** for the final device.
- Design a **reliable package** as a protection for the final device.

Following these guidelines, we can define several **trade-offs** that appear when working on the transmitter, depending on the parameters and components that may be modified. The most relevant of them are explained in the following subchapters.

5.1.1 Output envelope – Output power

The waveform of the **AM envelope** must remain similar to the **audio signal**. On the other hand, the **output power** of the transmitter should be maximized.

Output power will increase by increasing the gain of the BJT in the modulator, and by increasing the carrier amplitude. Nevertheless, the gain of the BJT is variable, since it is a modulated-gain transistor as explained in Chapter 4.1.5. The gain of the BJT may get saturated if the addition of the three voltage components in the base (carrier signal, audio signal and DC bias point) reaches the base-emitter saturation voltage. See Figure 25. This saturation voltage will depend on the BJT model.

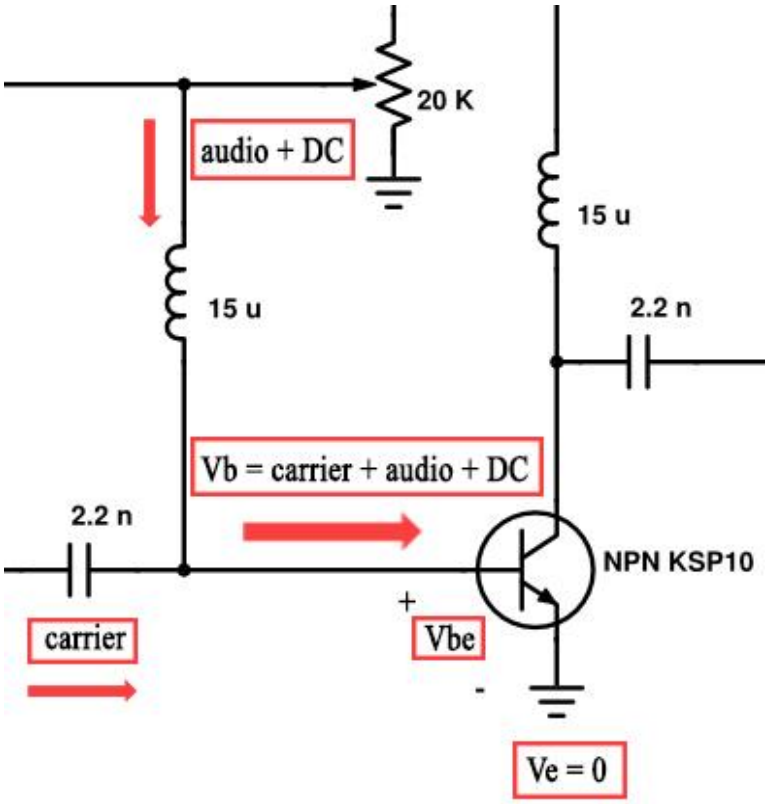

Figure 25 Detail of the voltage components on the base for the amplitude modulator.

If this happens, the carrier amplitude will not be linearly modified according to the audio waveform, and the envelope of the output AM signal will not be correct.

Because of that, we should reduce the carrier amplitude and the bias point of the BJT, giving a certain margin for the base voltage to change with the audio variations. This voltage reduction implies a **lower power efficiency** for the BJT, and a lower power delivery, but ensures the quality of the modulation.

5.1.2 Schematic simplicity – Cost

The original transmitter schematic used two **different BJT models** for the audio amplifier and the amplitude modulator blocks. In addition, the improved schematic will require three transistors, since one of them will be used for the oscillator block as shown in Chapter 5.3.

Using different transistor models, the list of components and their characteristics increases, which slightly makes the schematic more **complex**. On the other hand, using the same BJT model will make it easier for the students to understand their purposes. All the transistors in the schematic are actually performing amplifications, and it is simpler to study the characteristics of one BJT model rather than two or three models.

The BJT model must comply with the three blocks requirements. This may result on an increased cost because of the use of a more expensive BJT model. However, ordering and storing of components becomes simpler when using just one model.

5.1.3 Simplicity – Power consumption

The **crystal oscillator block** presents several weaknesses itself. First, we notice that it is generating a 4.5 Vpp signal that is actually being attenuated into around 60 mVpp. The original module requires 22.5 mW DC to produce it, which results in a power efficiency of less than 3%. In addition to that, the oscillator is a costly module. From a didactic point of view, it does not provide detailed information about how the carrier oscillation is being produced. On the other hand, it ensures good frequency stability and low harmonics in small size.

A custom oscillator design may help to **reduce the power consumption**, providing a good example of simple oscillator design, and even reduce the cost of the oscillator.

5.1.4 Stability – Output power

The stability resistor $\boldsymbol{R_{stab}}$ placed at the output of the schematic (see Figure 17) is is stabilizing the BJT and preventing it to start oscillating. But this resistor is actually loading the output in parallel with the antenna and dissipating a certain amount of power, decreasing the output power delivery.

If we remove or excessively increase the resistance of R_{stab}, oscillations may take place at some frequencies. This may happen because of the negative feedback generated through from the stray capacitances and inductances in the transistor. On the other hand, by increasing R_{stab} the output power delivered to the antenna increases.

5.2 Modifications

From these trade-offs, several **minor improvements** have been carried out. In addition to that, we have implemented a **bigger modification** involving the replacement of the **crystal oscillator**.

Table 5 summarizes all the final modifications and improvements implemented, and every single one will be described in the following subchapters.

Table 5 Modifications and improvements implemented.

Modifications	Components involved	Improvements
Replacement of the crystal oscillator module with a new custom designed crystal oscillator (Chapter 5.3)	Removed: Crystal oscillator Added: 18.432 MHz quartz crystal SS9018 BJT 20 kΩ potentiometer 15 µH inductor 820 pF capacitor 4.7 pF capacitor	The DC current consumption of the oscillator has been reduced by a factor of 5.
Replacement of the Audio Amplifier and the Amplitude Modulator transistors (Chapter 5.2.1)	2N3904 BJT and KSP10 BJT replaced by SS9018 BJTs	DC current consumption decreased by 4 mA. Increased simplicity of the schematic by using the same transistor model in all the different steps.
Modification of the output stability resistor (Chapter 5.2.2)	100 Ω resistor changed to 1 kΩ resistor	Output voltage increased by a factor of 3, higher power efficiency.
Modification of the decoupling and coupling capacitors values (Chapter 5.2.3)	2.2 nF capacitors changed to 68 nF capacitors	Impedance for the 18 MHz signal reduced from 4 Ω to 0.13 Ω. Capacitors purpose is clearer.
Modification of the LED indicator's resistor value (Chapter 5.2.4)	4.7 kΩ resistor changed to 20 kΩ resistor	DC current consumption of the LED indicator has been reduced from 1 mA to 0.2 mA.

5.2.1 BJT replacement

Using the **same BJT model** for all three blocks (audio amplifier, oscillator and amplitude modulator) makes the **schematic simpler**. By doing this, we avoid to use different component models for the same purpose, which is signal amplification.

To reduce the power consumption, it is necessary to select a **low-current transistor** able to work with **high gain**. Not only the current consumption can be decreased in this way, but we can also increase the power efficiency if the output voltage is higher because of the higher gain of the BJT. Because of that, the **current gain** (**h_{FE}**) should be high even when working with low collector currents.

It is also necessary to have an adequate **gain-bandwidth product** [49] since it will be operating with 18 MHz frequencies. Transistors should operate below the **transition frequency (f_T)** [49] when working as amplifiers, so the selected transistor will have **f_T** higher than 18 MHz. Another key parameter to take into account is the **price,** which will affect the final cost of the transmitter.

The following table shows the comparison of these parameters for some different NPN BJT models intended to use in low-current tasks. Prices in the Table 6 have been taken from Farnell.fi and DigiKey.fi at the dates shown in the references.

Table 6 Transistor models comparison.

NPN BJT	h_{FE}	f_T	Price (€)
2N3904 [40]	100 (Ic=10 mA)	270 MHz	0.04
KSP10 [45]	60 (Ic=4 mA)	650 MHz	0.29
SS9018 [50]	100 (Ic=1 mA)	1100 MHz	0.29
2N930A [51]	100 (Ic=0.01 mA)	min45 MHz	1.09
2N2857 [52]	30-150 (Ic=3 mA)	1-1.9 GHz	-
2N5088 [53]	300 (Ic=0.1 mA)	min50 MHz	0.34
2N5179 [54]	25-250 (Ic=3 mA)	900-2000 MHz	14
2N2484 [55]	max800 (Ic=10 mA)	min60 MHz	0.991
2N5210 [56]	250-600 (Ic=1mA)	min30 MHz	0.313
KSC1845 [57]	580 (Ic=0.1 mA)	110 MHz	0.311
NTE107 [58]	75 (Ic=8 mA)	700-2100 MHz	2.36

As it can be seen, BJTs **SS9018** and **KSC1845** provide very good characteristics for the project purpose and they have been used for the prototypes measurements.

5.2.2 Adjustment of the stabilization resistor (*Rstab*) value

By adjusting the value of R_{stab} we can check how much it can be increased without affecting negatively the performance of the modulator. For this reason, the output has been measured with different values of R_{stab}, so that we can check the output power and waveform. This resistor is dissipating so much power at the output, so that increasing its value will result on a **higher power delivery to the antenna**.

The following cases show the simulated power efficiency for different values. This simulated efficiency does not correspond with the real one, but we can get an idea of how much is this resistor affecting the performance.

Table 7 Simulated transmitter efficiency with different values for R_{stab}.

R_{stab} (Ω)	AM output power	Transmitter Power Efficiency
10	0.597 mW	0.474 %
100	10 mW	7.723 %
1000	13 mW	9.929 %

By lowering the *Rstab* value from the original 100 Ω value, it will dissipate more power, and the output power delivered to the antenna will be reduced as it can be seen in Table 7. The lower the value, the worse the transmitter power efficiency.

Increasing the *Rstab* value will make it bigger than the antenna impedance (assumed as 50 Ω), so that the load current through the *Rstab* will be lower. The output power increases, but there is a trade-off: when the audio input is high (30 mVpp), the output can get distorted because of the BJT saturation.

In order to avoid this problem, the carrier level has to be reduced, in this case by changing the attenuator by using one with a factor of 1/141. Table 7 shows also simulation results with a normal 20 mVpp input and *Rstab* = 1 kΩ.

Nevertheless, this has some limits. Increasing farther the *Rstab* value or removing it from the circuit results again on a saturation of the modulator BJT. We can keep reducing the input signal levels, but then the signal to noise ratio will be worsened.

5.2.3 Adjustment of the 2.2 nF capacitors

2.2 nF capacitors have been used in the original design for blocking the DC component while they provide a **low-impedance path** for the 18 MHz signal.

There are different ways to select a DC block capacitor. The main idea is to make the impedance very low for the desired frequency [59]. We can achieve this just by using capacitors with an adequate value of capacitance, so that the impedance for the operation frequency is low enough as

$$Z_C = \frac{1}{j2\pi fC} \tag{17}$$

where Z_C is the impedance, f is the frequency and C is the capacitance.

Other way is using a capacitor with its self-resonance frequency (FSR) corresponding to the working frequency, making the impedance to be the equivalent series resistance of the real capacitor [59], [60]. Nevertheless, if the working frequency rises above the FSR, the impedance of the capacitor will get inductive. It will work then as an inductor, which

is an undesired behavior. Because of that, working with frequencies below the FSR will be safer.

If we go deeper on the function of the capacitors used, we can calculate the impedance for an 18 MHz signal from equation (17) as

$$Z_C = \frac{1}{j2\pi \cdot 18 \cdot 10^6 \cdot 2.2 \cdot 10^{-9}} = -4j\ \Omega \tag{18}$$

Which is in fact a low impedance path. Nevertheless, we can improve this without big cost just by increasing the capacitance using 68 nF capacitors, so that the impedance results in

$$Z_C = \frac{1}{j2\pi \cdot 18 \cdot 10^6 \cdot 68 \cdot 10^{-9}} = -0.13j\ \Omega \tag{19}$$

Which is **30 times lower** than the previous impedance. Now, the capacitors are performing better their function and **their purpose is much more clear** as a low impedance path.

However, in these calculation we have considered ideal capacitors. Real capacitors will have a certain series inductance, which will also modify the total impedance.

5.2.4 Adjustment of the resistor for the LED indicator

The red LED indicator is intended to indicate when the power is connected. Since the typical LED forward voltage [61] is 1.85 V and the voltage supply for the circuit is 4.5 V, it needs an additional series resistor. This resistor will provide the voltage difference left from the forward voltage of the LED to the 4.5 V supply. By making the resistor value higher, the current flowing through this LED path will be lower (and also will **decrease the brightness** as it can be seen in Figure 26).

There is not a minimum current to produce light, since every current will produce a certain amount of photons [62]. On the other hand, if the resistor is too big, the current will decrease so that the luminous intensity of the LED may be unappreciable for the human eye.

Since the LED brightness is not a very important issue for the transmitter behavior, we can reduce the DC current flowing there by **increasing the series resistor** from 4.7 kΩ to 20 kΩ. The current decreases then from approximately **1 mA to 0.2 mA**, and the light is still visible. See Figure 24.

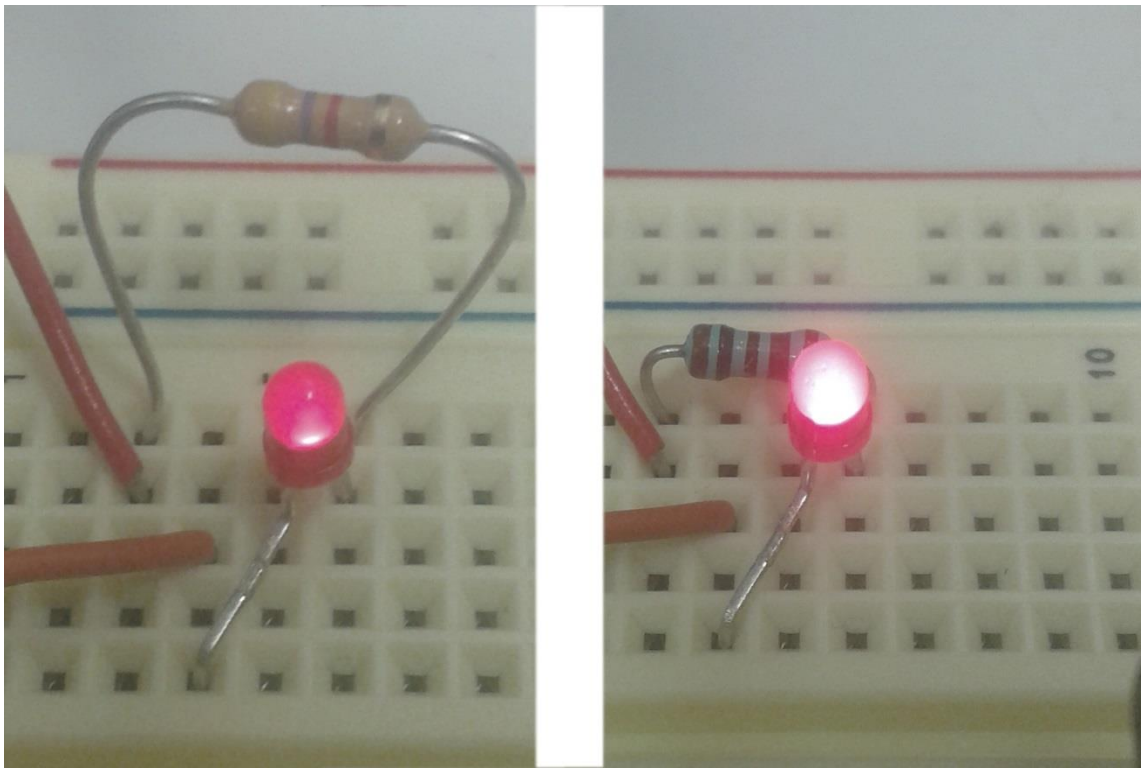

Figure 26 Comparison of LED brightness with 20 kΩ resistor (left) and 4.7 kΩ resistor (right).

5.3 Oscillator design

While the original Crystal Oscillator module was working with a DC current consumption of 5 mA, the objective is to design a **more efficient oscillator** with lower power consumption (at least half of the original DC current) by applying the basic oscillator theory seen in Chapter 2.3. To achieve this goal, the selection of a low current BJT has been commented in Chapter 5.2.1.

This step has been approached from different basic oscillator schemes. First, we try to build an **LC oscillator** taking the basic Colpitts and Clapp schematics as a reference. The intention is to see how the behavior of the real oscillator differs from the theory, and check if it is useful for the purposes of the transmitter. Once the LC oscillator has been tested, we can build and test a **crystal oscillator** and decide which one is more convenient.

Since this transmitter has not strict requisites about the working frequency, the desired oscillation frequency is not necessarily exactly the same as in the previous oscillator, but **any frequency** around the **18.4 MHz** (or even from 18 to 19 MHz) should be acceptable, if the oscillation is **stable** enough. Short-term stability must ensure the radio transmission and reception, which can be checked during field testing.

Summary tables showing the performance of different oscillator configurations, testing various BJTs, can be seen in the Appendix 4.

5.3.1 LC Oscillator design

As a first approach we design a **Colpitts oscillator.** The oscillator is simulated in ADS using the schematic from Figure 27. R_1 and R_2 correspond to the resistive parts of a potentiometer used for biasing the base of the BJT. Two coupling capacitors and an RF choke are blocking DC and AC components, respectively.

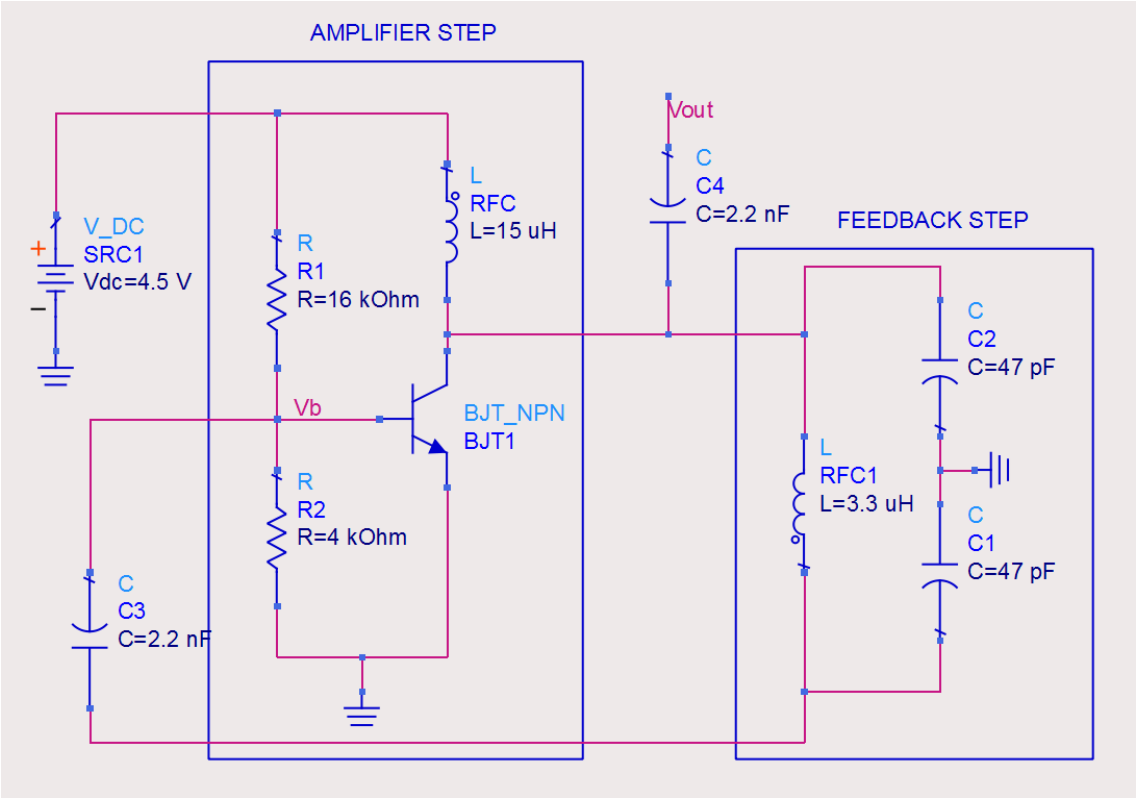

Figure 27 ADS Schematic for the LC Colpitts oscillator.

The values for the components in the tank circuit are selected after setting one of them in a fixed value as a reference. In this case, L = 3.3 µH is selected first so that we can work with capacitors in the order of pF. Both capacitors have been selected then to attain a **theoretical oscillation frequency of 18.07 MHz** according to equation (10).

Simulations predict a stable 18.2 MHz oscillation frequency, 0.72% over the theoretical one. The waveform can be seen in Figure 28. DC current consumption is around 3.8 mA, which is less than the original case but still not as low as it was desired.

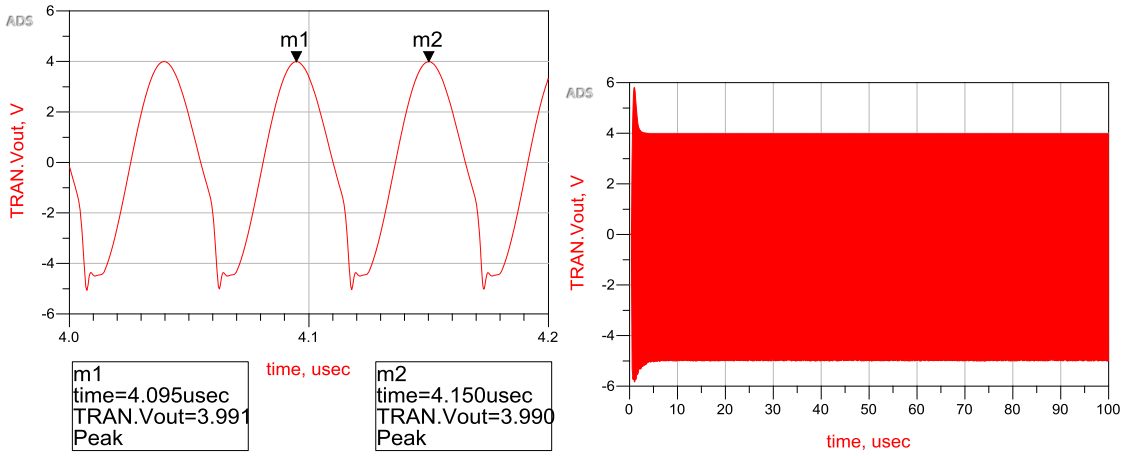

Figure 28 Output signal from the Colpitts Oscillator simulations. f_o = 18.20 MHz.

A prototype of the oscillator is built on a **breadboard using TH components**. See Figure 29. Using the same theoretical values for the inductor and the capacitors, the oscillation frequency measured at the output is around 12 MHz, when testing with different BJTs.

Table 8 Colpitts oscillator components, simulation and measurement results.

C_1	47 pF
C_2	47 pf
L	3.3 µH
I_c **(no load)**	17 mA
I_c **(transmitter load)**	18 mA
I_c **(simulation, no load)**	3.82 mA
f_o **(theoretical)**	18.07 MHz
f_o **(simulation)**	18.20 MHz
f_o **(measured)**	12.03 MHz
BJT	2N3904

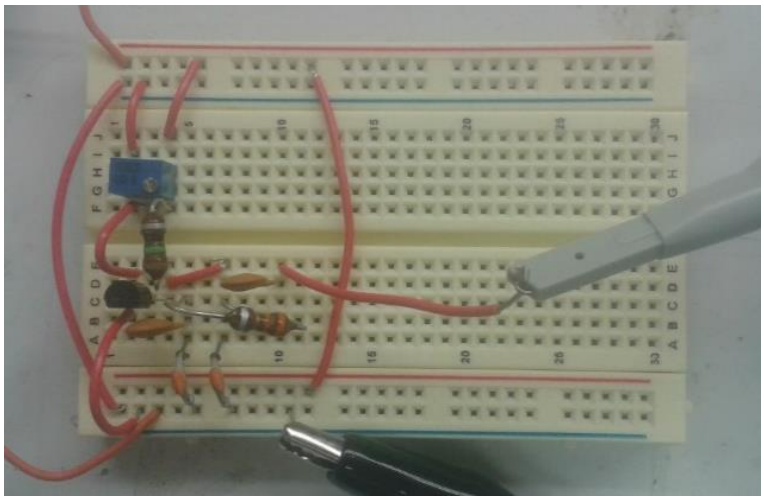

Figure 29 Breadboard prototype for the Colpitts Oscillator.

This Colpitts experiment help us to understand the differences between the theory and the real devices. Oscillation frequency is **around 33% lower** than the intended 18.07 MHz. This is caused by **parasitic** capacitances and inductances in the real circuit that are not considered in the simulations or the theoretical calculations. For example, stray capacitances of the BJT junctions affect in parallel the values of L, or C_1 and C_2 [63], [64], modifying the resonance frequency. Another problem is the power consumption: the DC current is more than 3 times higher than in the Crystal Oscillator module. Table 8 shows the values of the tank circuit, the simulated and the measured current, and the difference between the oscillation frequencies.

Using the datasheet of the 2N3904 as a reference [40], we can define two stray capacitors as *Cbc* = 4 pF and *Cbe* = 18 pF, where *Cbc* is the capacitance between the base and the collector, and *Cbe* is the capacitance between the base and the emitter. Figure 30 shows the schematic of a Colpitts oscillator, using the same components as before, including these two *Cbc* and *Cbe* capacitors. Figure 31 shows the simulated oscillation produced by this schematic, with f_o = 16.72 MHz.

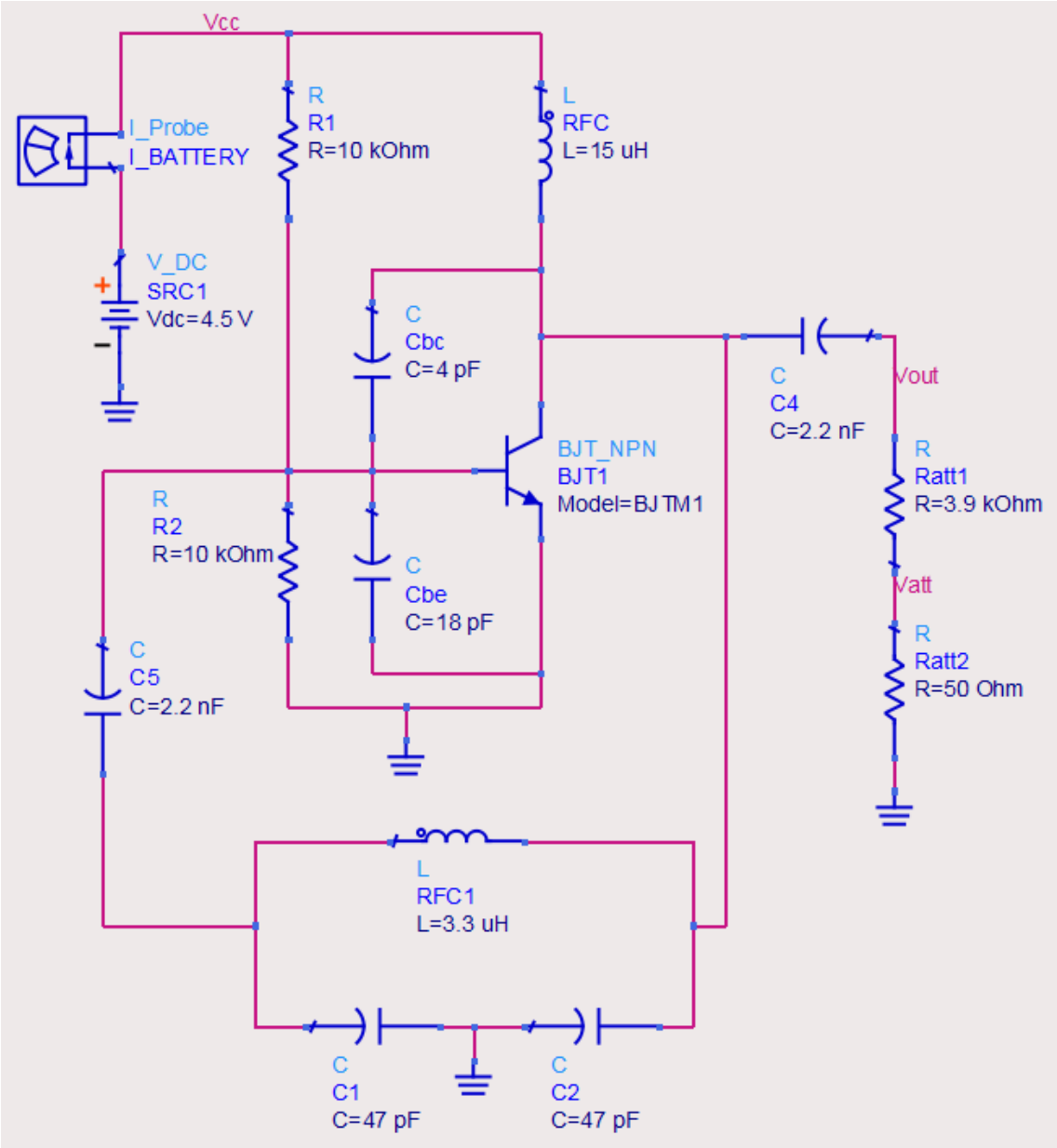

Figure 30 ADS schematic for the simulation of Colpitts oscillator with stray capacitors.

This result proves that the stray capacitances of the BJT decrease the theoretical oscillation frequency. However, the real device presents still a lower frequency. Other parasitic capacitances and inductances may affect the resonance, such as the **stray capacitances** between the lines of the **breadboard**. Their value is around 2 pF between adjacent files, according to the experiments in [65], and it is in the same order of magnitude of C_1 and C_2, so that it is more likely to affect their values when placed in parallel.

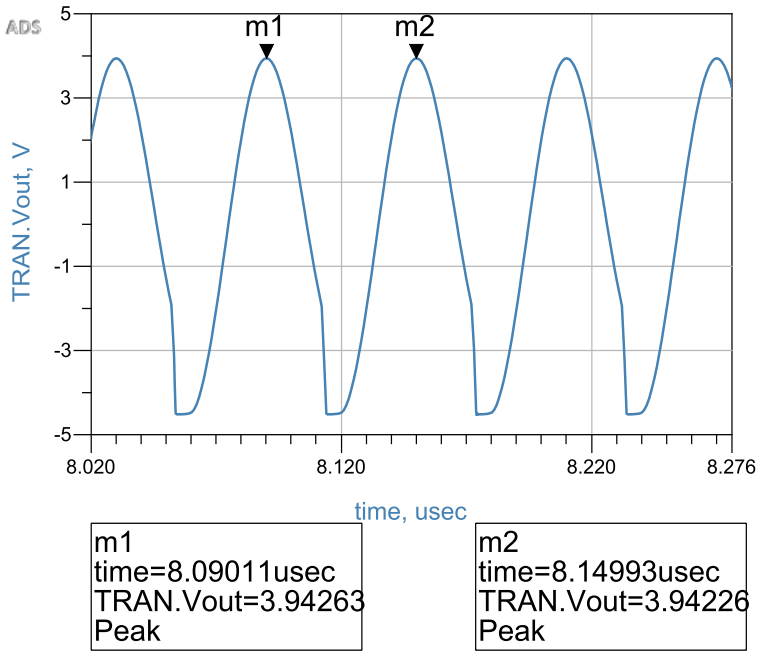

Figure 31 Output signal from the Colpitts Oscillator simulations with stray capacitors. f_o = 16.72 MHz.

In order to **adjust the frequency** to the desired 18 MHz range, there are several approaches that we can take:

1. Modify the values of the components in the feedback network. Modifying the capacitors or the inductor to get a higher theoretical frequency may produce the 18 MHz oscillation with the real device.
2. Develop a more complex oscillation model, taking into account the stray effects of the circuit into the calculation of the frequency. Use this model to select the components with more precision.
3. Include an additional series capacitor for tuning the frequency, working with a more accurate Clapp oscillator schematic.

To improve the LC oscillator performance, we decide to add the series capacitor C_S next to the 3.3 µH inductor, so that the schematic represents a **Clapp oscillator**. This option allows us to test a real circuit based on the Clapp schematic, without making the oscillator to be very complex or very different from the basic theory.

According to the theory seen in Chapter 2.3.2, the oscillation frequency can be set by C_S when using higher values of C_1 and C_2. Table 9 shows the theoretical components used for the first simulation, and the simulation results. The simulated frequency corresponds with the theoretical one this time. Figure 32 shows the simulated oscillation waveform.

Table 9 Clapp oscillator components and simulation results.

C_1	C_2	C_S	L	I_c (simulated)	f_o (simulated)	f_o (theoretical)
150 pF	150 pF	33pF	3.3 µH	1.3 mA	18.31 MHz	18.30 MHz

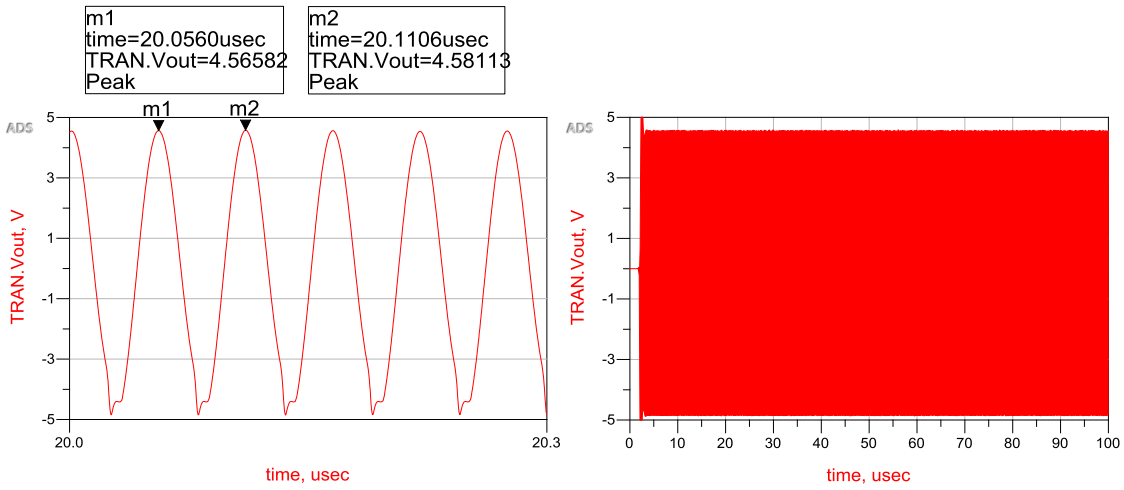

Figure 32 Output signal from the Clapp Oscillator simulations. f_o = 18.31 MHz.

Nevertheless, the real measured frequency when building the prototype is around 16 MHz. The difference is not that big as it was with previous Colpitts oscillator, but there is a significant difference (more than 10%) between the theory and the practical results again.

We can do a fine adjustment of the components to increase the measured oscillation frequency up to the 18 MHz range. The theoretical frequency will be higher, but the real one gets affected again by parasitic effects of the circuit.

Table 10 shows the final components selected according to iterative measurements. Figure 33 shows the waveform of the oscillation. By making C_1 greater than C_2 we can change the feedback ratio of the capacitive divider, so that the required gain of the BJT is modified according to the amplitude condition of the Barkhausen Criterion, seen in Chapter 2.3 and 2.3.1. Using the potentiometer (R_1 and R_2 in Figure 30), the DC current of the BJT can be adjusted to the minimum, which is related to the gain.

On the other hand, if the value of C_2 is reduced so that it is comparable with C_S, it will affect the oscillation frequency. The frequency is calculated according to equation (10) as

$$f_o = \frac{1}{2\pi\sqrt{3.3 \cdot 10^{-6} \cdot 1.53 \cdot 10^{-11}}} = 22.36\ MHz \tag{20}$$

Table 10 Clapp oscillator components and measurement results.

BJT	C_1	C_2	C_S	L	I_c (no load)	I_c (transmitter)	f_o (theoretical)	f_o (measured)
SS9018	220 pF	33 pF	33 pF	3.3 µH	4 mA	4 mA	22.36 MHz	18.03 MHz

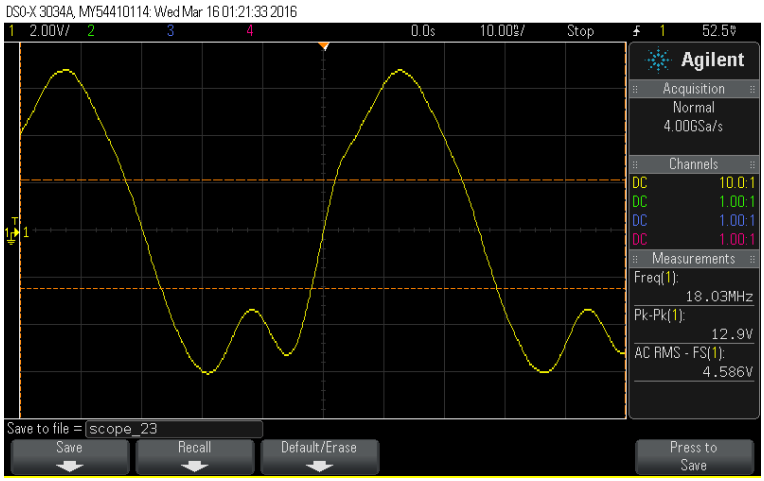

Figure 33 Output of the Clapp oscillator without any load. f_o = 18.03 MHz. Scale: 2.00 V/division vert. 10.00 ms/division horiz.

The spectrum analysis provides more information about the oscillator behavior. Even when the power efficiency has been improved in respect to the original oscillator, the **frequency stability is very low**. Any movement or object approaching the oscillator makes the frequency to shift more than ±50 kHz (around ±0.3% or ±3000 PPM), because the inductances and capacitances of the tank circuit get affected.

While testing with a **real receiver**, the radio signal was being transmitted without problems until one puts the hand close to the oscillator. In that moment, the **reception gets interrupted** so that the transmission is not reliable. This could be avoided in some measure by protecting the oscillator circuit from external issues using some kind of electromagnetic shielding (EMC shielding) structure.

Nevertheless, another easier option is building a more stable **crystal oscillator** whose tank circuit is based on a piezoelectric material (see the theory from Chapter 2.3.3).

5.3.2 Crystal Oscillator design

Once we have seen the limitations and differences between the real and the theoretical LC oscillators, we can try a custom-designed crystal oscillator. We use an 18.432 MHz **quartz crystal** [66] and both capacitors C_1 and C_2 to set the feedback network of a Pierce crystal oscillator as seen in Chapter 2.3.3.

Table 11 Crystal oscillator components and measurement results.

BJT	**C_1**	**C_2**	**I_c (no load)**	**I_c (transmitter)**	**f_o**
SS9018	820 pF	4.7 pF	1 mA	2 mA	18.44 MHz

Table 11 shows the characteristics of crystal oscillator with one fifth of the original current. Figure 34 shows the waveform of the oscillation, together with the frequency and amplitude measurements.

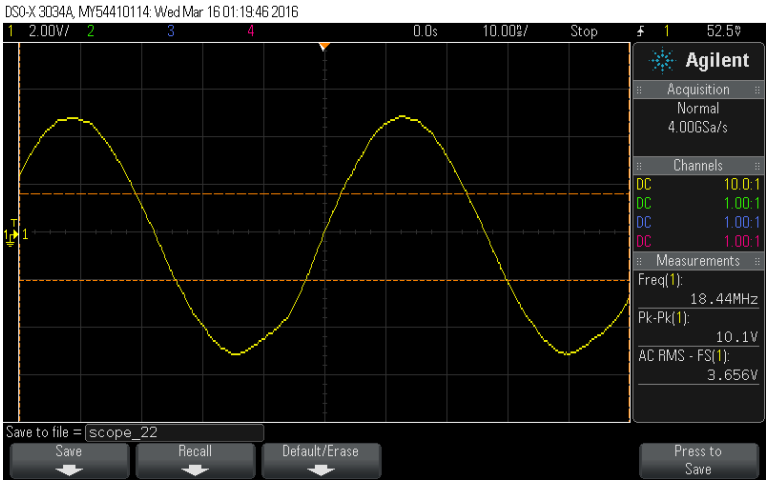

Figure 34 Output of the crystal oscillator without any load. f_o = 18.44 MHz. Scale: 2.00 V/division vert. (both) 10.00 ms/division horiz.

We can estimate the value of the **minimum collector DC current I_C** which will meet the amplitude contidion of the Barkhausen Criteria from the following definition of g_m and equation (12) as

$$g_m = \frac{I_C}{V_T} = \omega_o^2 R_e C_1 C_2 \tag{21}$$

where V_T is the thermal voltage (25.85 mV in normal conditions) and R_e has a maximum value of 30 Ω according to the datasheet [66]. Notice that, since the base current is much lower than the collector current in the BJT, I_C will be approximately the DC current consumption of the oscillator block. The potentiometer adjusts I_C to reach this minimum, ensuring that the circuit will produce the desired oscillation.

Using the values from Table 11 in equation (21) we estimate a current consumption **around 0.02 mA**. Nevertheless, the real minimum DC current measured in the prototype is much higher – **around 1 mA** without any output load. This increase may be produced by different factors:

- The value of C_2, which is in the order of several pF, will get affected by the stray capacitances as it was discussed in Chapter 5.3.1. However, if we consider all the other components with the same values of Table 11 except for C_2, the capacitance must have increased from 4.7 pF to around 200 pF, which is more than 40 times higher. C_1 may be affected also by parasitic components.
- R_e may be higher than the 30 Ω assumed from the datasheet. It may be again because of stray components and the effect of the non-solder connections in the

breadboard. However, the series resistance should increase up to around 700 Ω to produce I_C = 1 mA, which is more than 20 times higher.

Both of these factors combined together can affect much more the current than separately. For example, if C_2 increases to 90 pF and R_e increases to 400 Ω, the minimum current I_C ≈ 1 mA according to equation (21). Nevertheless, further research can be done about this problem to identify the exact reasons for this current consumption. We can select then different components taking into account more accurate models, and the effects of the breadboard.

Taking the results from Table 11, the current consumption without output load is **one fifth of the current** of the original oscillator. Additionally, field testing proved that the signal can be transmitted and received without interruptions so that this oscillator presents enough short-term stability. The oscillation frequency does not get affected by the approach of external objects. This oscillator has been used in the final improved device because of its stability, simplicity and power efficiency as the results in Chapter 6 will show.

5.4 Design of the PCB transmitter

The next design step after the transmitter prototyping is the final **PCB design and miniaturization** of the device.

Most of the components are exactly the same as in the breadboard prototype, but a few resistor values have been slightly adjusted for adapting to the standard SMD components available. Figure 35 shows the final schematic used for the PCB design and assembly, gathering together all the modifications commented in the previous chapters.

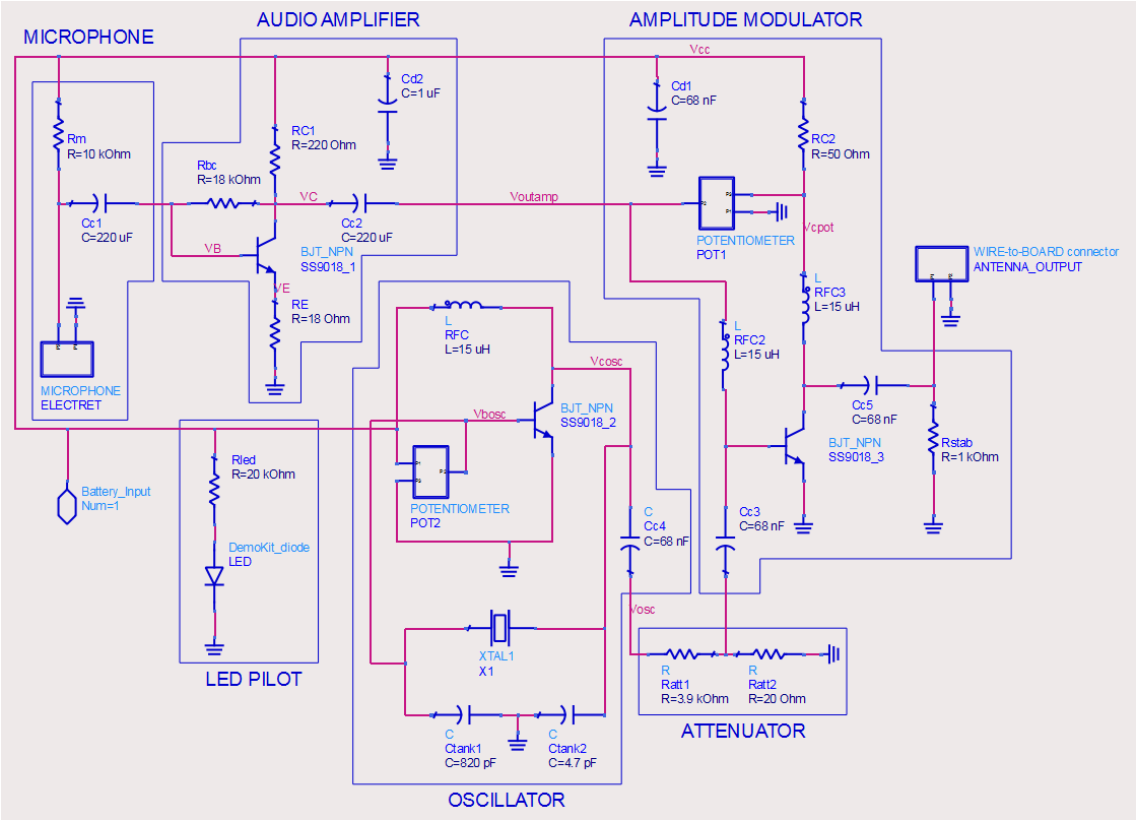

Figure 35 Final schematic for the PCB design and assembly of the improved transmitter.

5.4.1 Transmitter layout

As described in the Chapter 3.2, ADS has been used for the PCB design. The final device has been designed for a **double-sided board** [67], so that two copper layers and several connection vias have been placed. The complete dimensions of the PCB designed are 52 x 40 mm, corresponding to the size of the ground plane. Figure 36 shows a picture of the PCB layout in ADS.

SMD components have been placed on the **top layer** together with most of the copper traces, as seen in Figure 37 (left). Most of the TH components and the ground plane have been placed in the **bottom layer**, as seen in Figure 37 (right). Connections to the ground layer from the top traces were thought to be done by soldering little wires through the vias.

For the output antenna connection, a 2 pin *wire-to-board* connector [68] has been used. This connector makes it easy to connect and disconnect the antenna from the circuit, just requiring a screwdriver to secure the contact. On the other hand, two vias have been placed for soldering the battery holder wires directly to the board without the need of any additional connector. Furthermore, a push-button has been added to the design so that the

battery supply will only reach the device when the button is pushed. The AM transmitter will work then as a “push-to-talk” device.

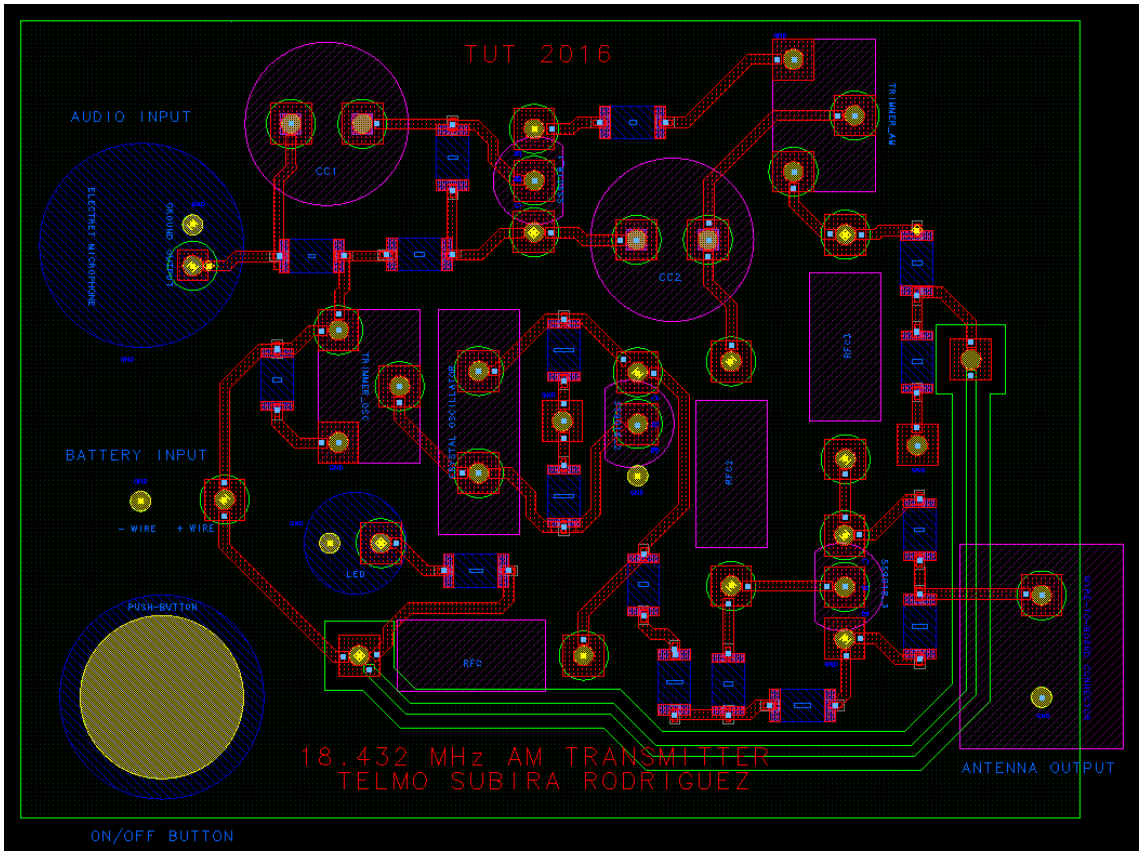

Figure 36 Preview of the PCB layout and tracing design.

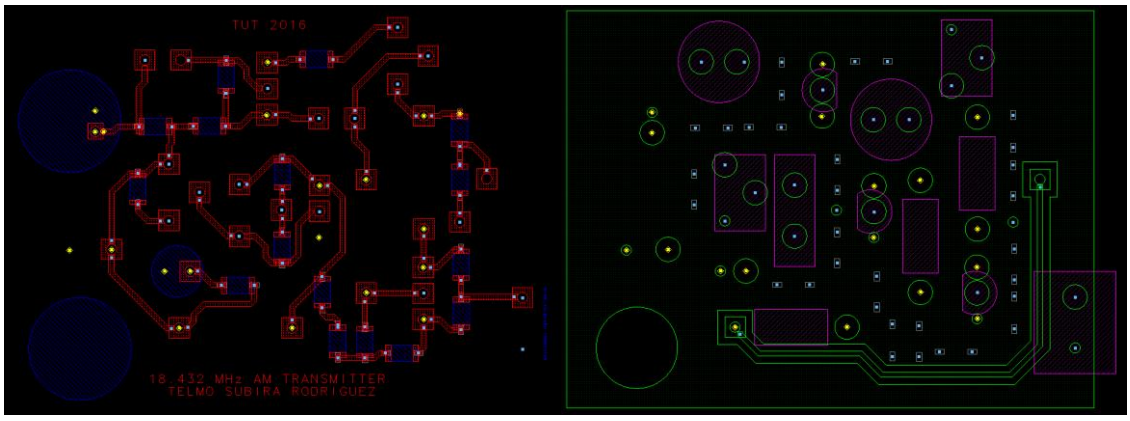

Figure 37 Preview of the top layer (left) and bottom layer (right) traces, components layout and ground plane.

All the components and materials used can be seen in the Table 13 from Chapter 6.1.

Some of the TH components have been placed in the top layer instead of the bottom one intentionally. These are the push-button, the LED indicator, the input microphone and the antenna connector. The reason for placing them in the top layer is to provide an **easier**

usability of the device. In this way, every component that may be accessed by the user is placed in the top side of the transmitter.

5.4.2 Transmitter manufacturing

The **assembly drawings** for the placement of the components and drillings are shown in the Figure 38. **Gerber** files of the layout can be seen in the Figure 39. These gerber images are exported into PDF to be printed as the exposure masks. Notice that the gerber images include alignment marks (bullseye-like parts), used for the alignment of the exposure masks with the board.

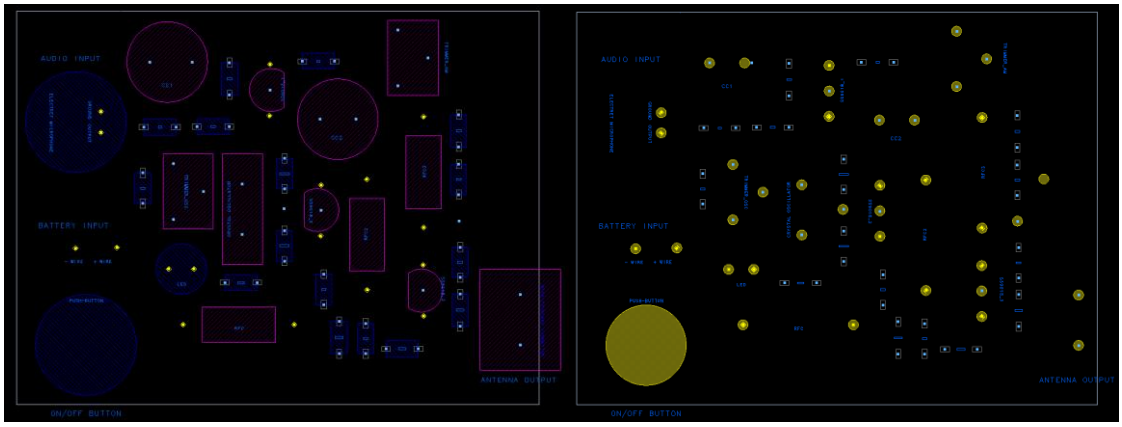

Figure 38 Preview of the assembly drawings. Both layers components placement (left) and drill position for vias and TH (right).

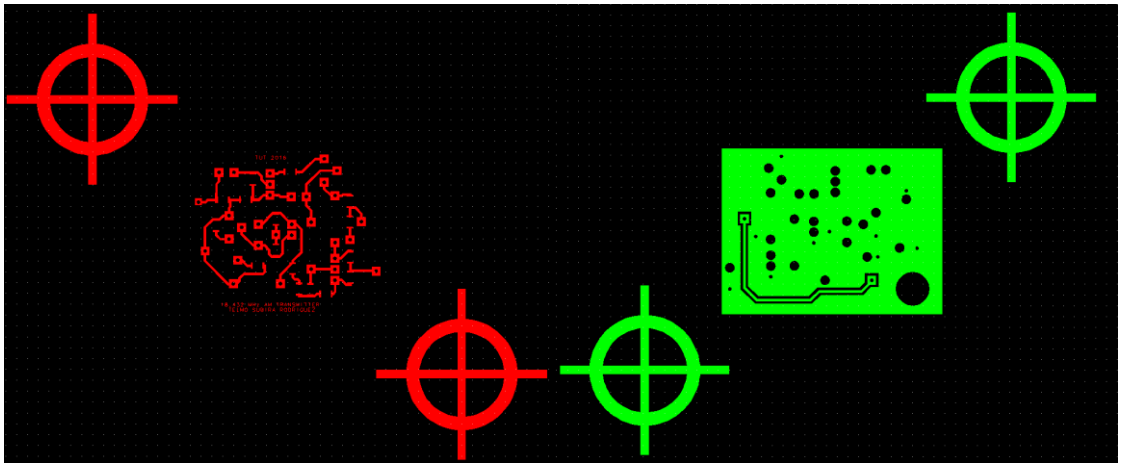

Figure 39 Preview of the top (left) and bottom (right) gerber files for exposure masks.

Following the manufacturing process described in the Chapter 3.3 (Figure 40), the final PCB result can be seen in the Figure 41.

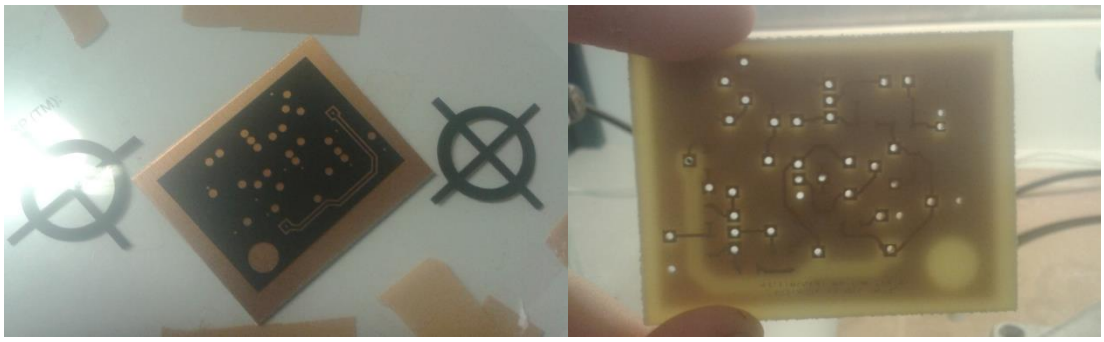

Figure 40 Alignment of masks for the UV exposure (left) and drilling process (right).

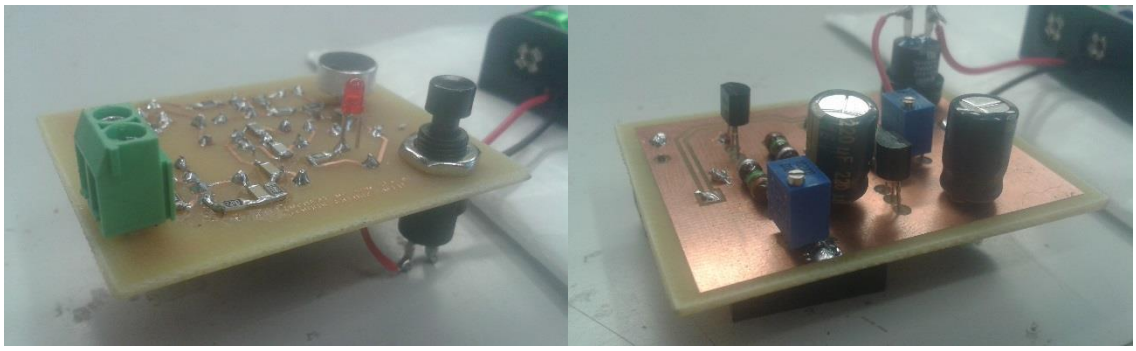

Figure 41 Top view (left) and bottom view (right) for the final PCB transmitter. Connections to the battery holder from the right.

Notice that the final layout is a mirrored version of the original PCB design. Since there were no problems with any component placement, the device was fabricated this way.

5.5 3D package design

A 3D model for the package has been designed using SolidWorks 2013 Edition [69]. It consists of 3 parts that are assembled as seen in Figure 42. The central part which will be holding the PCB on one side and the batteries on the other side. The bottom part will be used as the batteries cover, and the top part will be the PCB cover. This top part includes round holes for the button, LED, and microphone positions. There is also a cavity for the antenna connector. The purpose for this package is to fix and/or cover every part of the transmitter (e.g. PCB, cables, batteries and connectors). This improves the reliability [70], [71] of the device against environmental stresses [72] such as mechanical shocks, vibrations, dust accumulation, or liquids.

The models for the package parts have been exported into .stl files, which is a common CAD format, so that it could be printed using 3D printers. The following images show the **assembly drawing** (Figure 42) and realistic images (Figure 43) rendered using KeyShot v4 [73], which is a 3D rendering software. Figure 44 shows the real 3D-printed parts using a Prenta DUO 3D printer [74].

Additionally, Appendix 5 includes drawing images for the three separated parts.

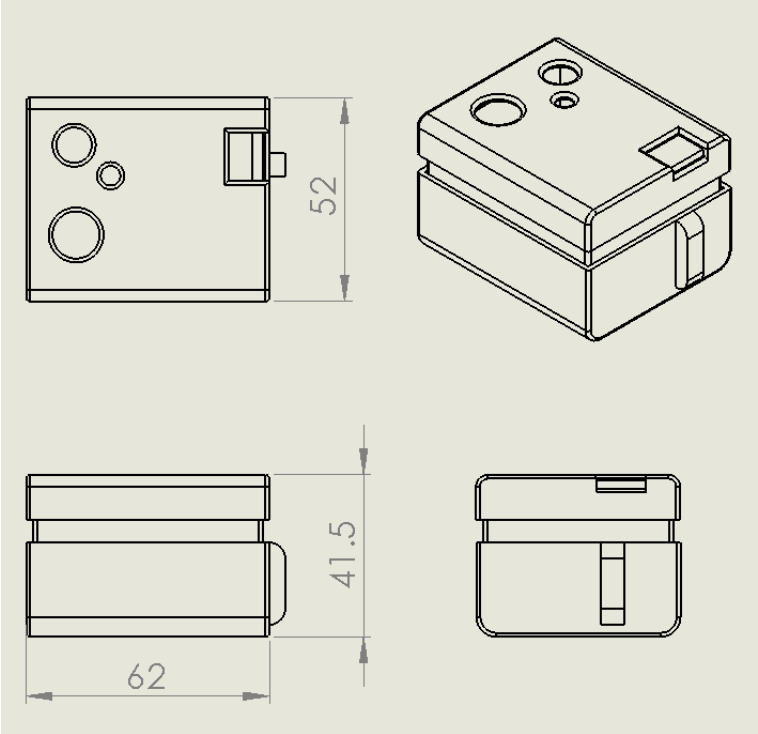

Figure 42 SolidWorks drawings for the complete assembly of the package.

Figure 43 KeyShot render images with metallic covering aspect.

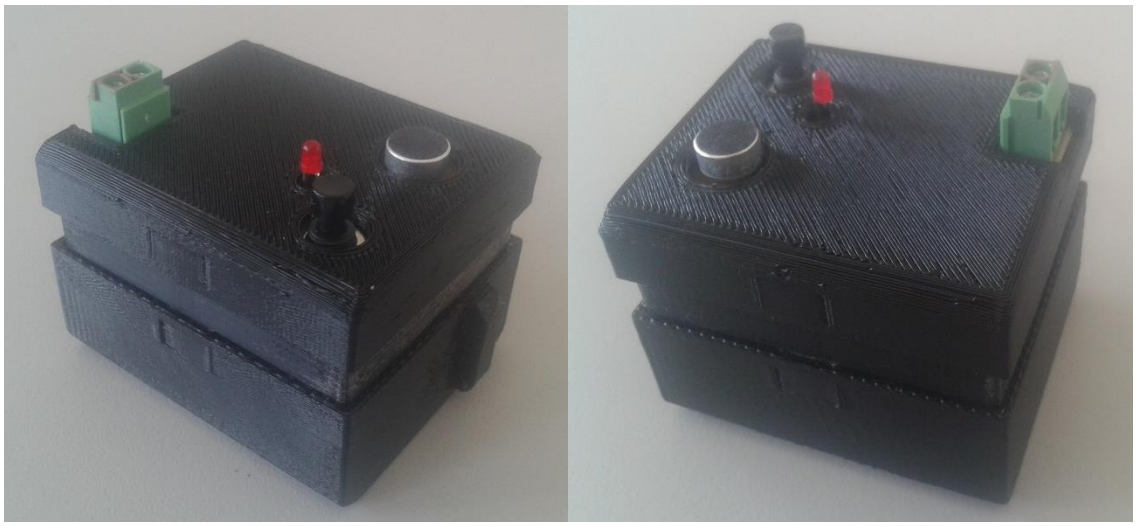

Figure 44 Final AM transmitter inside the 3D-printed package.

6. RESULTS AND COMPARISONS

This chapter shows and compares the results obtained from the spectrum measurements and from the time-domain **path-analysis mentioned in Chapter 3.1.2**, for three different versions of the AM transmitter:

1. The breadboard prototype of the **original AM transmitter** discussed in Chapter 4. It is based on the original schematic from the *Practical RF Electronics* course.
2. The **breadboard prototype of the optimized schematic,** with all the implemented modifications detailed in Chapter 5.2 and 5.3.
3. The **final PCB transmitter**, built from the optimized schematic and detailed in Chapter 5.4.

In all cases the input signal received by the microphone is the **standard 4 kHz** tone defined in Chapter 3.1.2.

The **output of the microphone** presents, in all three cases, a high 18-MHz noise coming from the common ground and supply paths. It can be seen in Figure 45. There is an increase of the amplitude of the noise from the original transmitter to the improved breadboard, because the amplitude of the oscillation itself has been increased. On the other hand, there is an important reduction of the noise in the PCB transmitter, so that we can appreciate the improvement in the quality of the audio signal from the breadboard to the PCB design.

The same 18-MHz noise from Figure 45 can be seen at the **output of the audio amplifier** in Figure 46. Noise has been amplified together with the audio signal, and we can appreciate again that the audio waveform is clearer in the PCB transmitter.

Figure 47 shows big differences between the original crystal module and the custom crystal **oscillator outputs**: the first one is a square wave with significant underdamped peaks on every voltage switch, while the crystal oscillator explained in Chapter 5.2.3 presents a more sinusoidal-like waveform. Additionally, the peak-to-peak amplitude is much higher, so the attenuation in the voltage divider had to be increased. This high amplitude is the reason of the increased high-frequency noise in the breadboard prototype.

At the **base of the modulated transistor**, the waveform should present the addition of the audio signal and the carrier signal as it can be seen in Figure 48. Since the output of the audio amplifier presents a big 18-MHz component, they look very similar. We can appreciate that the lower cycles of the 4 kHz signal are deeper than the upper cycles. This is because of the effect of the forwarded base-emitter PN junction in the modulated transistor, loading the output of the audio amplifier (more details in Appendix 3).

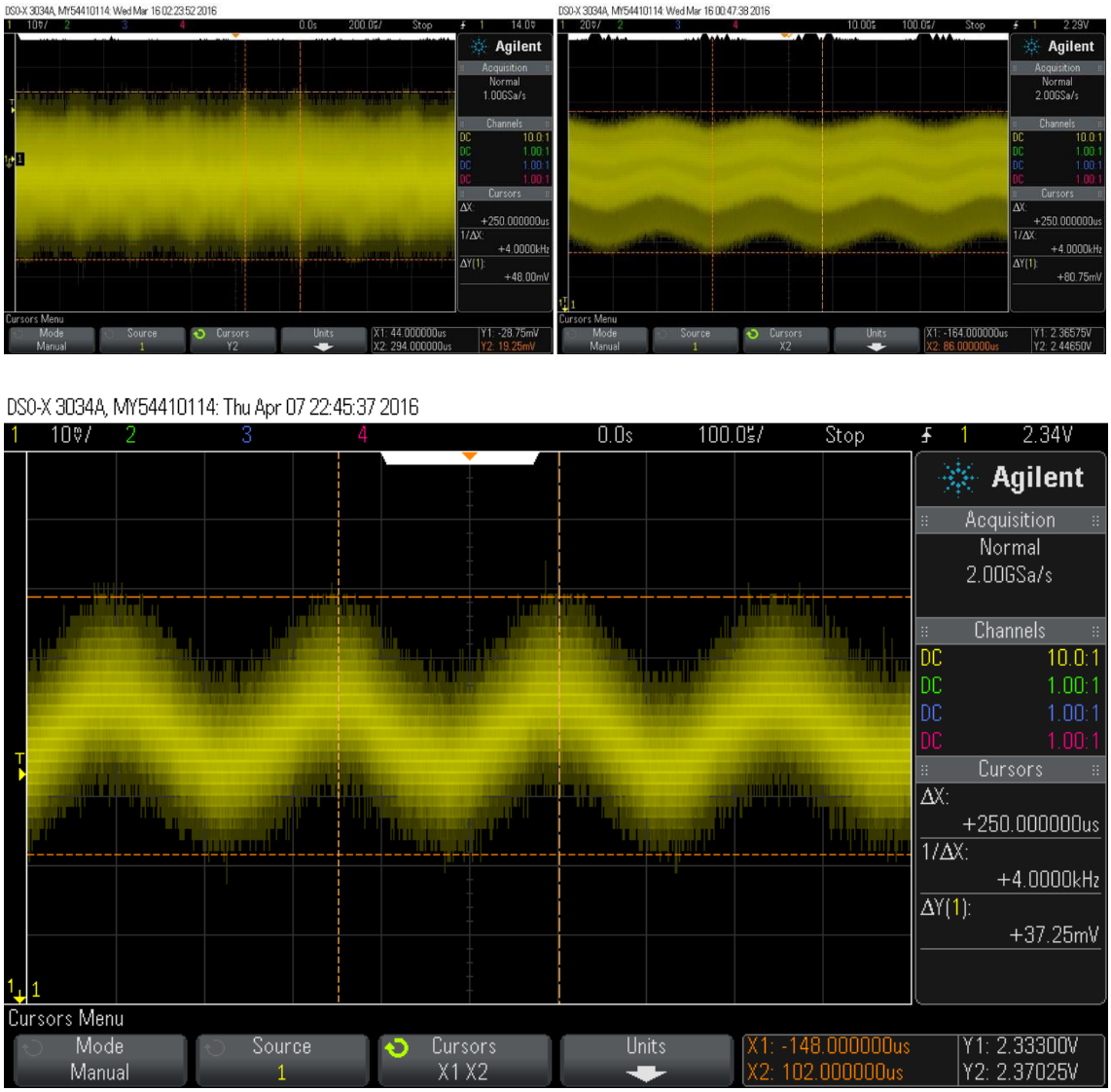

Figure 45 Microphone output waveforms comparison.

Original AM transmitter (top left). 10.00 mV/division vert. 200.00 ms/division horiz.

Improved breadboard (top right). 20.00 mV/division vert. 100.00 ms/division horiz.

Final PCB transmitter (bottom). 10.00 mV/division vert. 100.00 ms/division horiz.

At the **output of the AM transmitter** we can clearly see (Figure 49) the difference between the original version and the final device. The carrier amplitude has been increased from around 1 Vpp to almost 5 Vpp, but the modulation depth has been decreased from 51% to 39%. However, the output AM power has been increased around 3.8 times despite the lower modulation depth. The modulation depth can be adjusted by modifying the biasing of the modulated transistor, but there is a limit on the modification of the biasing. The transistor may start working out of the linear region, so that the amplitude modulation would not represent the audio signal anymore.

There is also another difference between the original output and the PCB output: the waveform in the bottom picture in Figure 49 looks much more “clear”, without the internal lines close to the envelope present in the top-left picture in Figure 49. This is because of the carrier waveform, which has not that many peaks that were present in the original oscillator output.

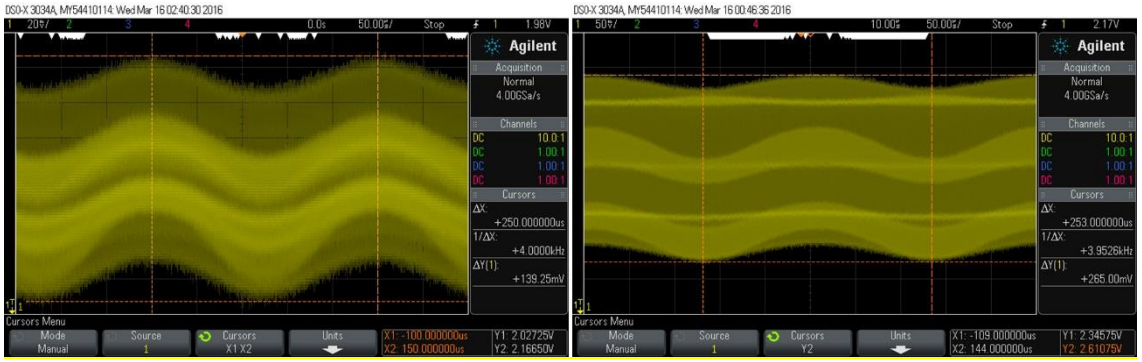

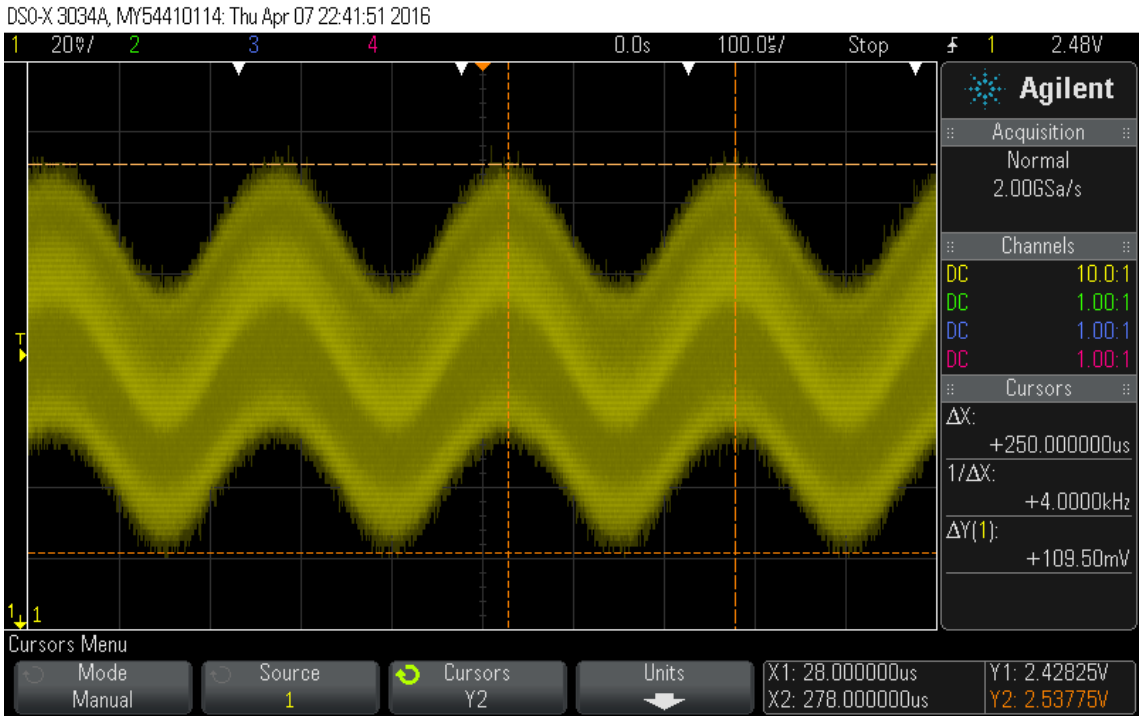

Figure 46 Audio Amplifier output waveforms comparison.

Original AM transmitter (top left). 20.00 mV/division vert. 50.00 ms/division horiz.

Improved breadboard (top right). 50.00 mV/division vert. 50.00 ms/division horiz.

Final PCB transmitter (bottom). 20.00 mV/division vert. 100.00 ms/division horiz.

Figure 47 Oscillator output waveforms comparison.

Original AM transmitter (top left). 2.00 V/division vert. 10.00 ms/division horiz.

Improved breadboard (top right). 2.00 V/division vert. 10.00 ms/division horiz.

Final PCB transmitter (bottom). 2.00 V/division vert. 10.00 ms/division horiz.

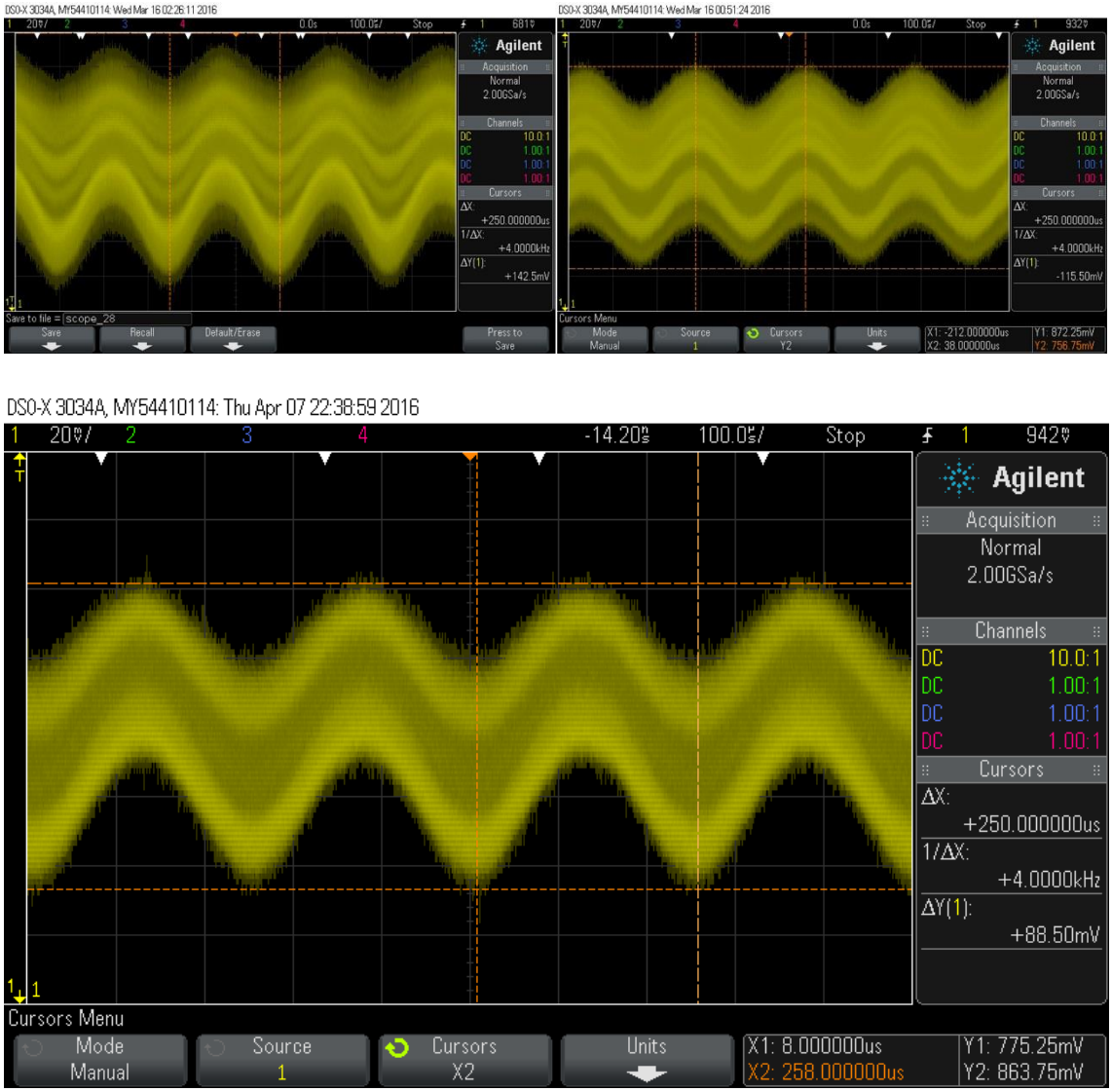

Figure 48 Modulated transistor base waveforms comparison.

Original AM transmitter (top left). 20.00 mV/division vert. 100.00 ms/division horiz.

Improved breadboard (top right). 20.00 mV/division vert. 100.00 ms/division horiz.

Final PCB transmitter (bottom). 20.00 mV/division vert. 100.00 ms/division horiz.

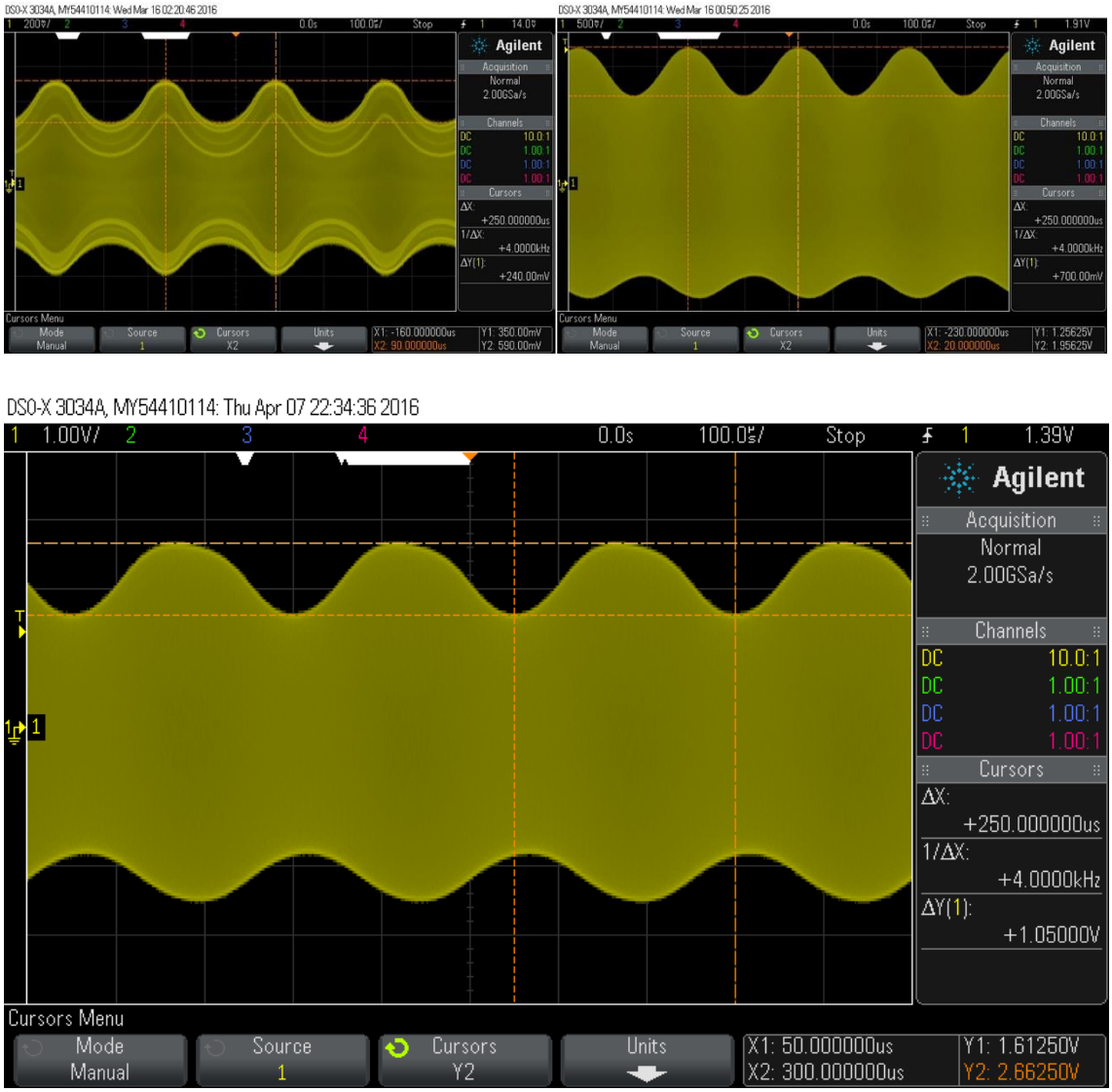

Figure 49 Antenna connection / AM transmitter output waveforms comparison. Original AM transmitter (top left). 200.00 mV/division vert. 100.00 ms/division horiz. Improved breadboard (top right). 500.00 mV/division vert. 100.00 ms/division horiz. Final PCB transmitter (bottom). 1.00 V/division vert. 100.00 ms/division horiz.

From the spectrum measurements, we can clearly see the differences between the different versions again. C/N of the carrier has increased around 10 dB from the original to the final device. However, the harmonics amplitude has been increased too, worsening the first harmonic distortion about 9 dB.

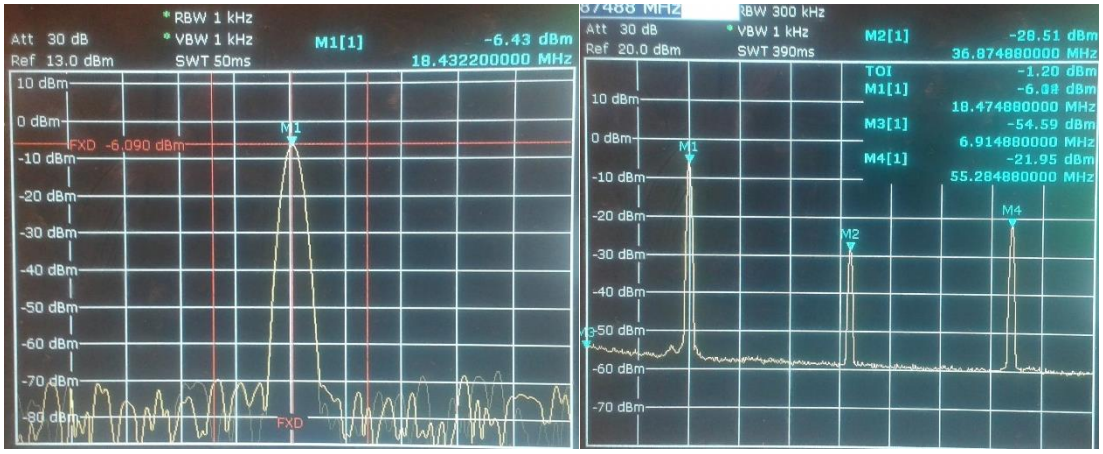

Figure 50 Original basic transmitter C/N (left) and P_{HD} (right) measurements.

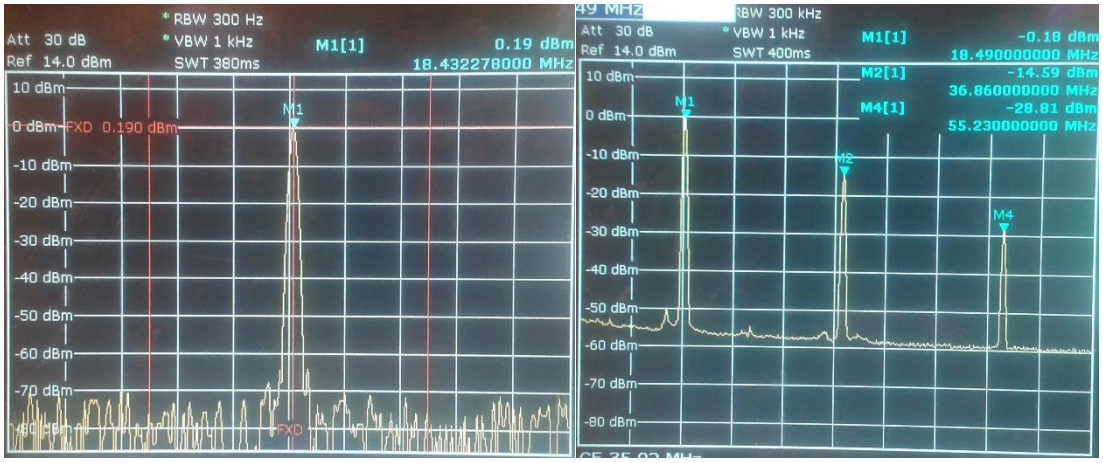

Figure 51 Improved breadboard transmitter C/N (left) and P_{HD} (right) measurements.

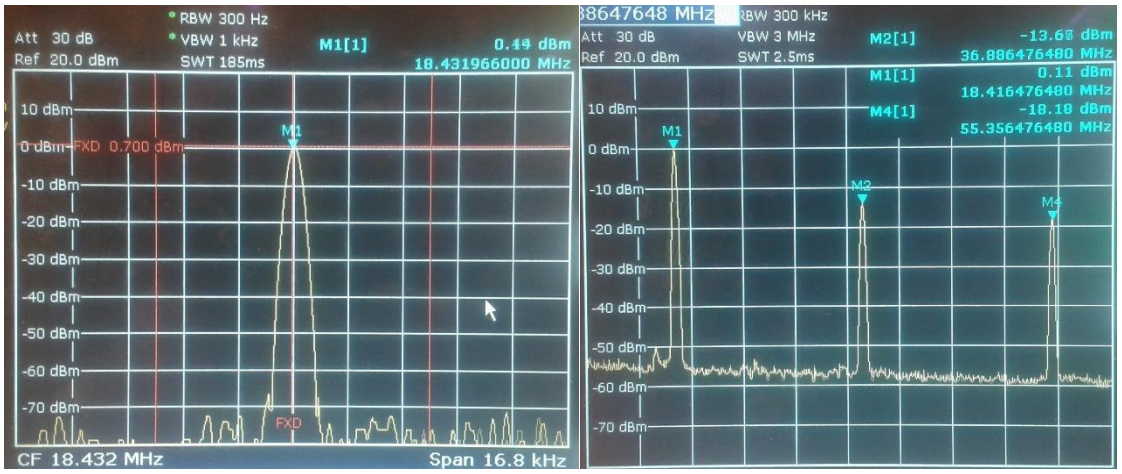

Figure 52 Final PCB transmitter C/N (left) and P_{HD} (right) measurements.

Field testing provides good reception and stability results for both the original and the final device. Voice is received and clearly recognizable. The distance reached by the PCB transmitter is much higher than the original one. Google Maps measurements [75] from field testing show that the **distance is approximately doubled**, as it can be seen in Figure 53 and Figure 54.

Figure 53 Approximate distance (65 m) reached by the original transmitter.

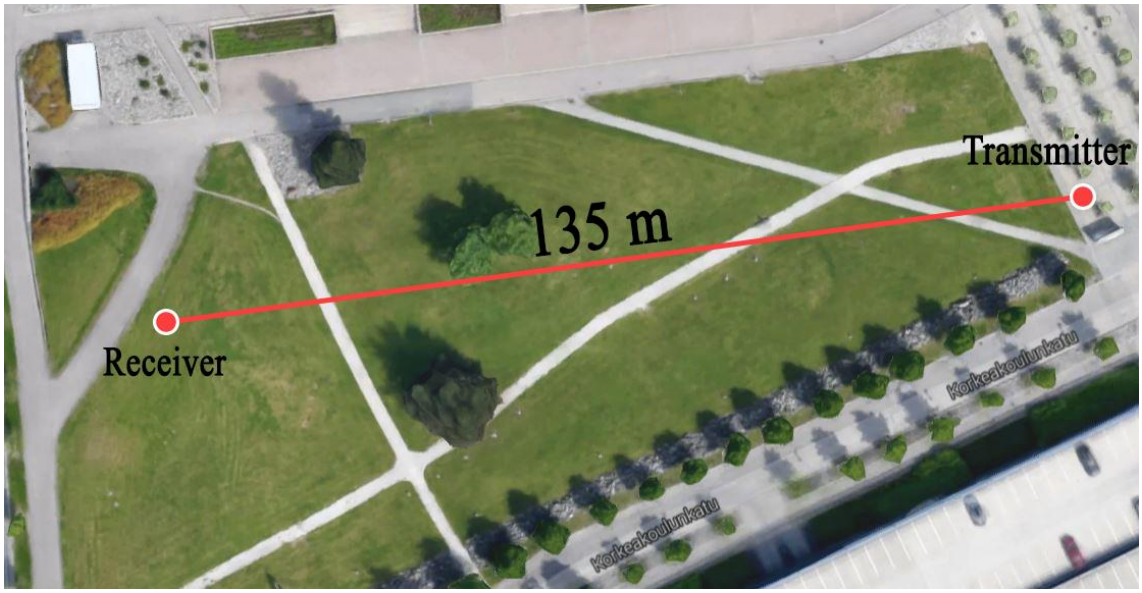

Figure 54 Approximate distance (135 m) reached by the PCB transmitter.

6.1 Materials and components

This section shows all the components used for the AM transmitter prototypes and final PCB design. Prices from the original and the final device are compared. Prices have been taken from Farnell.fi and Digikey.fi at the dates shown in the references, and they may vary in time. They have been taken for 50+ orders in all the cases.

Table 12 Bill of materials for the original basic AM transmitter. Prices at 05/05/16.

Component	Units	Price/unit (€)	Price (€)	Package
18 Ω resistor [76]	1	0.024	0.024	Axial Leaded TH
50 Ω resistor [76]	2	0.07	0.14	Axial Leaded TH
100 Ω resistor [76]	1	0.016	0.016	Axial Leaded TH
220 Ω resistor [76]	1	0.042	0.042	Axial Leaded TH
3.9 kΩ resistor [76]	1	0.029	0.029	Axial Leaded TH
4.7 kΩ resistor [76]	1	0.04	0.04	Axial Leaded TH
10 kΩ resistor [76]	1	0.025	0.025	Axial Leaded TH
18 kΩ resistor [76]	1	0.034	0.034	Axial Leaded TH
20 kΩ (trimmer) Potentiometer [77]	1	1.49	1.49	Square TH
2.2 nF capacitor [78]	4	0.07	0.28	Radial Leaded TH
1 µF capacitor [79]	1	0.037	0.037	Radial Leaded TH
220 µF capacitor [79]	2	0.0561	0.1122	Radial Leaded TH
15 µH inductor [80]	2	0.381	0.762	Axial Leaded TH
2N3904 BJT [40]	1	0.0647	0.0647	TO-92
KSP10 BJT [45]	1	0.298	0.298	TO-92
Red LED [61]	1	0.434	0.434	Radial Leaded TH
ECS-2100 Crystal Oscillator [43]	1	2.125	2.125	4-pin square TH
Electret Microphone [35]	1	1.14	1.14	Round - 4 mm diameter x 1.5 mm width

Table 12 contains all the components and prices for the original transmitter. Table 13 contains all the components for the final PCB transmitter, in which an additional connector and a push-button have been added. Table 13 shows also Assembly ID information for every component, according to the schematic and PCB design in Chapter 5.3.

Table 13 Bill of materials for the final PCB transmitter. Prices at 05/05/16.

Component	Units	Price/unit (€)	Price (€)	Package	Assembly ID
18 Ω resistor [81]	1	0.024	0.024	SMD 1206	RE
22 Ω resistor [81]	1	0.027	0.027	SMD 1207	Ratt2
47 Ω resistor [81]	1	0.07	0.07	SMD 1206	RC2
220 Ω resistor [81]	1	0.042	0.042	SMD 1206	RC1
1 kΩ resistor [81]	1	0.016	0.016	SMD 1207	Rstab
3.9 kΩ resistor [81]	1	0.029	0.029	SMD 1206	Ratt1
10 kΩ resistor [81]	1	0.025	0.025	SMD 1206	Rm
18 kΩ resistor [81]	2	0.04	0.08	SMD 1206	Rbc, Rled
20 kΩ (trimmer) potentiometer [77]	2	1.49	2.98	Square TH	POT1, POT2
68 nF capacitor [82]	4	0.09	0.36	SMD 1206	Cd1, Cc3, Cc4, Cc5
1 µF capacitor [82]	1	0.037	0.037	SMD 1206	Cd2
220 µF capacitor [79]	2	0.0561	0.1122	Radial Leaded TH	Cc1, Cc2
15 µH inductor [80]	3	0.381	1.143	Radial Leaded TH	RFC, RFC2, RFC3
4.7 pF capacitor [82]	1	0.26	0.26	SMD 1206	Ctank2
820 pF capacitor [82]	1	0.0642	0.0642	SMD 1206	Ctank1
Red LED [61]	1	0.434	0.434	Radial Leaded TH	LED
SS9018 BJT [50]	3	0.29	0.87	TO-92	SS9018_1, SS9018_2, SS9018_3
18.432 MHz Quartz Crystal [66]	1	0.284	0.284	Radial Leaded TH	XTAL1
Electret Microphone [83]	1	0.169	0.169	Round d9.7 mm	ELECTRET MICROPHONE
Push-button [84]	1	0.981	0.981	Round d10.6 mm	PUSH-BUTTON
2 pin Wire-to-board connector [68]	1	0.208	0.208	Square TH	WIRE-TO-BOARD CONNECTOR

In addition to the previous components, prototypes require a non-soldering breadboard. PCB transmitter used a double-sided substrate board. There are included in Table 14. The unit price for the breadboard is divided by 4 since the board can be cut so that up to 4 transmitters could be done using the 100 x 160 mm substrate.

Table 14 Substrates prices. Prices at 05/05/16.

Board	Units	Price/unit (€)	Total Price (€)	Package

Breadboard [30]	1	2.11	2.11	400 holes – d0.8 mm holes
Double-sided board [67]	1	7.75 / 4	1.94	100 x 160 mm (52 x 40 mm minimum)

With all the component and substrates information, Table 15 summarizes and compares the prices for the fabrication of the three different versions of the transmitter.

Table 15 Comparison of prices for different versions. Prices at 05/05/16.

Transmitter version	**Total cost (€)**
Original schematic – breadboard prototype	9.20
Optimized schematic – breadboard prototype	10.10
Optimized schematic – PCB	10.14

The price of the original transmitter is the lowest of all of them. It includes the original components and the breadboard price.

The prototype for the breadboard prototype of the optimized schematic includes the components and the breadboard prices. It **increases around 10% the overall price**. It is mainly because of the BJT prices and the addition of the second potentiometer, used in the oscillator block. Replacing this potentiometer with fixed value resistors would decrease the cost considerably: from 10.10 € to 8.67 € according to the prices at 05/05/16. This means that the improved schematic could be prototyped on a breadboard with less cost than the original one.

The final PCB version has a higher price also, because of the addition of the connector, the push-button, and the substrate.

6.2 Comparison of results

With all the previous results, the PCB transmitter performance has been summarized and compared to the previous prototype and the original device as it can be seen in the Table 16.

Table 16 Comparison between characteristics of the original transmitter, the optimized breadboard prototype and the optimized PCB transmitter.

	Original schematic - breadboard	**Optimized sch. - breadboard**	**Optimized sch. - PCB**
Carrier C/N	~65 dB	~75 dB	~75 dB
P_{HD}	22.5 dBc	14.4 dBc	13.8 dBc

DC Voltage	4.5 V	4.5 V	4.5 V
DC Current	38 mA	29 mA	28 mA
Output AM Power (4 kHz tone)	0.287 mW	1.129 mW	1.097 mW
Power Efficiency (4 kHz tone)	0.168 %	0.865 %	0.870 %
Alkaline battery lifetime	~26.3 h	~34.5 h	~35.7 h
Transmission distance	~65 m	-	~130 m
Price	9.2 €	10.10 €	10.14 €

Carrier C/N ratio has been increased around 10 dB from the original to the improved version, which is translated into a better signal delivery to the antenna. On the other hand, the **first harmonic distortion has been worsened more than 9 dB**: this is the weakest point of the PCB transmitter. Even when the custom crystal oscillator design is better in terms of power consumption, we have to face the trade-off of the decreasing value for the P_{HD} since it is not as good as the original in rejecting harmonics. Nevertheless, the transmission distance has been increased (around the double) because of the higher power delivery to the antenna.

Results for the PCB transmitter are around **5 times higher** than the original one in terms of **power efficiency**. Efficiency remains under the 1%, so it is still obviously very low, but taking into account that the circuit design has been kept as simple as the original, this increase can be considered as a good result.

The lifetime of the batteries has been increased because of the reduced power consumption. Considering that the typical **capacity for alkaline batteries** is around 1000 mAh [85]–[87], the batteries lifetime for this device will be approximately 35.7 hours of use, against the ~26.3 hours of the original device.

Additionally, the PCB design has other advantages such as **reliability** against external stresses, and a **smaller** and more **user-friendly form factor** than the breadboard prototype. For the user, the transmitter appears as a black-box with a push-to-talk button and the antenna connector. The LED will also indicate the user that the battery is still working and he can use the device when pushing the button.

From a commercial perspective, the performance of the final device is not really competitive. Current consumption is much higher compared to the 5 mA of some commercial modules [4], [88], [89] for sensing, remote control or security tasks. For broadcasting, AM broadcast transmitter TR-6000 [90] reaches 41% power efficiency, with 10 watts output power. P_{HD} is 35 dBc minimum, which is considerably better than the 13.8 dBc of our AM transmitter.

6.3 Debug information

The following tables (from Table 17 to Table 21) show detailed information of the **different blocks** of the AM transmitter. They provide measurements for different parameters so that they could be checked and tested when replicating the transmitter fabrication. All data refers to the **improved schematic**, built on the **breadboard** prototype and the final **PCB** version.

Notice that almost every value remains very similar between the PCB and the breadboard prototype, but the noise measured in at the microphone and the LED has been reduced.

Table 17 Microphone block debug information.

	Breadboard transmitter	**PCB transmitter**
Output DC Voltage	2.41 V	2.34 V
High-frequency Noise (without audio input)	50 mVpp	27 mVpp

Table 18 Audio amplifier block debug information.

	Breadboard transmitter	**PCB transmitter**
Base DC voltage $V_{B\text{-}AMP}$	1 V	0.98 V
DC Current	9.20 mA	9.15 mA
Gain	12 dB	7.7 dB

Table 19 Amplitude modulator block debug information.

	Breadboard transmitter	**PCB transmitter**
Base DC voltage $V_{B\text{-}MOD}$	0.82 V	0.82 V
DC Current	17.4 mA	15.5 mA
Gain (without audio input)	32 dB	37.2 dB

Table 20 Oscillator + attenuator blocks debug information.

	Breadboard transmitter	**PCB transmitter**
Oscillation frequency f_o	18.432 MHz	18.432 MHz
DC Current	2.10 mA	3.21 mA
Base DC voltage $V_{B\text{-}OSC}$	0.74 V	0.73 V
Oscillator output voltage	10.6 Vpp	13.8 Vpp
Attenuator output voltage	65 mVpp	70 mVpp
Attenuation	44.25 dB	45.89 dB

Table 21 LED indicator block debug information.

	Breadboard transmitter	**PCB transmitter**

DC Current	0.15 mA	0.16 mA
High-frequency Noise	300 mVpp	45 mVpp

7. CONCLUSIONS

The process of optimizing a transmitter requires a wide technical background, in which very different matters are essential to get the final results. This project itself combines many different engineering tasks such as circuit analysis, laboratory equipment usage, circuit simulation, circuit design, PCB layout and fabrication, or 3D modelling. An organized methodology and schedule, and complete documentation of every task are essential for the project to run smoothly. Table 22 helps to have an overview of the project.

Analytic characterization has been very important in the optimization process. Analog and RF electronics concepts are essential to understand the transmitter working, and how changes may affect the circuit behavior. In addition to that, decision making and trade-off analysis played important roles. They were necessary when implementing improvements to the schematic, and also when designing the PCB and the user interface for the final device.

As it was commented in Chapter 6.2, commercial devices offer better characteristics. These comparisons are just for providing some additional information. The original purpose of the AM transmitter optimized in this project is very different from the commercial cases. For that reason, from an optimization point of view the results are good. Optimization itself implies the improvement of the device characteristics so that they fit the best as possible with the cases of use, without any waste of resources.

All the objectives and requirements have been considered during the whole project, and the final schematic complies with the simplicity restriction. Power efficiency, signal-to-noise ratio, transmission distance, and power consumption have been quantitatively improved. Moreover, a reliable and small-sized product has been fabricated which will be used as the demonstration device in the *Practical RF Electronics* course.

Table 22 Summary of the characteristics and results of the optimization project.

Objective	Optimization and fabrication of a basic AM transmitter
Case of use	Didactic demonstration for RF students
Main restrictions	Keep it as simple as the original one
Strengths of the optimized transmitter	26% decreased power consumption +9.4 h battery lifetime x5 power efficiency x2 transmission distance Simple schematic Reduced size More reliable PCB form factor User-friendly interface
Weaknesses of the optimized transmitter	-9 dB P_{HD}
Technical background	Analog electronics Audio amplifiers Power efficiency Feedback Oscillators AM modulation PCB design and fabrication 3D design and printing

Further research can be done to improve certain points of the transmitter. We could work on the characterization of the parasitic elements of the circuit, affecting the behavior of the LC oscillator. From there, one can develop a more precise model to design and select the frequency and current consumption of the LC oscillator and the crystal oscillator. Additionally, EMC shields can be designed together with the packaging part to isolate the PCB from external electromagnetic interferences. This may help to reduce the variations in the frequency when using an LC oscillator.

Another point is the design and fabrication of the antenna, as an additional component matching the purpose of the transmitter.

If the **modifications for** the transmitter were **not that restricted**, many varied approaches could have been taken for this optimization. More complex schematic designs for the audio amplifier block such as Class-B, C, E or AB amplifiers [13], [38], [91], [92] would provide much higher power efficiency, at expense of a more distorted signal.

Using a high-level amplitude modulator [1], [93], [94] would increase the output power and also the efficiency. We could even include additional amplifier blocks, or filter blocks to reduce the harmonics power [95]. After studying the characteristics of the antenna, which was not included as mentioned before, an impedance matching network [96]–[98] could have been designed to provide the maximum power delivery from the output of the modulator to the antenna.

PCB design could be approached differently also, if the fabrication were carried out with industrial equipment. Wave soldering techniques [99] and computer controlled manufacturing processes can produce smaller circuits and also place much smaller components [100] without any problem.

REFERENCES

[1] C. V. Domine Leenaerts Johan van der Tang, *Circuit Design for RF Transceivers*. Kluwer Academic Publishers, 2001.

[2] "Amplitude Modulation: What is AM," *Radio-electronics*. [Online]. Available: http://www.radio-electronics.com/info/rf-technology-design/am-amplitude-modulation/what-is-am-tutorial.php. [Accessed: 05-May-2016].

[3] "Reginald Fessenden," *Wikipedia*. [Online]. Available: https://en.wikipedia.org/wiki/Reginald_Fessenden. [Accessed: 05-May-2016].

[4] "AM Transmitter Module QAM-TX1," *Quasar UK*. [Online]. Available: http://docs-europe.electrocomponents.com/webdocs/087d/0900766b8087d2df.pdf. [Accessed: 05-May-2016].

[5] "Airband," *Wikipedia*. [Online]. Available: https://en.wikipedia.org/wiki/Airband. [Accessed: 05-May-2016].

[6] "ELT-41727 Study Guide 2015-2016," *Tampere University of Technology*. [Online]. Available: http://www.tut.fi/wwwoppaat/opas2015-2016/kv/laitokset/Elektroniikka_ja_tietoliikennetekniikka/ELT-41727.html. [Accessed: 05-May-2016].

[7] D. Kennedy, *Electronic Communication Systems*. McGRAW-HILL, 1993.

[8] "Data Communications course," *La Trobe University*. [Online]. Available: http://ironbark.xtelco.com.au/subjects/DC/lectures/7/. [Accessed: 05-May-2016].

[9] "Ampplitude Modulation Fundamentals," *PA2OLD*. [Online]. Available: http://www.pa2old.nl/files/am_fundamentals.pdf. [Accessed: 05-May-2016].

[10] "Electrical efficiency," *Wikipedia*. [Online]. Available: https://en.wikipedia.org/wiki/Electrical_efficiency. [Accessed: 05-May-2016].

[11] "Electric Power Efficiency," *RapidTables*. [Online]. Available: http://www.rapidtables.com/electric/efficiency.htm. [Accessed: 05-May-2016].

[12] "Power Amplifier Efficiency Explained," *Elliot Sound Products*. [Online]. Available: http://sound.westhost.com/efficiency.htm. [Accessed: 05-May-2016].

[13] G. Hanington, P. F. Chen, V. Radisic, T. Itoh, and P. M. Asbeck, "Microwave power amplifier efficiency improvement with a 10 MHz HBT DC-DC converter," in *Microwave Symposium Digest, 1998 IEEE MTT-S International*, 1998, vol. 2, pp. 589–592.

[14] "Feedback Oscillators," *University of St Andrews*. [Online]. Available: https://www.st-

andrews.ac.uk/~www_pa/Scots_Guide/RadCom/part4/page1.html. [Accessed: 05-May-2016].

[15] E. Messer, "Oscillators Theory and Practice," in *Harris/Intersll Amateur Radio Club*.

[16] "Barkhausen Stability Criterion," *MIT*. [Online]. Available: http://web.mit.edu/klund/www/weblatex/node4.html. [Accessed: 05-May-2016].

[17] "Barkhausen Stability Criterion," *Wikipedia*. [Online]. Available: https://en.wikipedia.org/wiki/Barkhausen_stability_criterion. [Accessed: 05-May-2016].

[18] "Oscillators," *Majmaah University*. [Online]. Available: http://faculty.mu.edu.sa/public/uploads/1400394697.1447Ch16 - Oscillators.pdf. [Accessed: 05-May-2016].

[19] G. Gonzalez, *Foundations of Oscillator Circuit Design*. Artech House, 2007.

[20] "Oscillator Stability," *The University of Kansas*. [Online]. Available: http://www.ittc.ku.edu/~jstiles/622/handouts/Oscillator Stability.pdf.

[21] "Clock Oscillator Stability," *DigiKey*. [Online]. Available: http://www.digikey.kr/en/pdf/c/cardinal/clock-oscillator-stability. [Accessed: 05-May-2016].

[22] "Colpitts Oscillator," *CircuitsToday*. [Online]. Available: http://www.circuitstoday.com/colpitts-oscillator. [Accessed: 05-May-2016].

[23] "LC Oscillators and Types," *CircuitsToday*. [Online]. Available: http://www.circuitstoday.com/lc-oscillators-and-types. [Accessed: 05-May-2016].

[24] "Simple Parallel (Tank Circuit) Resonance," *All About Circuits*. [Online]. Available: http://www.allaboutcircuits.com/textbook/alternating-current/chpt-6/parallel-tank-circuit-resonance/. [Accessed: 05-May-2016].

[25] "Clapp Oscillator," *CircuitsToday*. [Online]. Available: http://www.circuitstoday.com/clapp-oscillator. [Accessed: 05-May-2016].

[26] "Quartz Crystal Theory," *Jauch Quartz GmbH*. [Online]. Available: http://www.jauch.de/ablage/med_00000818_1327049076_Quartz Crystal Theory 2007.pdf. [Accessed: 05-May-2016].

[27] R. J. Matthys, *Crystal Oscillator Circuits*. Krieger Pub Co, 1991.

[28] "Who uses ADS?," *KeySight Technologies*. [Online]. Available: http://www.keysight.com/main/editorial.jspx?cc=FI&lc=fin&ckey=1788468&nid=-34346.0.02&id=1788468. [Accessed: 05-May-2016].

[29] "ADS Key Features," *KeySight Technologies*. [Online]. Available: http://literature.cdn.keysight.com/litweb/pdf/5990-6464EN.pdf?id=1608816. [Accessed: 05-May-2016].

[30] "Breadboard 400 pin," *Farnell*. [Online]. Available: http://fi.farnell.com/pro-signal/psg-bb-400/breadboard-400-pin-white/dp/2503765?MER=en-me-sr-b-all. [Accessed: 05-May-2016].

[31] "Human Speech Spectrum, Frequency Range, Formants," *AV Info*. [Online]. Available: http://www.bnoack.com/index.html?http&&&www.bnoack.com/audio/speech-level.html. [Accessed: 05-May-2016].

[32] S. A. Gelfand, *Essentials of audiology*. New York: Thieme, 2007, 2007.

[33] "AN-1149 Layout Guidelines for Switching Power Supplies," *Texas Instruments*. [Online]. Available: http://www.ti.com/lit/an/snva021c/snva021c.pdf. [Accessed: 05-May-2016].

[34] "Via," *Wikipedia*. [Online]. Available: https://en.wikipedia.org/wiki/Via_(electronics). [Accessed: 05-May-2016].

[35] "Pro-Signal ABM-715-RC Electret Microphone," *Farnell*. [Online]. Available: http://fi.farnell.com/pro-signal/abm-715-rc/electret-microphone-omni-leads/dp/2066501. [Accessed: 05-May-2016].

[36] "Electret Microphone," *Wikipedia*. [Online]. Available: https://en.wikipedia.org/wiki/Electret_microphone. [Accessed: 05-May-2016].

[37] "Electret Condenser Microphone Basics," *Digi-Key*. [Online]. Available: http://www.digikey.pt/en/pdf/p/pui-audio/pui-audio-electret-condenser-microphone-basics?redirected=1. [Accessed: 05-May-2016].

[38] "Amplifier Classes," *ElectronicsTutorials*. [Online]. Available: http://www.electronics-tutorials.ws/amplifier/amplifier-classes.html. [Accessed: 05-May-2016].

[39] B. G. Ludwig Reinhold, *RF Circuit Design: Theory and Applications*, First. Prentice Hall, 2008.

[40] "2N3904 BJT Datasheet," *Sparkfun*. [Online]. Available: https://www.sparkfun.com/datasheets/Components/2N3904.pdf. [Accessed: 05-May-2016].

[41] "What is a coupling capacitor," *LearningAboutElectronics*. [Online]. Available: http://www.learningaboutelectronics.com/Articles/What-is-a-coupling-capacitor. [Accessed: 05-May-2016].

[42] N. Storey, *Electronics: A systems approach*, Fourth. Pearson Education, 2009.

[43] “18.432 MHz ECS-2100 Crystal Oscillator,” *Digi-Key*. [Online]. Available: http://www.digikey.com/product-search/en?mpart=ECS-2100A-184&vendor=50. [Accessed: 05-May-2016].

[44] “Voltage Dividers,” *Sparkfun*. [Online]. Available: https://learn.sparkfun.com/tutorials/voltage-dividers. [Accessed: 05-May-2016].

[45] “KSP10 BJT Datasheet,” *Fairchild Semiconductor*. [Online]. Available: https://www.fairchildsemi.com/datasheets/KS/KSP10.pdf. [Accessed: 05-May-2016].

[46] “Choke (electronics),” *Wikipedia*. [Online]. Available: https://en.wikipedia.org/wiki/Choke_(electronics). [Accessed: 05-May-2016].

[47] H. Sekiya and M. K. Kazimierczuk, “Design of RF-choke inductors using core geometry coefficient,” in *Proc. Electrical Manufacturing and Coil Winding Conf*, 2009.

[48] “Harmonic Distortion Measurement White Paper,” *National Instruments*. [Online]. Available: http://www.ni.com/white-paper/3401/en/. [Accessed: 05-May-2016].

[49] M. H. Jones, *A practical introduction to electronic circuits*. Cambridge University Press, 1995, p. 148.

[50] “SS9018 BJT Datasheet,” *Fairchild Semiconductor*. [Online]. Available: https://www.fairchildsemi.com/datasheets/SS/SS9018.pdf. [Accessed: 05-May-2016].

[51] “2N930A BJT Datasheet,” *Farnell*. [Online]. Available: http://www.farnell.com/datasheets/1677188.pdf. [Accessed: 05-May-2016].

[52] “2N2857 BJT Datasheet,” *Central Semiconductor Corp*. [Online]. Available: https://www.centralsemi.com/get_document.php?cmp=1&mergetype=pd&mergepath=pd&pdf_id=2n2857.PDF. [Accessed: 05-May-2016].

[53] “2N5088 BJT Datasheet,” *Fairchild Semiconductor*. [Online]. Available: https://www.fairchildsemi.com/datasheets/2N/2N5088.pdf. [Accessed: 05-May-2016].

[54] “2N5179 BJT Datasheet,” *Microsemi*. [Online]. Available: http://www.microsemi.com/document-portal/doc_view/6087-2n5179-rev-pdf. [Accessed: 05-May-2016].

[55] “2N2484 BJT Datasheet,” *Central Semiconductor Corp*. [Online]. Available: https://www.centralsemi.com/get_document.php?cmp=1&mergetype=pd&mergepath=pd&pdf_id=2n2484.PDF. [Accessed: 05-May-2016].

[56] “2N5210 BJT Datasheet,” *Central Semiconductor Corp*. [Online]. Available: https://www.centralsemi.com/get_document.php?cmp=1&mergetype=pd&mergepath=pd&pdf_id=2N5209-10.PDF. [Accessed: 05-May-2016].

[57] “KSC1845 BJT Datasheet,” *Fairchild Semiconductor*. [Online]. Available: https://www.fairchildsemi.com/datasheets/KS/KSC1845.pdf. [Accessed: 05-May-2016].

[58] “NTE107 BJT Datasheet,” *NTE Electronics Inc*. [Online]. Available: http://www.nteinc.com/specs/100to199/pdf/nte107.pdf. [Accessed: 05-May-2016].

[59] R. Fiore, “Capacitors in Coupling and DC Blocking Applications,” *Circuit Des. Notebooks. ATC*, pp. 1–927, 2001.

[60] R. Fiore, “Practical Capacitor Tolerance Selection for Coupling, DC Blocking and Bypass Applications,” *Microw. Prod. Dig.*, 2001.

[61] “Kingbright L-934LSRD LED,” *Farnell*. [Online]. Available: http://fi.farnell.com/kingbright/l-934lsrd/led-low-current-3mm-red/dp/1142514. [Accessed: 05-May-2016].

[62] E. F. Schubert, T. Gessmann, and J. K. Kim, *Light emitting diodes*. Wiley Online Library, 2005.

[63] Y. Chen, K. Mouthaan, and B.-L. Ooi, “Performance enhancement of Colpitts oscillators by parasitic cancellation,” *Circuits Syst. II Express Briefs, IEEE Trans.*, vol. 55, no. 11, pp. 1114–1118, 2008.

[64] T. W. Brown, F. Farhabakhshian, A. G. Roy, T. S. Fiez, and K. Mayaram, “A 475 mV, 4.9 GHz enhanced swing differential Colpitts VCO with phase noise of-136 dBc/Hz at a 3 MHz offset frequency,” *Solid-State Circuits, IEEE J.*, vol. 46, no. 8, pp. 1782–1795, 2011.

[65] “Solderless Breadboard Capacitance,” *EEVblog*. [Online]. Available: http://www.eevblog.com/forum/blog/eevblog-568-solderless-breadboard-capacitance/. [Accessed: 05-May-2016].

[66] “TXC 9B-18.432MAAJ-B XTAL - 18.432 MHz,” *Farnell*. [Online]. Available: http://fi.farnell.com/txc/9b-18-432maaj-b/xtal-18-432mhz-18pf-hc-49s/dp/1842220. [Accessed: 05-May-2016].

[67] “PCB double-sided board - FR4, Epoxy Glass Composite,” *Farnell*. [Online]. Available: http://fi.farnell.com/mega/3204911/pcb-fr4-100x160-ss/dp/3204911/false. [Accessed: 05-May-2016].

[68] “Lumberg KRMC Wire-to-Board connector,” *Farnell*. [Online]. Available: http://fi.farnell.com/lumberg/krmc-02/terminal-block-wire-to-brd-2pos/dp/1217302/false. [Accessed: 05-May-2016].

[69] "SolidWorks," *Dassault Systems*. [Online]. Available: http://www.solidworks.com/.

[70] M. Pecht, D. Das, and A. Ramakrishnan, "The IEEE standards on reliability program and reliability prediction methods for electronic equipment," *Microelectron. Reliab.*, 2002.

[71] H. Lu, C. Bailey, and C. Yin, "Design for reliability of power electronics modules," *Microelectron. Reliab.*, vol. 49, no. 9, pp. 1250–1255, 2009.

[72] D. Kececioglu and F.-B. Sun, *Environmental Stress Screening: Its Quantification, Optimization and Management*. DEStech Publications, Inc, 2003.

[73] "KeyShot," *Luxion*. [Online]. Available: https://www.keyshot.com/.

[74] "Prenta DUO 3D Printer," *Prenta*. [Online]. Available: http://www.prenta.fi/en/3d-printers-services/3d-tulostimet/prenta-duo. [Accessed: 05-May-2016].

[75] "Measure distance between points," *Google Maps Help*. [Online]. Available: https://support.google.com/maps/answer/1628031?co=GENIE.Platform=Desktop&hl=en. [Accessed: 05-May-2016].

[76] "Through Hole Resistors," *Farnell*. [Online]. Available: http://fi.farnell.com/through-hole-resistors/prl/tulokset. [Accessed: 05-May-2016].

[77] "Trimmer Potentiometer 25 turns 20k," *Farnell*. [Online]. Available: http://fi.farnell.com/bourns/3296y-1-203lf/trimmer-25-turn-20k/dp/9353585. [Accessed: 05-May-2016].

[78] "Ceramic disc and plate capacitors," *Farnell*. [Online]. Available: http://fi.farnell.com/ceramic-disc-plate-capacitors/prl/tulokset. [Accessed: 05-May-2016].

[79] "Aluminium Electrolytic capacitors - leaded," *Farnell*. [Online]. Available: http://fi.farnell.com/aluminium-electrolytic-capacitors-leaded/prl/tulokset. [Accessed: 05-May-2016].

[80] "HF Axial Leaded Inductors," *Farnell*. [Online]. Available: http://fi.farnell.com/high-frequency-inductors-axial-leaded/prl/tulokset. [Accessed: 05-May-2016].

[81] "Chip SMD 1206 resistors," *Farnell*. [Online]. Available: http://fi.farnell.com/webapp/wcs/stores/servlet/Search?catalogId=15001&langId=358&storeId=10159&categoryId=700000005450&beginIndex=1&showResults=true&aa=true&pf=110421912. [Accessed: 05-May-2016].

[82] "Ceramic Multilayer MLCC Capacitors - SMD 1206." [Online]. Available: http://fi.farnell.com/webapp/wcs/stores/servlet/Search?catalogId=15001&langId=

358&storeId=10159&categoryId=700000005423&beginIndex=1&showResults=true&aa=true&pf=111854956. [Accessed: 05-May-2016].

[83] "MULTICOMP MCKPCM-97H45P-40DB-4808 MICROPHONE," *Farnell*. [Online]. Available: http://fi.farnell.com/multicomp/mckpcm-97h45p-40db-4808/microphone-omnidirection-16khz/dp/2396073?selectedCategoryId=&exaMfpn=true&categoryId=&searchRef=SearchLookAhead. [Accessed: 05-May-2016].

[84] "MULTICOMP R13-509A-05-BB Pushbutton Switch," *Farnell*. [Online]. Available: http://fi.farnell.com/multicomp/r13-509a-05-bb/switch-spst-no-mom-black-3a/dp/1634682. [Accessed: 05-May-2016].

[85] "4903 AAA Alkaline Battery Datasheet," *Farnell*. [Online]. Available: http://www.farnell.com/datasheets/39630.pdf. [Accessed: 05-May-2016].

[86] "Battery Capacity," *Techlib*. [Online]. Available: http://www.techlib.com/reference/batteries.html. [Accessed: 05-May-2016].

[87] "Battery Life," *BatterySavers*. [Online]. Available: http://batterysavers.com/Compare-Batteries.html. [Accessed: 05-May-2016].

[88] "AM Transmitter Module QAM-TX3 Datasheet," *Quasar UK*. [Online]. Available: http://datasheet.octopart.com/QAM-TX3-Quasar-Remote-Controls-datasheet-11039545.pdf. [Accessed: 05-May-2016].

[89] "AM Transmitter Module QAMT2-XXX Datasheet," *Farnell*. [Online]. Available: http://www.farnell.com/datasheets/8039.pdf. [Accessed: 05-May-2016].

[90] "Radio Systems TR-6000 AM BROADCAST TRANSMITTER Operating Instructions," *TalkingHouse*. [Online]. Available: http://www.talkinghouse.com/manuals/TR-6000Manual04-12.pdf. [Accessed: 05-May-2016].

[91] "Class C Amplifier," *University of San Diego*. [Online]. Available: http://home.sandiego.edu/~ekim/e194rfs01/lec24ek.pdf. [Accessed: 05-May-2016].

[92] S. C. Cripps, "RF Power Amplifiers for Wireless Communications, (Artech House Microwave Library)," *Artech House*, 2006.

[93] D. R. Anderson and W. H. Cantrell, "High-efficiency high-level modulator for use in dynamic envelope tracking CDMA RF power amplifiers," in *Microwave Symposium Digest, 2001 IEEE MTT-S International*, 2001, vol. 3, pp. 1509–1512.

[94] M. Kazimierczuk, "Collector amplitude modulation of the class E tuned power amplifier," *Circuits Syst. IEEE Trans.*, vol. 31, no. 6, pp. 543–549, 1984.

[95] G. J. Wakileh, *Power systems harmonics: fundamentals, analysis and filter design*. Springer Science & Business Media, 2001.

[96] "Impedance Matching," *Electronic Design*. [Online]. Available: http://electronicdesign.com/communications/back-basics-impedance-matching-part-1. [Accessed: 05-May-2016].

[97] G. Marrocco, "The art of UHF RFID antenna design: impedance-matching and size-reduction techniques," *Antennas Propag. Mag. IEEE*, vol. 50, no. 1, pp. 66–79, 2008.

[98] H. F. Pues and A. R. Van De Capelle, "An impedance-matching technique for increasing the bandwidth of microstrip antennas," *Antennas Propagation, IEEE Trans.*, vol. 37, no. 11, pp. 1345–1354, 1989.

[99] T. A. Updike, R. S. King, and M. T. Coles, "Method of wave soldering thin laminate circuit boards." Google Patents, 2001.

[100] "Pick and place machines," *SMTmax*. [Online]. Available: http://www.smtmax.com/category.php?id=15&gclid=CjwKEAjwxoG5BRCC7ezlzNmR8HUSJAAre36jkycVp46n-VYRPDDVv0c97t7RnPAiReYKJmM38s1vDBoCbUzw_wcB. [Accessed: 27-Apr-2016].

[101] "33120A Function/Arbitrary Waveform Generator Datasheet," *KeySight Technologies*. [Online]. Available: http://literature.cdn.keysight.com/litweb/pdf/5968-0125EN.pdf?id=1000032746:epsg:dow. [Accessed: 05-May-2016].

[102] "InfiniiVision 3000 X-Series Oscilloscopes Datasheet," *KeySight Technologies*. [Online]. Available: http://literature.cdn.keysight.com/litweb/pdf/5990-6619EN.pdf?id=2002858. [Accessed: 05-May-2016].

[103] "PL & PL-P series Datasheet," *TTi*. [Online]. Available: http://www.farnell.com/datasheets/1796750.pdf. [Accessed: 05-May-2016].

[104] "R&S FSL Spectrum Analyzer Datasheet," *Rohde & Schwarz*. [Online]. Available: https://cdn.rohde-schwarz.com/pws/dl_downloads/dl_common_library/dl_brochures_and_datasheets/pdf_1/FSL_dat-sw_en_0758-2790-22_v1100.pdf. [Accessed: 05-May-2016].

[105] "UV-Belichtungsgeräte AKTINA S Serie," *Walter Lemmen*. [Online]. Available: http://www.walterlemmen.de/images/pdf/UV-Belichtungsgeraete_AKTINA-S.pdf. [Accessed: 05-May-2016].

[106] "Manufacture of Printed Circuit Boards," *TechnologyStudent*. [Online]. Available: http://www.technologystudent.com/pcb/PCB3A.htm. [Accessed: 05-May-2016].

[107] “EPEC How to Build a Circuit Board,” *SlideShare*. [Online]. Available: http://www.slideshare.net/epectec/how-to-build-a-circuit-board-boot-camp. [Accessed: 05-May-2016].

[108] K. Arita and T. Nishimura, “Soldering flux.” Google Patents, 1995.

APPENDIX 1. LABORATORY EQUIPMENT

Waveform Generator HP 33120A. [101]

Oscilloscope Keysight InfiniiVision DSO-X 3035A. [102]

DC Power Supply TTI PL303QMD. [103]

Spectrum Analyzer Rohde & Schwarz FSL. [104]

Ultra-violet exposure unit Aktina S from Walter Lemmen. [105]

APPENDIX 2. PCB FABRICATION PROCESS

The process involves many different steps [106], [107]:

1. **Export** and **print** on transparencies the exposure masks for both top and bottom copper layers in the circuit board. Top layer mask may be flipped when printing, so that the final result will be right when flipping again the transparency over the board.
2. Cut the circuit board to the **final circuit size** and remove the protective tape layer.
3. **Align** both masks together using printed alignment marks and place the circuit board between them so that the masks fit correctly.
4. Figure 55 includes a picture of the exposure unit [105] used for the **exposure** step. The board is exposed to the UV radiation during 50 seconds while the traces layout is masked by the transparency prints.

Figure 55 Walter Lemmen Aktina S UV exposure unit. [105]

5. **Develop**: acetone is used just some seconds to reveal the copper by removing the exposed photoresist layer. Masked photoresist will stay covering the copper.
6. **Etch**: remove the copper that has not been covered by the exposure mask, so that the desired pattern stays over the substrate. A chemical etching solution made of 80 ml H_2O + 30 ml H_2O_2 + 30 ml HCl is used for this step. The PCB may be cleaned with water afterwards.
7. **Remove** the photoresist using acetone again. Clean and dry the PCB.
8. Visual and electrical **inspection**. Check all the traces visually and electrically using a multimeter.
9. **Drill** all the required holes in the board for the TH connections and vias.
10. Check the schematic and the PCB assembly drawings, **solder** every component on the correct place and position. No-clean **Flux** have been added to the pads for facilitate the soldering and prevent oxidation [108].
11. Final visual and electrical **inspection**, checking every connection using a multimeter and looking for possible errors or short circuits.

APPENDIX 3. ANALYSIS OF THE AUDIO AMPLIFIER DISTORTION

Looking for the source of the audio amplifier distortion, we add a diode in parallel to the resistive load at the output. This diode simulates the PN junction of the transistor from the AM step. Figure 56 includes the schematic for the simulations in ADS.

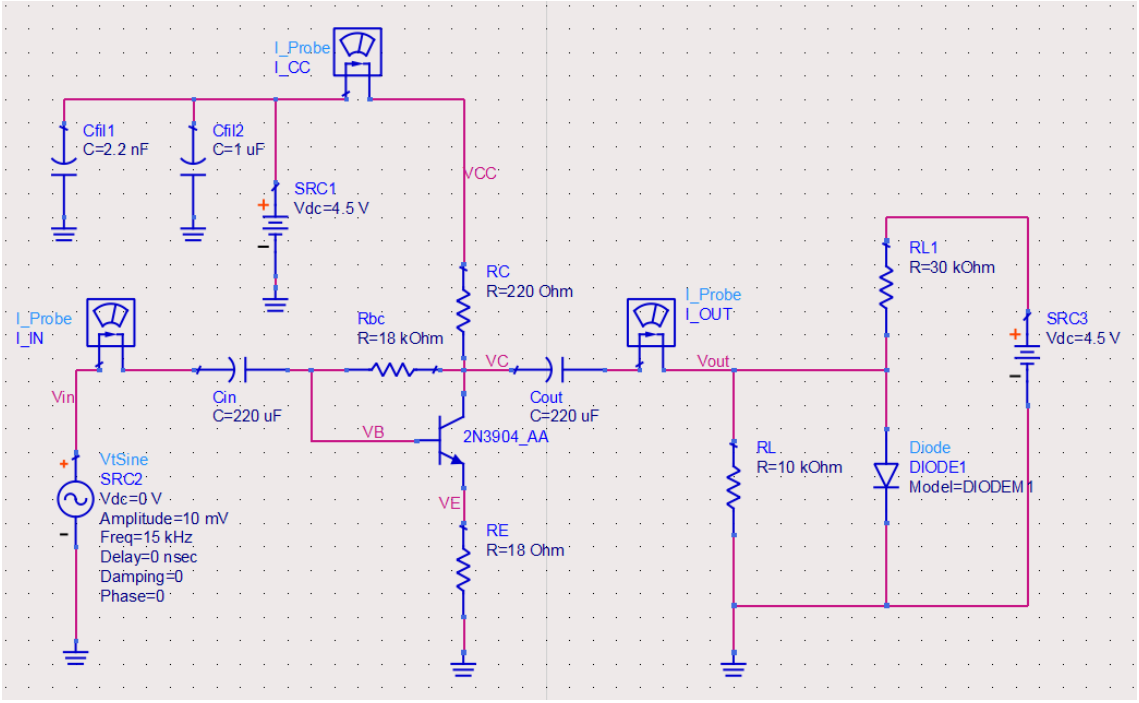

Figure 56 ADS schematic for the Audio Amplifier non-linearity study. Diode load.

The PN junction has also a biasing circuit that makes it work forwarded, and we can appreciate that during the upper cycles of the input signal the gain is higher because the amplifier signal can go deeper. During the lower input cycles, the gain is lower when the voltage in the PN junction gets saturated. See Figure 57.

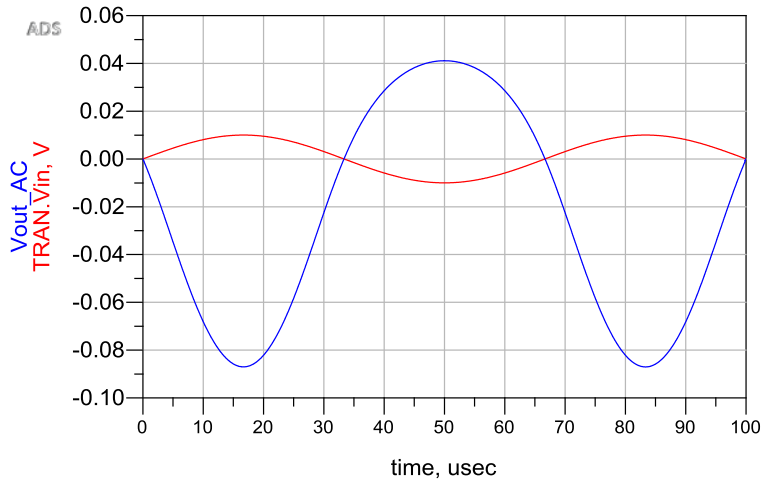

Figure 57 Audio Amplifier output (blue) and input (red) voltages with PN junction load.

This is almost the same waveform that be obtained when simulating the entire system. It makes the transmitter to distort the final AM signal, since the modulation is made according to the distorted waveform coming from the audio amplifier.

For improving this, we can add a resistor between the PN junction and the ground as seen in Figure 58. The output voltage of the amplifier will not be the same as the PN junction voltage, but the junction voltage added to the voltage drop in the series resistor. This voltage will adapt to the input variations.

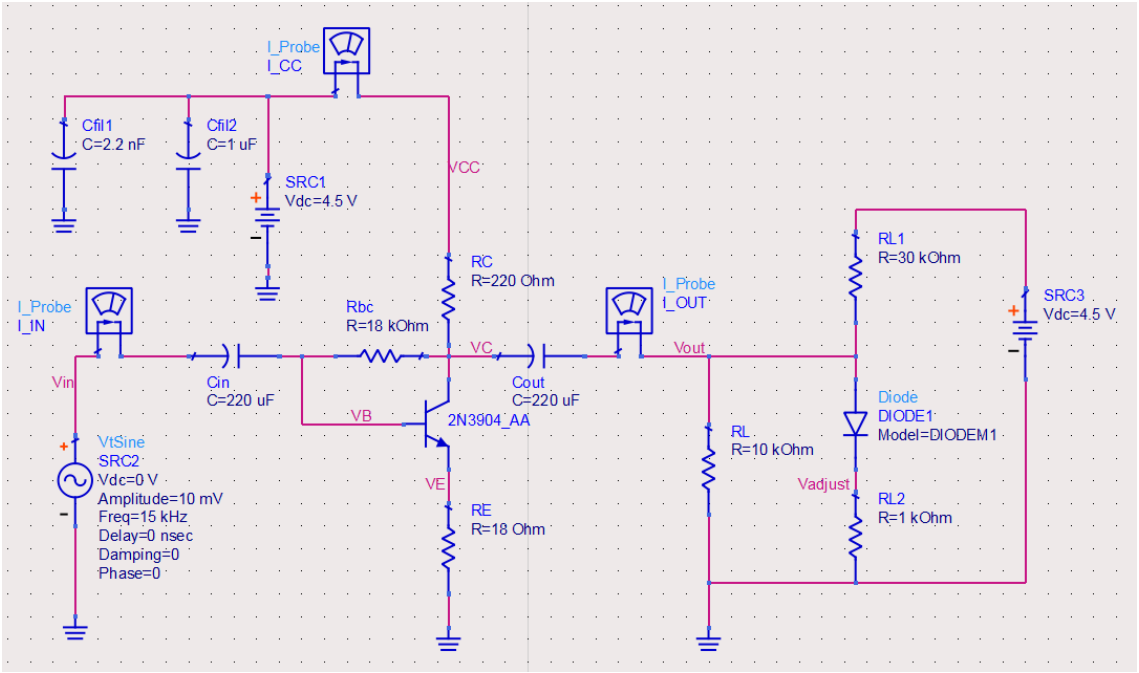

Figure 58 ADS schematic for the Audio Amplifier non-linearity study. Diode and series resistor load.

Now, the gain has been reduced because the load impedance has been lowered, but the amplifier works linearly and the waveform looks more similar to the sinusoidal input as it can be seen in Figure 59.

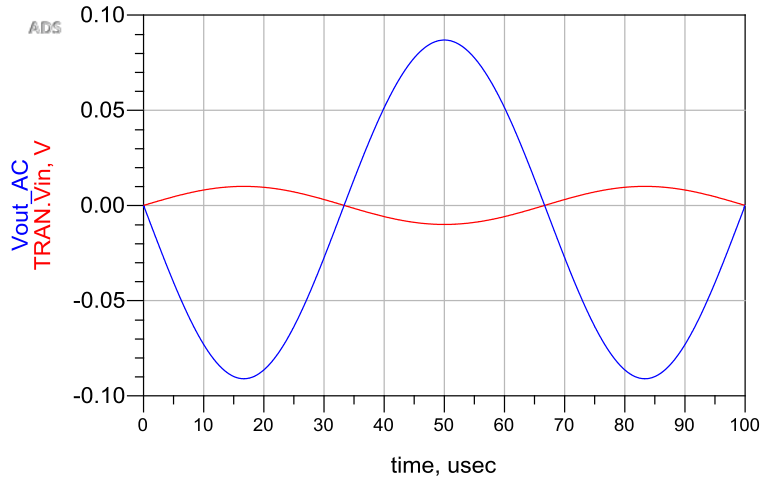

Figure 59 Audio Amplifier output (blue) and input (red) voltages with PN junction and resistive load.

We have to take into account that in our real circuit, there is not a diode but a BJT. The maximum gain that this modulated amplifier can achieve will be reduced also when adding this emitter resistor, so the output power delivered for the transmitter would be lower.

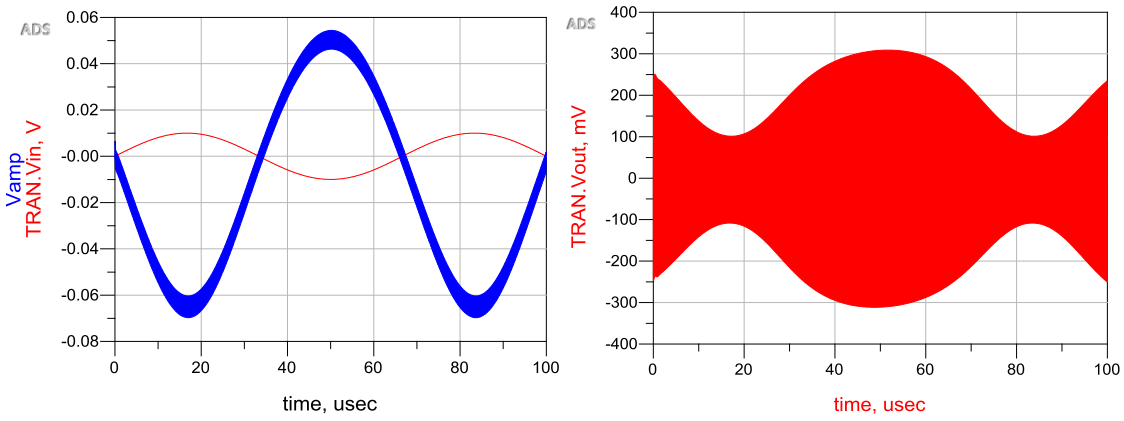

Figure 60 Audio amplifier (left) and amplitude modulator (right) simulations with an emitter resistor in the AM BJT.

As we can see from the Figure 60, the audio amplifier works more linearly when adding the emitter resistor to the modulated transistor. On the other hand, the gain of the modulated transistor decreases, and the output power delivered to the antenna is lower.

It can be seen also that the AM waveform gets more distorted (with thicker upper cycles) when increasing the resistor value, so that fixing the audio amplifier distortions does not really improve the overall performance of the transmitter.

APPENDIX 4. SUMMARY OF OSCILLATOR BEHAVIORS

The following tables show measurement results for different oscillators. Notice that even when the feedback networks were the same in some cases, the power consumption and the oscillation frequencies varied because of the use of different BJT models in the amplifier. Table 23 shows oscillators using the BJT 2N3904, Table 24 uses the BJT SS9018 and Table 25 uses the BJT KSC1845.

(Green: good value Orange: acceptable value Red: Unacceptable value)

Table 23 Oscillator comparison using BJT 2N3904.

Oscillator type	Colpitts oscillator	Clapp oscillator	Clapp oscillator	Clapp oscillator	Clapp oscillator	Crystal oscillator	Crystal (original)
L	3.3 µH	3.3 µH	3.3 µH	3.3 µH	3.3 µH	-	-
C_S	-	22 pF	27 pF	22 pF	22 pF	-	-
C_1	47 pF	150 pF	150 pF	220 pF	220 pF	33 pF	-
C_2	47 pF	150 pF	150 pF	220 pF	150 pF	33 pF	-
f_o	12.6 MHz	18.7 MHz	17.8 MHz	18.1 MHz	18.5 MHz	18.4 MHz	18.4 MHz
I_c	8 mA	24 mA	21 mA	35 mA	18 mA	13 mA	5 mA

Table 24 Oscillator comparison using BJT SS9018.

Oscillator type	Colpitts oscillator	Clapp oscillator	Clapp oscillator	Clapp oscillator	Crystal oscillator	Crystal oscillator	Crystal (original)
L	3.3 µH	3.3 µH	3.3 µH	3.3 µH	-	-	-
C_S	-	22 pF	22 pF	33 pF	-	-	-
C_1	47 pF	150 pF	470 pF	220 pF	33 pF	820 pF	-
C_2	47 pF	150 pF	150 pF	33 pF	33 pF	4.7 pF	-
f_o	12.1 MHz	18.8 MHz	18.3 MHz	18.0 MHz	18.4 MHz	18.4 MHz	18.4 MHz
I_c	10 mA	18 mA	9 mA	4 mA	8 mA	1 mA	5 mA

Table 25 Oscillator comparison using BJT KSC1845.

Oscillator type	Colpitts oscillator	Clapp oscillator	Clapp oscillator	Clapp oscillator	Clapp oscillator	Crystal oscillator	Crystal (original)
L	3.3 µH	3.3 µH	3.3 µH	3.3 µH	3.3 µH	-	-
C_S	-	22 pF	22 pF	22 pF	22 pF	-	-
C_1	47 pF	150 pF	470 pF	220 pF	220 pF	33 pF	-
C_2	47 pF	150 pF	150 pF	220 pF	150 pF	33 pF	-
f_o	10.4 MHz	18.5 MHz	18.0 MHz	17.9 MHz	18.3 MHz	18.4 MHz	18.4 MHz
I_c	12 mA	9 mA	10 mA	10 mA	8 mA	9 mA	5 mA

APPENDIX 5. DRAWINGS OF PACKAGE PARTS

Technical drawings for the three parts of the package are shown in this appendix. Figure 61 shows the middle part of the package, Figure 62 shows the bottom part which covers the battery, and Figure 63 shows the top part which covers the PCB. All the distances shown are measured in mm. Every figure shows the front, top and side view of the part together with the isometric view.

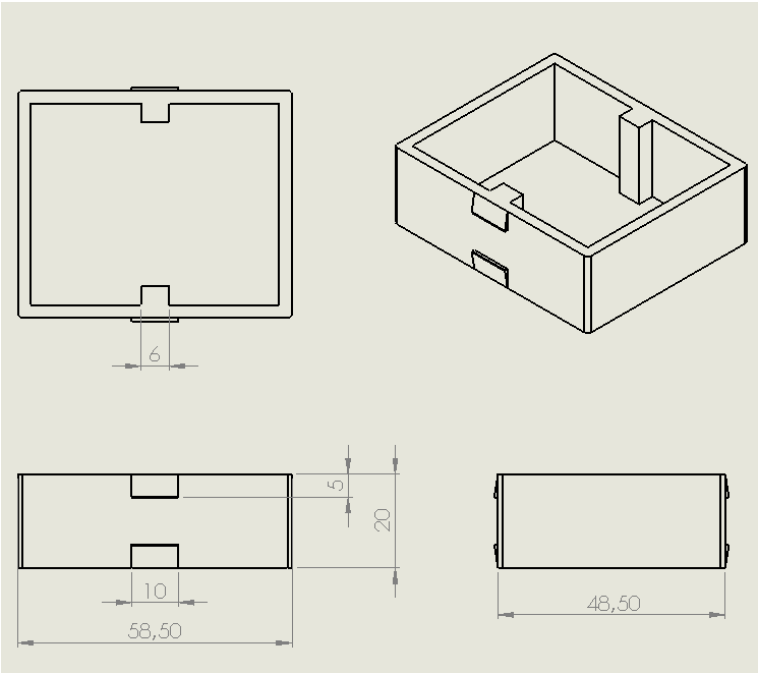

Figure 61 SolidWorks drawings for the middle part of the package.

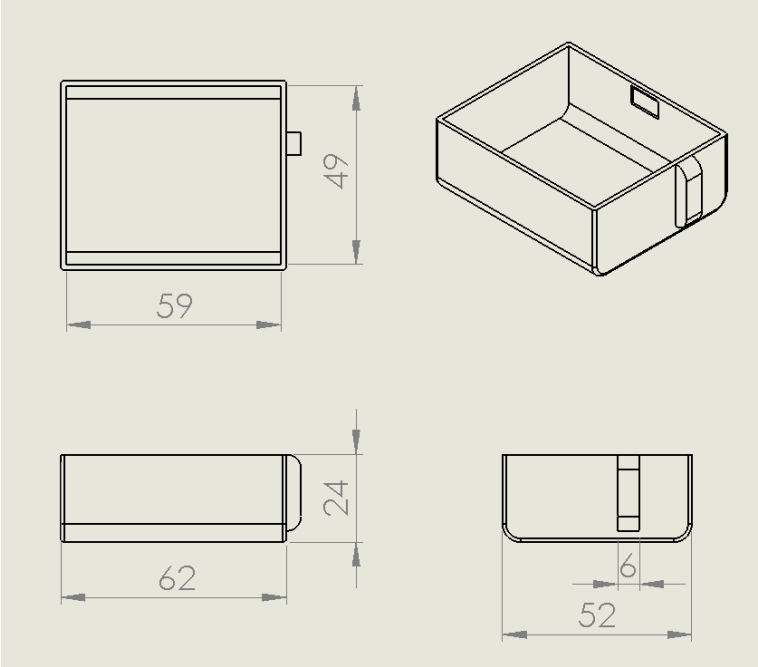

Figure 62 SolidWorks drawings for the bottom cover of the package.

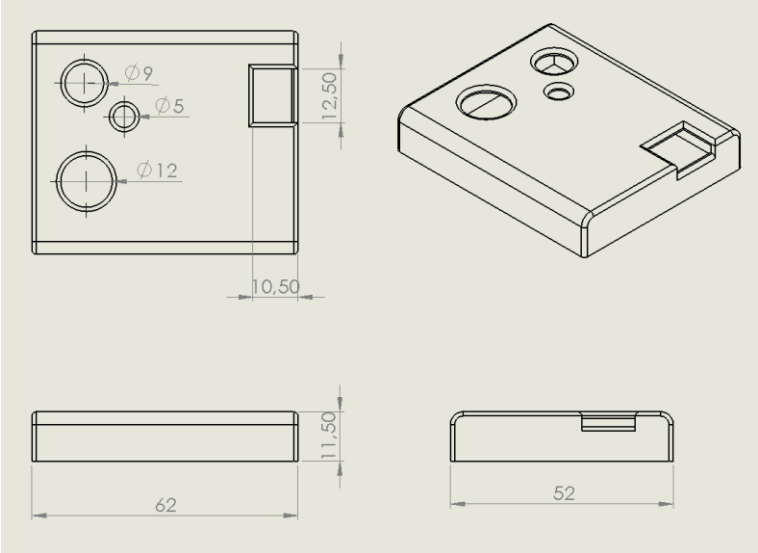

Figure 63 SolidWorks drawings for the top cover of the package.